January 2015

PHYSICAL CHEMISTRY OF COLLOIDAL-NANOPARTICLE INTERACTIONS

NECLA Mine Eren
Purdue University

Graduate School Form 30
Updated 1/15/2015

PURDUE UNIVERSITY
GRADUATE SCHOOL
Thesis/Dissertation Acceptance

This is to certify that the thesis/dissertation prepared

By NECLA MINE EREN

Entitled

PHYSICAL CHEMISTRY OF COLLOIDAL-NANOPARTICLE INTERACTIONS

For the degree of Doctor of Philosophy

Is approved by the final examining committee:

OSVALDO CAMPANELLA
Chair

GANESAN NARSIMHAN

MARTIN OKOS

OWEN JONES

To the best of my knowledge and as understood by the student in the Thesis/Dissertation Agreement, Publication Delay, and Certification Disclaimer (Graduate School Form 32), this thesis/dissertation adheres to the provisions of Purdue University's "Policy of Integrity in Research" and the use of copyright material.

Approved by Major Professor(s): OSVALDO CAMPANELLA

Approved by: BERNARD ENGEL 7/27/2015

Head of the Departmental Graduate Program Date

PHYSICAL CHEMISTRY OF COLLOIDAL-NANOPARTICLE INTERACTIONS

A Dissertation

Submitted to the Faculty

of

Purdue University

by

Necla Mine Eren

In Partial Fulfillment of the

Requirements for the Degree

of

Doctor of Philosophy

August 2015

Purdue University

West Lafayette, Indiana

Dedicated to all the children on earth especially to my nephews…

ACKNOWLEDGEMENTS

First of all, I would like to express my sincere gratitude to my academic advisor Dr. Campanella who encouraged me throughout my graduate studies. Without his guidance, support and trust, this work would not have been possible. His touch converted an ordinary student into an enthusiastic PhD. Everything I learnt from him will guide me through the rest of my academic career!

I also thank Dr. Narsimhan and Dr. Okos for always inspiring me and their willingness to help me regardless the topic. I am in debt to Dr. Narsimhan for investing time on me, as if I am one of his graduate students. His dedication makes a difference! Also, I will never forget the long conversations with Dr. Okos that shaped my understanding, expectations and attitude to my PhD and academic career. Without him, I would not have an academic strategy! Last but not least, I would like to thank Dr. Jones for his endless patience with all my experimental questions and concerns and for his ongoing support with all the instruments that I used in his lab, I never felt an outsider in his lab. In addition to my committee members, there are so many Purdue scholars that contributed to my academic and professional development. To name a few, Associate Dean of Engineering: Dr. Fentiman, ABE Department Head: Dr. Engel, Director of Whistler Center: Dr. Hamaker, Director of Dane O. Kildsig Center: Dr. Pinal. I would like to extend my appreciation to all of them.

I am thankful not only to my teachers at Purdue University, but to the ones in Turkey that has inspired me to pursue an academic career. I would like to thank all of them, especially to Dr. Aziz Tekin, Dr. Ayla Soyer, Dr. Osman Kola and Dr. Behic Mert.

I also owe many thanks to my family for being the best family on earth! Their unconditional love and support kept me going! A note to my nephews, to be read in the future, I apologize that I could not witness you growing up, I was not there neither to watch the first steps nor to hear the first words, but I accumulated lots of experience here, I will walk by you through the rest of your life and listen you endlessly to make up this past 3 years!

And of course friends…Life would have been so tough and boring without them. All my friends in Turkey, ABE friends, Rheology Lab and Pinal Lab lab mates, Turkish friends and Oliva, I am thankful for having all of you in my life.

TABLE OF CONTENTS

Page

Page

LIST OF TABLES

LIST OF FIGURES

Figure Page

Figure Page

Figure Page

Figure Page

Figure Page

Figure Page

Figure Page

Appendix Figure

ABSTRACT

Eren, Necla M. Ph.D., Purdue University, August 2015. Physical Chemistry of Colloidal-Nanoparticle Interactions. Major Professor: Osvaldo Campanella.

Following the advances in the design and characterization of engineered nanoparticles, biomaterials came into contact with the nano-world. Among many implementations of bio-nanotechnology, there is an increasing scientific and industrial interest in designing complex/hybrid structures (micro/macro) by merging the advantageous of inorganic colloidal particles (fixed shape, hard matter) with organic biopolymers (flexible shape, soft matter).In the current dissertation, nanostructured silica suspensions with tunable rheological characteristics were designed via steric and electrostatic interactions. Perturbation of short range interactions, protein bridging and silica re-dispersion were reported to play key roles in the macro-structure formation as determined by light scattering, steady state shear and small angle oscillatory shear rheology. Tunable rheology was attributed to the physiochemical interactions of disordered fractal microstructures that are formed via spontaneous, non-directional and random complexation. The thermodynamic nature of complexation was resolved by discriminating the free energy change into its enthalpic and entropic contributions through circular dichroism and isothermal titration calorimetry. The dominant entropic pathway of complexation, showed that the assembly of supra-colloid microstructures by

using nano-particles and biopolymers as building blocks is not limited by unfavorable enthalpic restrictions.

CHAPTER 1. INTRODUCTION

1.1 Research motivation

Advances in electronics, computer applications, data storage, communications, energy storage, environmental remediation and defense that related to the design and characterization of engineered nanoparticles, inspired biological engineers to create "bio-nanotechnology"[1-3]. As a result of that inspiration, nanoparticles came into contact with humans and bio-world[4, 5].

Bio-nanotechnology mainly focuses to elucidate the unknowns of "protein corona"[6-9], "nano-bio interfacing"[10, 11] and "nano-bio hybridization"[12-15]. Protein corona investigates the dynamic identity of the nanoparticle that is gained upon contact to the biological fluids (*in vivo* interactions)[6]. Whereas, "nano-bio interfacing" and "nano-bio hybridization", investigates the *in vitro* interactions of nanoparticles with biomaterials. In both *in vivo* and *in vitro* interactions, the common idea is to understand how nanoparticles interacts with biological entities such as membranes, proteins, phospholipids, endocytic vesicles, organelles, DNA and biological fluids[1]. Yet, the ultimate goal is diverse: understanding of the *in vivo* interactions is expected to guide applications in biomoleculer transport, drug delivery and regenerative medicine, whereas a deeper knowledge *in vivo* interactions is expected to lead new generation biosensors and nano-bio hybrid materials. .

The focus of the current thesis is on the field of bio-nanotechnology through nano-bio hybrid materials design. The main objective was to initiate a systematic hybridization approach in the design of disordered fractal microstructures. The main motivation was to gain a benefit from those microstructures in the manipulation of rheological characteristics of concentrated suspensions containing nano-systems. Two complementary approaches were integrated to meet the main objective:

1. The rheological consequences of biopolymer-nanoparticle interactions were investigated along with the mechanisms that could explain them using a physicochemical approach.
2. The thermodynamic nature of bio-polymer nanoparticle complexation was investigated along with the binding mechanisms governing the complexation.

In light of the above remarks the motivation of the current thesis could be summarized as follows:

1. There is a growing scientific and industrial interest on interfacing the nanotechnology with the bio-word.
2. The diversity of possible applications merges many basic sciences into an interdisciplinary research field that provides various tools to develop new bio nanotechnology approaches for the benefit of human beings.

Manipulation of the rheological characteristics of nano-structured suspensions in a systematic manner is expected to open up the floor for application of these principles in 3-dimensional printing, wastewater purification, ceramic slurry processing, fuel design with increased safety, personal care products with desired properties and functions, artistic paints with fine-tuned consistency among many others.

1.2 Thesis Organization

The main focus, objectives and relevance to the fundamental and applied science is summarized in the Section 1.1

Chapter 2 includes the fundamental background of principles used in the thesis. Physicochemical descriptions of colloidal interactions are presented in Section 2.1. The experimental progress in establishing relationships between colloidal interactions and macroscopic structure is surveyed in Section 2.2 with a focus on rheological consequences of depletion and steric (due to adsorption) interactions. And finally, the thermodynamic nature of colloidal interactions is summarized in Section 2.3 with a focus on complex formation and thermal equilibrium.

Working principles of instrumentations that are used heavily within the thesis, is described in Chapter 3 with relevant fundamental information required to understand the operation, data analysis and data interpretation.

In Chapter 4, rheological consequences of colloidal interactions of silica with α-lactalbumin are reported from a macroscopic and microscopic standpoint, along the description of mechanisms that could explain this behavior.

In Chapter 5, thermodynamic signature of protein (lysozyme) adsorption induced silica flocculation was explored with a focus in an understanding of complexation mechanism.

1. Finally in Chapter 6, key findings of the thesis are summarized and short term outcomes emphasized including recommendations for future medium and long term research..

CHAPTER 2. STATE OF THE ART

Within this chapter, many concepts and approaches that a relevant to the current thesis were surveyed briefly with no claim to provide a detailed literature review. Due to the complexity of concepts a "state of art relation map" is provided in Figure 2.1 in order to guide the reader through the chapter.

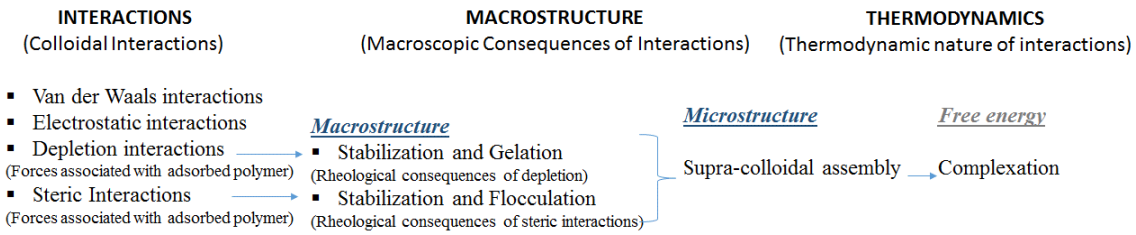

Figure 2-1 State of art relation map

2.1 Colloidal Interactions

Colloidal dispersions are two-component systems in which the dispersed phase is too small (≤1μm) to be affected by gravitational forces but large enough (>1nm) to be different than true solutions. The size of colloidal particles ranges from 1 nm to 1000 nm; just to compare the diameters of atoms are below 0.5nm. At the colloidal scale the particle motion is significantly governed by thermal energy, also known as Brownian motion (Figure 2.2).

Interparticle interactions that are observed in colloidal systems are described in subsections (2.1.1-2.1.4) following reference[1], which for the sake of simplicity is not cited through the text again. Derivations of the equations that are presented in the text are taken from lectures of the Colloidal Class that is taught by Dr. Narsimhan at Purdue University (unpublished). Theoretical calculation of interaction potential for different geometries, using different approximations, is beyond the scope of the thesis, but can be found in the literature *(16-20)*

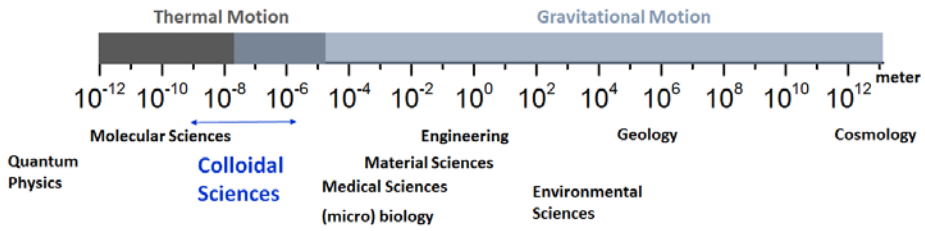

Figure 2-2 Particle motion based on Colloid Scale (adapted from Norde 2010)

2.1.1 Van der Waals Interaction

Macroscopic and microscopic properties of colloidal systems are determined by a large variety of interparticle forces. Just like atoms experiencing inter-atomic force through their fluctuating dipole moments, colloidal particles experience an attractive interparticle potential, known as the van der Waals interaction.

Van der Waals interaction is a consequence of permanent dipole-permanent dipole, permanent dipole-induced dipole, and induced dipole-induced dipole interactions

between colloidal particles. By assuming pairwise additivity the net interaction potential *(Va)* between two spherical colloidal particles of radii R_1 and R_2 is given by

$$Va = -\frac{A}{6}\left[\frac{2R_1R_2}{s^2+2R_1s+2R_2s}+\frac{2R_1R_2}{s^2+2R_1s+2R_2s+4R_1R_2}+\ln\left(\frac{s^2+2R_1s+2R_2s}{s^2+2R_1s+2R_2s+4R_1R_2}\right)\right] \quad (2.1)$$

Where *A* is the Hamaker constant and *s* is the surface to surface distance.

Van der Waals interaction causes colloidal particles to attract each other when they are separated by short distances. Colloidal particles tend to approach each other due to Brownian motion, convection, gravity and other forces, which may bring the particles to the required short distance to promote particle-particle interaction. At this point, if there is no counterattacking force the particles will aggregate as a consequence of van der Waals attraction and the colloidal system is destabilized.

Stabilization of colloidal systems is feasible through balancing attractive forces with repulsive forces such as electrostatics and forces associated with the presence of a second macromolecule in the system

2.1.2 Electrostatic Interactions

Whenever charged colloidal particles are dispersed in a liquid medium, oppositely charged groups (ions) in the continuous phase are attracted to the colloidal particles as a consequence of electro-neutrality. The region where neutralization occurs is called electrical double layer (Figure 2.3). When two colloidal particles approach each other, the overlap of double layers causes an electrostatic repulsion and the variation of electrical potential with the distance from a charged surface is calculated from the assumed double layer thickness and nanoparticle surface potential. For example when the double layer

around the colloids is thin, the Derjaguin approximation is used and electrostatic repulsion (V_R) for two colloidal spheres is given by:

$$V_R = 2\pi\varepsilon_0\varepsilon R\psi_0^{\,2}\ln\left(1+\exp(\kappa s)\right) \tag{2.2}$$

Where ε is dielectric constant of medium, ε_0 is permittivity of vacuum, R is the radius of the spherical particle, ψ is the surface potential of the colloid, s is the surface to surface distance and κ is the Debye-Huckel parameter. The Debye-Huckel parameter is given by the equation $\frac{1}{\kappa} = \left[\frac{\varepsilon_0\varepsilon kT}{e^2\sum z_i^{\,2} n_{i0}}\right]^{1/2}$ where; k is Boltzmann constant, T is the temperature, e is the elementary charge z_i and n_{i0} are the valence number and bulk number concentration of i^{th} ion respectively.

In the case of thick double layer (κR<5), Verwey and Overbeek approximation is used to calculate the electrostatic repulsion, which yields:

$$V_R = 2\pi\varepsilon_0\varepsilon R\psi_0^{\,2}\exp(\kappa s) \tag{2.3}$$

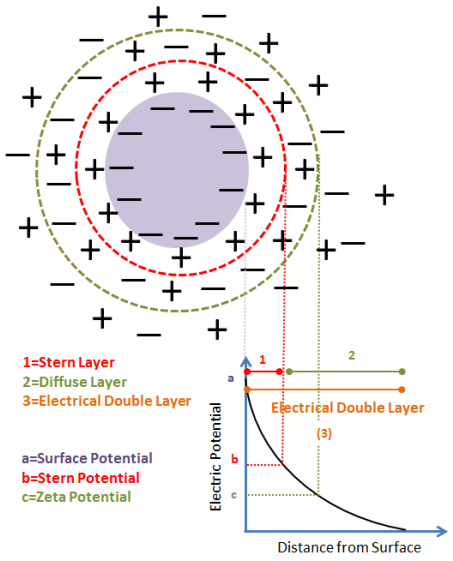

Figure 2-3Electrical Double Layer

2.1.3 Forces associated with adsorbed molecules

When a macromolecule is introduced to a colloidal suspension either adsorption of the polymer on the colloidal particle or depletion of the polymer from the vicinity of the particle occurs. When a macromolecule is adsorbed on the colloid surface, depending on the adsorbed layer thickness (L_s) and the distance between colloidal particles (d) two different phenomena or domains can be identified:

1. Non interacting domain ($d>2L_s$): There is no interaction between colloids.
2. Interpenetration domain ($L_s \leq d \leq 2L_s$): A steric interaction occurs due to the increase in the polymeric segment density in the interpenetrating region.

The resulting steric interaction can be either attractive or repulsive depending on the segment solvent interaction. In a good solvent ($\chi<0.5$) the resulting interaction is repulsive since free energy of mixing is positive due to thermodynamically unfavorable interpenetration of segments. (In good solvents interaction between adsorbed segment and solvent are favorable). On the other hand, in a bad solvent ($\chi \geq 0.5$) the resulting interaction is attractive since free energy of mixing is negative due to thermodynamically favorable interpenetration of segments. Steric interaction energy between two colloidal spheres is given by:

$$\Delta G(d) = 4\pi akT\left(\frac{v_2^{\,2}}{v_1}\right)\left(\frac{1}{2}-\chi\right)\omega^2\left(1-\frac{d}{2L_s}\right)^2 \qquad (2.4)$$

Where a is the radius of colloidal particle, T is the temperature, k is Boltzmann constant, v_2 is the partial specific volume of the polymer, v_1 is the volume of solvent molecule, χ is Flory-Huggins parameter, ω is the weight of polymer per unit area.

In the case of smaller separation distance ($d<L_s$), the adsorbed segments are compressed leading to a decrease in the configurational entropy. This causes an increase in the free energy and the resulting steric interaction is repulsive regardless the goodness of the solvent. Steric interaction energy in the interpenetration plus compression regimes is given by the following equation:

$$\Delta G(d) = 4\pi akT(\frac{v_2^{\ 2}}{v_1})\left(\frac{1}{2}-\chi\right)\omega^2\left\{\ln\left(\frac{L_s}{d}\right)-\frac{1}{2}+\frac{d}{2L_s}\right\}+2\pi akTv\left[d(\ln\left(\frac{d}{L_s}\right)-1+L_s\right]+\pi akT\left(\frac{v_2^{\ 2}}{v_1}\right)\left(\frac{1}{2}-\chi\right)\omega^2 \quad (2.5)$$

where v is the number of chains per unit area.

2.1.4 Forces associated with free molecules

If a macromolecule is not adsorbed on the colloid surface, its concentration between two colloidal particles changes due to geometric factors. Again the characteristic of the resulting interaction (repulsive or attractive) depends on the goodness of the solvent, separation distance and concentration of free polymer in solution.

For example, in a good solvent the interaction between the solvent and the macromolecule is favorable and changes in the conformation of the macromolecule due to geometric constrains result in an increase in the free energy, which turns into a repulsive force. Once colloids overcome this energy barrier and get closer, non-adsorbed macromolecules surrounding the colloidal particles are completely squeezed out of the region between two colloids and demixing of the macromolecule and the solvent causes a further increase in the free energy. At larger separation distances between colloids, the potential energy diagram will have an energy barrier. However at very small separation distances, the solvent between colloidal particles is squeezed out and causes demixing of

the solvent with the non-adsorbed molecules in the bulk. This should cause a decrease in the free energy and particles will experience attraction. The height of the energy barrier and the depth of the potential will depend on the concentration of free macromolecule in the solution. At low free (non-adsorbed) molecule concentration, the energy barrier is small and depletion leads destabilization, or in other words depletion flocculation occurs (due to attraction). At higher free molecule concentrations, the energy barrier is large enough to impart kinetic stability and depletion leads stabilization (due to repulsion).

The attractive potential due to depletion flocculation is given by:

$$\begin{aligned} &\Delta G = 0 \text{ if } d \geq 2a+\Delta \\ &\Delta G = -\pi_0(\pi/12)\left\{2(2a+\Delta)^3 - 3(2a+\Delta)^2 d + d^3\right\} \text{ if } 2a \leq d \leq 2a+\Delta \end{aligned} \tag{2.6}$$

Where a is the colloid radius, Δ is the macromolecule diameter (macromolecule is assumed to be rigid and spherical) and d is the separation distance of colloids, π_o is the limiting Van't Hoff osmotic pressure of the dissolved polymer and is given by $\pi_0 = kTN_2 / V$. (N_2 is the number of polymer molecules and V is the volume)

The theoretical calculation of the interparticle interaction energy in colloid systems is summarized in Section 2.1. A summary on the phase behavior of colloidal particles due to electrostatic, depletion and steric interaction is given in Figure 2.4. This theoretical background is expected to provide a framework while building a deeper understanding of the rheological consequences of interactions due to presence of a polymer in colloidal media. The following section reviews the experimental progress in the macroscopic scale research of colloid-polymer mixtures. .

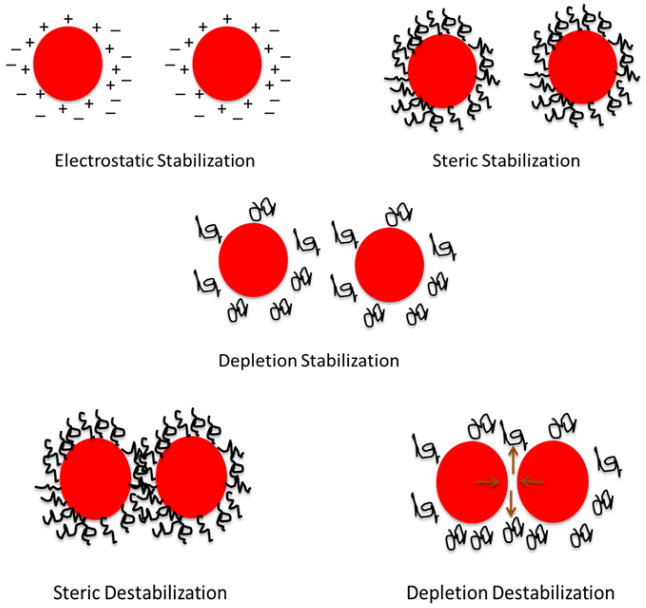

Figure 2-4 Summary of electrostatic/polymeric stabilization and destabilization

2.2 Macroscopic Consequences of Interactions

When a polymer is introduced into a colloidal system, the phase behavior of the polymer in the bulk and in the vicinity of colloid is different due to polymer's conformational degrees of freedom. In the case of adsorption there is an increase in polymer segment density and in the case of depletion there is a reduction of the polymer segment density close to the surface of the colloid. The competition of these two factors determines the resulting phenomena. The first factor is the attractive potential between polymer segments and colloid surface and the second one is an entropic repulsion. The attractive potential tries to bind the polymer segments to the colloid surface, on the other hand the entropic repulsion pushes the polymer segments far away from the surface in order to maximize entropy (Since colloid surface is impenetrable, polymer conformational degrees of freedom is reduced at the surface and causes a decrease in the

entropy). If the attractive potential dominates, the polymer is adsorbed on the surface and if entropic repulsion dominates polymer stays in the solution[21, 22]

Resulting forces due to adsorption or depletion can be either attractive or repulsive and that are described in the Sections 2.1.3 and 2.1.4. In this section, the first objective is to review the "old school" progress in establishing relationship between depletion (Section 2.2.1) or steric (due to adsorption, Section 2.2.2) interactions and macrostructure by focusing on the rheology of colloid-polymer mixtures. The second objective is to present a brief literature survey on the recent interest in the field of "colloidal interactions and macrostructure of materials" by focusing on supra-colloidal assembly (Section 2.2.3).

2.2.1 Rheological Consequences of Depletion Interactions

The first manuscript indicating an attractive force between two bodies immersed in a solution was published in 1954 by two Japanese Physicists [23]without naming it as "depletion" but foreseeing the importance of the force on the behavior of suspended particles. Since then a great amount of research (2045 citations on J. Che. Phys., 22(1954), p.1255)) has been dedicated on the topic.

To make a long story short, only important remarks that might be relevant to the current thesis are summarized. First Asakura and Oosawa (1954) concluded that the magnitude of the attractive force between particles depends on the osmotic pressure of the solution and the range of attraction depends on the diameter of particles. They also proposed that the phase behavior of suspended particles might be affected by this attractive force[24]. Experimental support to that hypothesis followed right after using a

styrene-divinylbenzene microgel-polystyrene model system. In the model system, addition of free polymer creates attractive forces between particles. Colloidal particles that are attracted to each other via this attractive force, aggregate and experience phase separation [(25)].

Later it was shown that addition of free polymer to a nanoparticles suspension can also stabilize the system and this third type (the first type was electrostatic and the second type was steric, Figure 2.3) of stabilization was termed "depletion stabilization"[(26)]. Theory of "depletion stabilization" and "depletion flocculation" was supported by experiments through years with different approaches.

However, bringing a rheological approach to the topic was a relatively slow process. Finally the effect of interparticle forces due to addition of a non-adsorbing polymer on rheology has been investigated with model systems [(27)]and it was found to link both hydrodynamic and thermodynamic interactions to predict the resulting rheology of separated phase or flocculated dispersions[(28)]. Later, rheological investigations on weakly flocculated dispersions at low particle volume fractions ($\Phi<0.55$) were conducted [(29)]which seems to lead the 21 Century's research trend on the topic, that is more focusing on beyond the gelation boundary and investigating the location of gel transition and mechanical properties of depletion flocculated gels [(30)].

Through years, as a consequence of ubiquity and significance of the topic, numerous scenarios based on kinetic phenomenon have been proposed to explain the gelation mechanism. Later on, despite the purely kinetic theories, the simple picture of gelation is concluded as being a direct consequence of equilibrium liquid gas-separation with experiments, simulations and theory [(31)].).

2.2.2 Rheological Consequences of Steric Interactions

The history of steric interactions is even longer than depletion and dates back at least 4000 years to the preparation in of ancient Egyptian inks where carbon black was dissolved in water using natural protective macromolecules such as gum Arabic, egg albumin or casein [32]. Despite the long history of steric stabilization, the first manuscript differentiating the protective action of natural macromolecules from today's steric stabilization agents was published in 1954, in the same volume of the Journal of Chemical Physics that Asakura and Oosawa's had published their first manuscript about today's depletion [33].

Recognition of steric interactions as stabilizing and destabilizing factors was faster compared to depletion most probably due to its technological application history. In other words the mechanism responsible for the stabilization was explained after it had been used for 4000 years. The mechanism of steric interactions is summarized in Section 2.1.3, in the following subsections progress on the rheology of sterically stabilized concentrated suspensions and concentrated suspensions that are flocculated and coagulated due to steric interactions are reviewed.

2.2.2.1 Sterically Stabilized Suspensions

As mentioned in Section 2.1.3, steric interaction is repulsive as long as $\chi<0.5$. The rheological character of suspensions that are sterically stabilized under this condition first depends on the chain length of adsorbed or grafted polymer. In the case of short chains the interactions are weak and colloidal particles are not interacting so rheological behavior approaches to that of hard spheres. [34, 35] In the non-interacting domain,

hydrodynamic interaction and Brownian motion are the only forces responsible for the flow [(36)].

However, most of the times the adsorbed or grafted layer is thicker and causes interactions that are 'soft" in nature as a result of the longer range of interaction. In this interpenetration/compression domain rheological behavior can change from being fluid-like to gel-like depending on the overlapping intensity, or in other words, how larger the surface to surface separation distance (d) is compared to the adsorbed/grafted layer thickness (L_s). Changing volume fraction is an easy way to tune d and this has been investigated in both non-aqueous and aqueous [(37, 38)] suspensions. That made possible to calculate the exact volume fraction at which the dispersion behavior changes from viscous to elastic by plotting G''/G'=tanδ versus volume fraction. The cross-over point is defined as the volume fraction at which tanδ is 1. Also, it is concluded that the cross-over volume fraction (Φ_{cr}) depends on the particle size (a). Smaller the particle, smaller is the Φ_{cr} due to higher compressibility of small particles (Compressibility is Ls/a).

The value of viscoelastic measurements in studying interactions has led studies that investigated the quantitative correlation of rheology with interparticle interactions [(39, 40)]. However, the lack of well-established instrumentation on direct measurement of interparticle interactions has moved the focus of the research to shift towards developing methodologies to design methods and technologies such as the Surface Force Apparatus, Atomic Force Microscopy, Total Internal Reflection Microscopy, and Optical Tweezers. Relevance of those methods and technologies to the macrostructure of interacting colloids is beyond the scope of the current thesis but could be found elsewhere. [(21)].

2.2.2.2 Strongly flocculated systems

As mentioned in Section 2.1.3, steric interactions in bad solvents ($\chi \geq 0.5$) are attractive. In other words, reduction of the solvency of suspension will eventually result in flocculation of the colloidal particles. If the solvency is being decreased by addition of electrolytes, the electrolyte concentration at which the particles start to flocculate is called as critical flocculation concentration (CFC). Actually CFC can be investigated by rheological methods by investigating changes on the suspension storage modulus with electrolyte concentration. Below CFC, decreasing of the solvency will cause a reduction in the effective radius of the sterically stabilized colloidal particles that turns into a decrease in the effective volume fraction that is monitored with the decrease of the storage modulus. Above the CFC a sharp increase in the storage modulus indicates the flocculation of colloidal particles [(41)].

Also rheological models have been developed to examine the structure of flocculates. According to the elastic floc structure model, flocculated units were assumed to be small flocs of particles (called flocculi) and the ability of flocculi to entrap the dispersion media is assumed to be the indicator of its structure [(42)]. If the attractive forces between flocculies are strong, flocculies have a loose, open structure. And in the case of weak attractive forces the flocculi has a very close packed structure. Flocculi are closed packed and entrap a little amount of water just above the CFC. On the other hand, far above the CCF, structure gets more and more open which entraps a considerable amount of liquid [(29)].

Since these initial efforts, a significant amount of work has been focused on the effect of steric interactions in the rheological properties of strongly flocculated systems

due to attractive forces that are steric in nature. Even though there are still debates on how to interpret the relationship between steric interactions and rheology , it is widely accepted that flocculation of colloidal particles results in unique macroscopic responses.[43]. .

2.3 Thermodynamic nature of Interactions

As summarized in Section 2.2.3, one of the main focuses in the nanoparticle colloidal research is to develop complex materials with targeted functionalities. The main approach is to play with the colloidal interactions (summarized in Section 2.1) to trigger the complex formation and control the aggregate morphology and structure. Here the fundamental thermodynamic principles that are needed to understand the thermodynamic nature of interactions that drive the complex formation is summarized in a general thermodynamic concept, more details could be found elsewhere in the literature [44-46].

According to the first law of thermodynamics the energy content of the universe or any isolated system is constant:

$$\Delta U_{system} + \Delta U_{surrounding} = 0 \tag{2.7}$$

The internal energy change in a system (ΔU) results from the work (w) and heat (q) exchange between the system and surrounding:

$$\Delta U = q + w \tag{2.8}$$

Here, U is a state function (i.e. its change from one state to other does not depend on the path taken,) whereas q and w are path dependent functions. So written is differential terms equation 2.8 may be written as:

$$dU = \delta q + \delta w \tag{2.9}$$

Where d represents a differential change in a state function such as *U*, whereas δ represents the differential change of a path dependent function. After including the mechanical, interfacial, electrical and chemical works in terms of state variables equation 2.9 may be written as:

$$dU = \delta q - pdV + \gamma dA + \psi dQ + \sum_i \mu_i dn_i \tag{2.10}$$

Where p (pressure), γ (interfacial tension), ψ (electric potential), μ_i (chemical potential of i^{th} component) are the intensive variables and V (Volume), A (interfacial area), Q (electric charge) and n_i (number of moles of i^{th} component) are the corresponding extensive variables of the equation.

According to the second law of thermodynamics the direction of energy flow of the universe is always towards a more disordered state. “Entropy” is the main representation of disorder in thermodynamics and the entropy of a system could be defined as the number of ways to store the energy within the system.

The entropy change in a system for a transition from state 1 to state 2 is formulated as:

$$\Delta S \geq \int_1^2 \frac{\delta q}{T} \tag{2.11}$$

In the above equation the equal sign corresponds to an ideal “reversible” process whereas the inequality sign corresponds to an irreversible and real process. So, for reversible processes equation 2.10 may be re-written as:

$$dU = TdS - pdV + \gamma dA + \psi dQ + \sum_i \mu_i dn_i \tag{2.12}$$

At equilibrium, and assuming that intensive variables are constant, equation 2.12 may be integrated to yield:

$$U = TS - pV + \gamma A + \psi Q + \sum_i \mu_i n_i \tag{2.13}$$

After defining the enthalpy (H) and Gibbs energy (G) as:

$$H \equiv U + pV \tag{2.14}$$

$$G \equiv U + pV - TS = H - TS \tag{2.15}$$

the Free energy change can be expressed as:

$$dG = -SdT + VdP + \gamma dA + \psi dQ + \sum_i \mu_i dn_i \tag{2.16}$$

Also at constant T, p,….,$n_{j\neq i}$, the chemical potential of component *i* in a mixture equals its partial molar Gibbs energy:

$$g_i \equiv \left(\frac{\partial G}{\partial n_i}\right)_{T,p,\ldots,n_{j\neq i}} = \mu_i \tag{2.17}$$

By cross differentiating equation 2.16 and assuming ideal gas behavior i.e.,

$$\nu_i = \frac{RT}{\rho_i} \tag{2.18}$$

the pressure and temperature dependence of the chemical potential can be derived (R is the universal gas constant). Further integration of this chemical potential of i^{th} component in an ideal solution may be written as:

$$\mu_i = \mu_i^o + RT \ln X_i \tag{2.19}$$

Where X_i is the mole fraction of i^{th} component in the solution, that is:

$$X_i \equiv \frac{n_i}{\sum_i n_i} \tag{2.20}$$

And μ_i^o is the molar free energy of the pure component, which can be obtained by extrapolating the function μ_i to $X_i=1$ and assuming ideal behavior.

For a chemical reaction as:

$aA+bB \leftrightarrow pP+qQ$

The equilibrium condition imposes that $\Delta G = 0$, that is $\Delta G = p\mu_p + q\mu_q - \left(a\mu_a + b\mu_b\right) = 0$, which at constant pressure and temperature, reduces to

$a\mu_A+b\mu_B=p\mu_P+q\mu_Q$

After defining the equilibrium constant K in terms of the molar concentrations of the *i* component denoted c_i as:

$$K \equiv \frac{c_P^p c_Q^q}{c_A^a c_B^b} \tag{2.21}$$

Equation 2.19 can be written in terms of the Gibbs energy of the reaction as:

$$RT \ln K = -\Delta G \tag{2.22}$$

Where T is the absolute temperature in Kelvin, R is the gas constant, K is the equilibrium association (or binding) constant.

To sum up Equations 2.15 and 2.22 are the fundamental relationships that help to understand the energy exchange that drive the complex formation between colloids and adsorbing polymers [(47)]. .

CHAPTER 3. METHODOLOGY AND MATERIALS

3.1 Light Scattering

Light is just a form of energy that physicists would prefer to call “electromagnetic radiation” most likely due to the way that it propagates. Light or electromagnetic waves are composed of electric and magnetic fields that oscillate perpendicular to each other and perpendicular to the direction of energy and wave propagation as depicted in Figure 3.1.

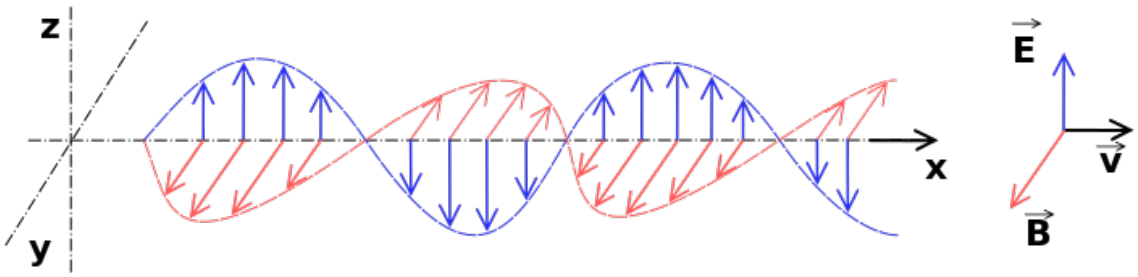

Figure 3-1 The electric field (E) is in the vertical plane and magnetic field (B) is in the horizontal plane. The wave is propagating from left to right (source: Wikipedia).

When light comes into contact with a molecule, the electric field of the light applies a force on the charges of the molecule and accelerates them by creating an oscillating polarization. According to the classical electromagnetic theory, an accelerated charge radiates scattered light that depends on the size, shape and molecular interactions in the scattering molecule.

As summarized in Figure 3.2, the purpose of the different type of light scattering experiments is to characterize the structure and molecular characteristics and dynamics of the tested materials by relating the measured spectral characteristics of the scattered light to the targeted structural and dynamic property via electrodynamic and time dependent statistical mechanical theories [48] A summary of the principles of dynamic, static and electrophoretic light scattering is depicted in Figure 3.3 and each method described further in the following sections.

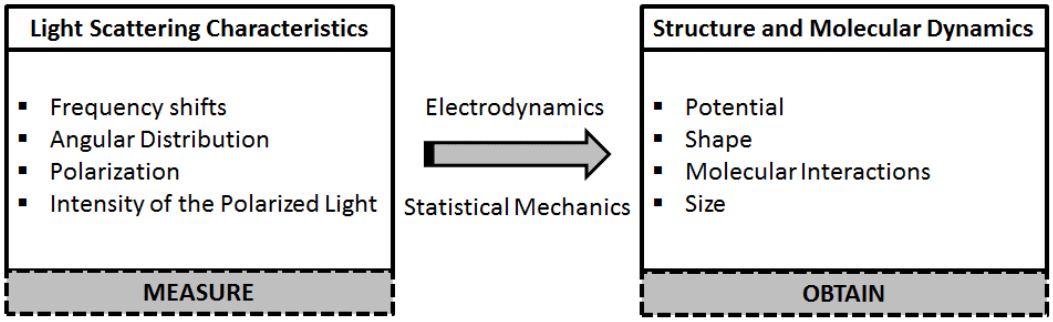

Figure 3-2 Light Scattering characteristic of a system combined with help of electrodynamics and the theory of time dependent statistical mechanics serves as the most important physical probes of the structure and dynamics of matter.

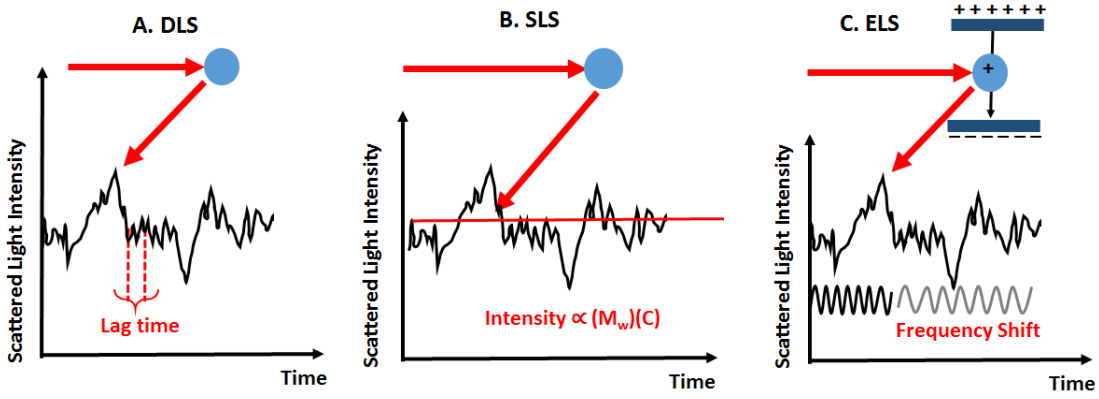

Figure 3-3 Principle of A. dynamic light scattering (DLS), B. static light scattering (SLS) and C. electrophoretic light scattering (ELS)

3.1.1 Dynamic Light Scattering

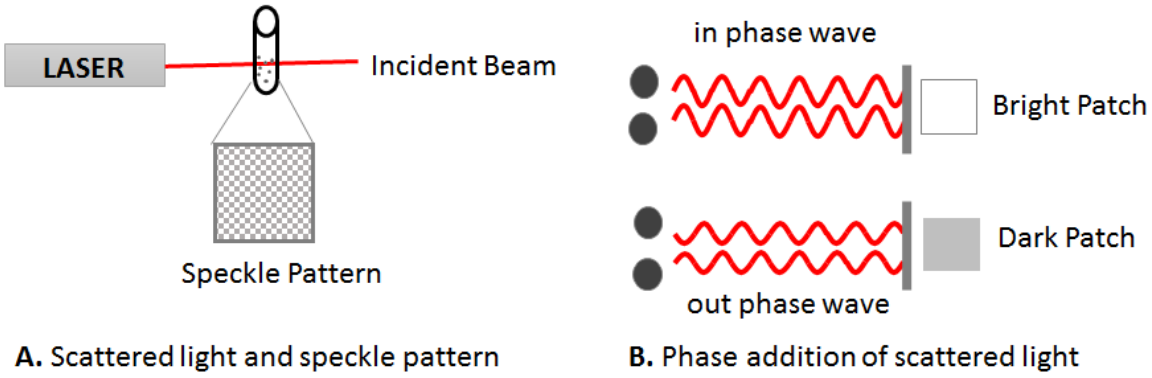

Figure 3-4 A) The signal collected at detector can be imagined as a speckle pattern due to the contribution of the scattered light generated by the molecules. B) The intensity of the signal depends on the phase addition of scattered light falling on the detector. If two beams arrive to the detector with the same phase and interfere constructively, they form a bright patch. In the opposite scenario, two beams arrive to the detector with different phases and interfere destructively; as a result they form a dark patch. As particles moves, speckle pattern will change and the rate of this change can be related to the size of particles under certain circumstances.

In a dynamic light scattering experiment, the intensity of scattered light is measured as a function of time to get information on the sizes of the molecules. How is the information on size from scattering intensity is obtained goes as back as 18th century when Brown, Rayleigh, Mie, Debye, Smoluchowski and Einstein developed theories such as Brownian motion, Rayleigh-Debye Scattering, Mie Scattering and Stokes-Einstein kinetic theory. Physically, to interpret the phenomenon, imagine a test tube containing particles dissolved or suspended in a solvent and the tube is illuminated with light. On one hand illuminated molecules will be translating, rotating and vibrating due to thermal interactions, consequently their exact position will be changing in time. On the other hand the electric filed amplitude of the scattered light depends on the exact position of the charges, so as they move the electric field will fluctuate. From the rate of fluctuation we can obtain information about the molecules positions which in turn is related to their

diffusion rates that further can be used to calculate the hydrodynamic size of the molecule. The mechanism of the DLS experiment is illustrated in Figure 3.3.

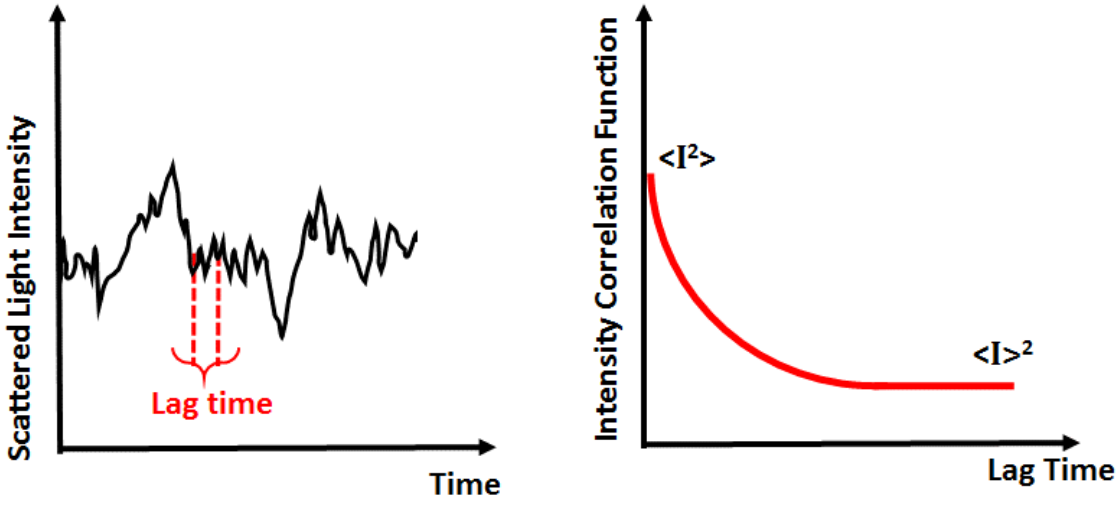

Figure 3-5 If the intensity of a signal is compared to the intensity at a very small time later (lag time) there will be a strong correlation between the signals. B) The correlation of the signal will decay like exponential as lag time increases**.**

The first step in the DLS experiment is to collect the photon counts over time which is proportional to the intensity of the scattered light. So what you measure directly is not more than intensity fluctuation. As shown in the Figure 3.4.A, this looks like just random noise and without the help of theory of noise and fluctuations, what we measure does not have a quantitative meaning. This is why all dynamic light scattering instruments have a correlator that is designed to convert the measured fluctuations to a quantitative form that is called correlation function.

The correlator computes the intensity correlation function $G_2(\tau)$ from the measured photon counts by comparing the signal as a function lag time (τ):

$$G_2(\tau) = \langle I(t)I(t+\tau)\rangle = \lim_{T\to\infty}\frac{1}{T}\int_0^T I(t)I(t+\tau)dt \quad (3.1)$$

Where, the angle brackets denote a time average, $I(t)$ is the intensity at time t and $I(t+\tau)$ is the intensity at time $t+\tau$, τ is the lag time between two points in time where the correlation is performed, T is the duration of DLS measurement.

Assuming photon counting as a Gaussian Process, the intensity correlation function can be expressed in terms of scattered field amplitudes via the Siegert relationship:

$$g_2(\tau) = 1 + \mathrm{b}g_1(\tau)^2 \quad (3.2)$$

Here, g_2 is intensity correlation function normalized by $G_2(\infty)$ and g_1 is field correlation function normalized by $G_1(0)$.

As shown in the Figure 3.5.B, for lag times very long compared to the correlation time, the correlation function decays from $\langle I^2\rangle$ to $\langle I\rangle^2$. And each particle in the illuminated volume contributes to this decay. If the system is mono-disperse, a simple exponential can describe the decay of this correlation function:

$$g_1(\tau) = \mathrm{e}^{-\Gamma\tau} \quad (3.3)$$

Where Γ is the decay constant, which is related to translational diffusion coefficient, D, via:

$$\Gamma = -Dq^2 \quad (3.4)$$

Where q is the magnitude of scattering vector and can be calculated as:

$$q = \frac{4\pi n}{\lambda}\sin\left(\frac{\theta}{2}\right) \quad (3.5)$$

Where n is the refractive index of the suspending liquid or solvent, λ is wavelength of the incident light in vacuum and θ is the scattering angle.

If the particles are spherical, translational diffusion coefficient, D, can be related to the hydrodynamic diameter of particles, R_h, via:

$$R_h = \frac{kT}{6\pi\eta D} \tag{3.6}$$

Where kT is the thermal energy (k is the Boltzmann constant and T is the absolute temperature) and η is the viscosity of the suspending liquid or solvent.

If the system is not mono-disperse, the exponential decay of each particle's diffusion coefficient contributes. And the following integral equation has to be inversed to obtain a distribution of Γ's.

$$g(\tau) = \int_0^\infty G(\Gamma)\, \mathrm{e}^{-\Gamma\tau}\, d\Gamma \tag{3.7}$$

Where is G(Γ) is a normalized distribution function of decay constant.

This is a first-kind Fredholm integral and due to high ill-posedness of the inverse problem, small perturbation in the data acquisition causes to large deviations in the decay constant distribution. To solve this problem three main approaches have been proposed: cumulant based methods[49], exponential sampling [50] and inverse Laplace Transform [51]. Numerous attempts have been made to test, modify and improve these approaches [52-65] and most DLS instruments provide user friendly software to apply these algorithms to measured correlation function. However, the complexity of the algorithms requires a

more conscious path than throwing the data in a black-box and reporting “physical parameters” with the hope that they will represent the data truly.

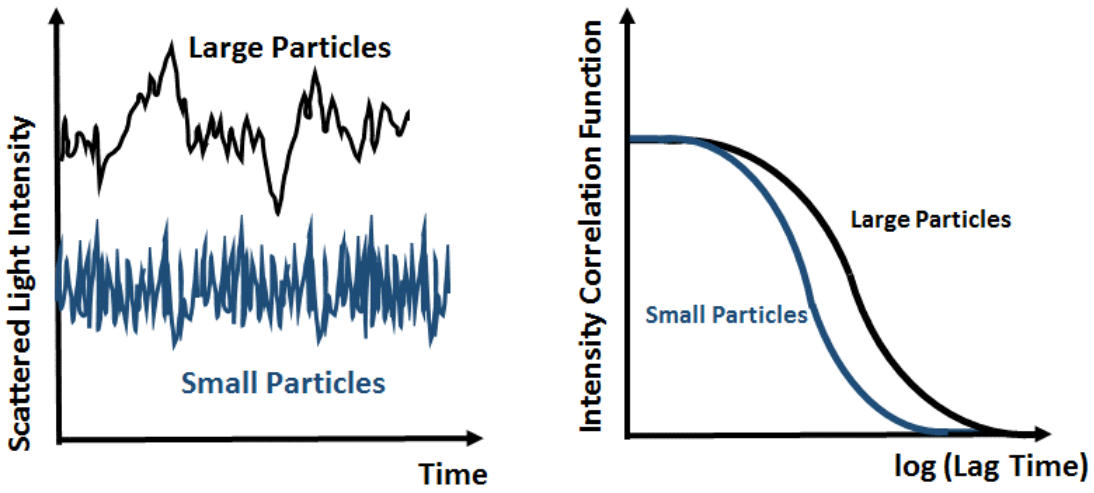

Figure 3-6 Small Particles will fluctuate faster and correlation of the signal will decay faster whereas correlation of the signal will take longer in the case of large particles due to slower fluctuations

Even though Correlation Function is quantitative compared to the intensity fluctuation (Figure 3.5), it is necessary to consciously extract physical parameters that truly represents the decay such as decay constant or decay constant distribution. We can further use this parameter to calculate the diffusion constant and particle size.

Based on the summary in this section, the selection of algorithms to extract the physical parameters from the DLS data were made carefully through this thesis. The selection was based on the system of interest in order to avoid misinterpretation of the results as much as possible, as summarized in the methods of each publication section.

3.1.2 Static Light Scattering

The intensity of light scattered by a particles/polymers is related to the concentration and molar mass of particles/polymers and the angle under which the scattered beam is measured via:

$$\frac{K^{*}c}{R(\theta,c)} = \frac{1}{M_w P(\theta)} + 2A_2 + \ldots \tag{3.8}$$

where $R(\theta,c)$ is the excess Rayleigh Ratio (cm^{-1}), c is the concentration of polymer (g/mL), M_w is weight average molecular weight , A_2 is the second viral coefficient related to the interaction between the solvent (mol mL/g^2) and the molecule, K^* is the optical constant. θ is the angle between the scattering direction and the incident light beam and $P(\theta)$ is the particle scattering function. (Further terms of equation can be neglected at low concentrations.)[66]

The particle scattering function $P(\theta)$ can be defined as:

$$\frac{1}{P(\theta)} = 1 + \frac{1}{3} n \frac{l^2}{6}\left[\frac{4\pi}{\lambda_0}\sin^2\left(\frac{\theta}{2}\right)\right]^2 + \frac{1}{36} n^2 \left[\frac{l^2}{6}\left[\frac{4\pi}{\lambda_0}\sin^2\left(\frac{\theta}{2}\right)\right]^2\right]^2 + \ldots \tag{3.9}$$

where n is number of elements in a random chain polymer, l is the length of elements and λ_0 is the incident radiation wavelength at vacuum.

By defining all the constants under one parameter (D) and neglecting the further terms, $P(\theta)$ can be reduced to:

$$\frac{1}{P(\theta)} \approx 1 + D\sin^2\left(\frac{\theta}{2}\right) \tag{3.10}$$

After plugging the Equation (3.10) into equation (3.8), for low concentration (c→0=) Equation (3.8) yields to:

$$\frac{K^{*}c}{R(\theta,c)} \approx \frac{1}{M_w} + (1 + \frac{16\pi^2}{3\lambda_0{}^2} < R_G{}^2 > \sin^2\frac{\theta}{2}) \tag{3.11}$$

*R(*θ*,c)* refers the angle-dependent intensity of light scattered by sample via:

$$R(\theta,c) = \frac{(I_\theta - I_{\theta,solvent})r^2}{I_0 V} = f\frac{\left(V_\theta - V_{\theta,solvent}\right)}{V_{laser}} \tag{3.12}$$

Where I_θ is the scattered light intensity of solution, $I_{\theta,solvent}$ is the scattered light intensity of solvent, both measured at an angle θ , I_0 is the intensity of the incident radiation, V is the volume of the scattering solution, r is the distance between the scattering volume and detector. V_θ, $V_{\theta,solvent}$, V_{laser} are detector signal voltages of the solution, solvent and laser, respectively and f is an instrumental constant depending on the geometry of the apparatus, structure of the scattering cell and the refractive indices[(66)].

While calculating the Rayleigh Ratio, it is assumed that light is vertically polarized and optical constant (K^*) for vertically polarized (polarization is the direction of electric field oscillation) incident light is:

$$K^{*} = \frac{4\pi^2 n_0{}^2}{\lambda_0{}^4 N_A}(dn/dc)^2 \tag{3.13}$$

where n_o is the refractive index of the solvent at incident wavelength, N_A is the Avogadro's number and dn/dc is the specific refractive index increment of scattering macromolecules with concentration.

3.1.3 Electrophoretic Light Scattering

As it is mentioned in the section 2.2.2 and shown Figure 2.2 the existence of charges on particles creates an electrical double layer. The potential at the electrical double layer is called zeta potential. The existence of charges on particles makes them also responsive to the applied electric field that is they will move under the influence of applied electric field (electrophoresis). The movement of particles in the applied electric field causes the scattered light to experience a frequency shift (Figure 3.7)[67].

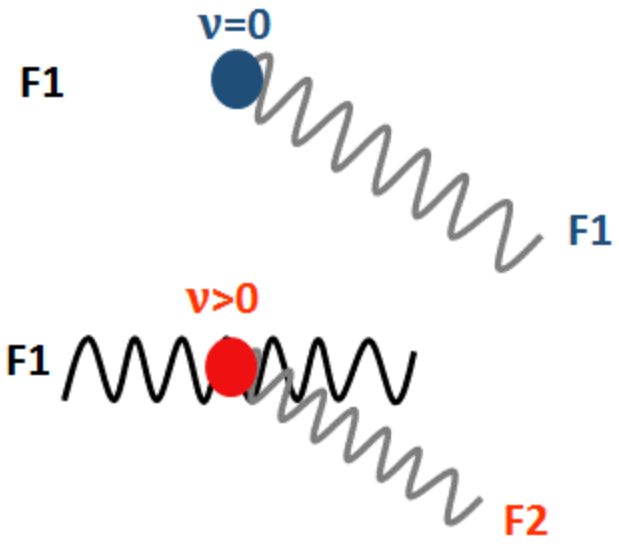

Figure 3-7 For a stationary particle (V=0), the frequency of the scattered light (F_1) will be same as the frequency of the incident light (F_1) whereas moving particles V > 0 will shift the frequency of the scattered light (F_2); V is the velocity of the particle.

The frequency shift ($\triangle f$) is related to the particle velocity (ν) via:

$$\Delta f = \frac{2\nu \sin\left(\frac{\theta}{2}\right)}{\lambda} \tag{3.14}$$

Where θ is the scattering angle and λ is the laser wavelength. From the velocity, electrophoretic mobility (U_e) could be obtained by dividing the velocity to the voltage gradient (E , due to applied electric field) imposed on the particle as follows;

$$U_e = \frac{\nu}{E} \tag{3.15}$$

Electrophoretic mobility (U_e) is proportional to particle's radius (a) and zeta potential (z), dielectric constant (ε) and viscosity (η) of the medium and the thickness of the electrical double layer (κ^{-1}). The contribution of the double layer thickness and size is defined by Henry function, f(κa), and in moderate electrolyte concentration in aqueous media f (κa) is 1.5 (Smoluchowski approximation).So finally from the electrophoretic mobility zeta potential could be calculated via:

$$U_e = \frac{2\varepsilon z f(\kappa a)}{3\eta} \tag{3.16}$$

3.2 Rheology

Rheology studies the flow and deformation of the material. The most common flow type in rheology is shear flow as depicted in Figure 3.8.

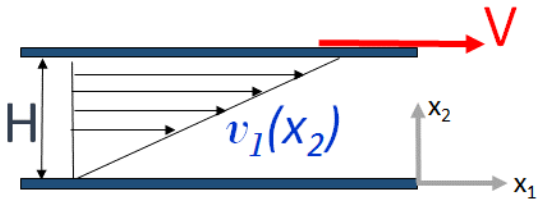

Figure 3-8 Velocity profile in a simple shear flow.

In a simple shear flow a liquid is sandwiched between two parallel plates a distance H apart. The velocity of the upper plate is V in the x_1 direction and lower plate is stationary. If there is no slip the velocity gradient $\frac{\partial v_1}{\partial x_2}$ is constant:

$$\frac{\partial v_1}{\partial x_2} = \frac{V}{H} = \dot{\gamma} \tag{3.17}$$

The velocity gradient calculated for the specific shear arrangement depicted in Figure 3.8 could be generalized for a three dimensional flow as:

$$\nabla v = \begin{bmatrix} \frac{\partial v_1}{\partial x_1} & \frac{\partial v_2}{\partial x_1} & \frac{\partial v_3}{\partial x_1} \\ \frac{\partial v_1}{\partial x_2} & \frac{\partial v_2}{\partial x_2} & \frac{\partial v_3}{\partial x_2} \\ \frac{\partial v_1}{\partial x_3} & \frac{\partial v_2}{\partial x_3} & \frac{\partial v_3}{\partial x_3} \end{bmatrix} \tag{3.18}$$

From which the shear rate tensor for simple shear flows could be obtained via:

$$\underline{\underline{\dot{\gamma}}} = \nabla \underline{v} + (\nabla \underline{v})^T \tag{3.19}$$

For a simple shear flow with the kinetics:

$$\underline{v} = \begin{bmatrix} v_1 \\ v_2 \\ v_3 \end{bmatrix}_{123} = \begin{bmatrix} \dot{\zeta}(t)\, x_2 \\ 0 \\ 0 \end{bmatrix} \tag{3.20}$$

the strain rate tensor simplifies to:

$$\underline{\underline{\dot{\gamma}}}(t) = \begin{bmatrix} 0 & \frac{\partial v_1}{\partial x_2} & 0 \\ \frac{\partial v_1}{\partial x_2} & 0 & 0 \\ 0 & 0 & 0 \end{bmatrix} \tag{3.21}$$

After defining the 21-component of shear rate tensor as:

$$\dot{\gamma}_{21}(t) = \frac{\partial v_1}{\partial x_2} = \dot{\zeta}(t) \tag{3.22}$$

To create the flow, a force has to be applied. By assuming a parallelepiped around a point in the fluid (Figure 3.9), such force or corresponding stress (Force per Area) can be written as a nine component tensor called stress tensor:

$$\underline{\underline{\tau}} = \begin{bmatrix} \tau_{11} & \tau_{12} & \tau_{13} \\ \tau_{21} & \tau_{22} & \tau_{23} \\ \tau_{31} & \tau_{32} & \tau_{33} \end{bmatrix} \tag{3.23}$$

Velocity gradient (profile) and stress are related through constitutive equations based on the kinematics (flow type such as shear or elongation and choice of the scalar function $\dot{\zeta}(t)$, which can be constant or function of time and on the material being tested. So by using constitutive equations and specified deformation flows we can determine the material properties under a defined flow deformation. Those material properties are quantified through material functions such as viscosity, storage modulus and loss modulus for shear flows among other for other types of flows.

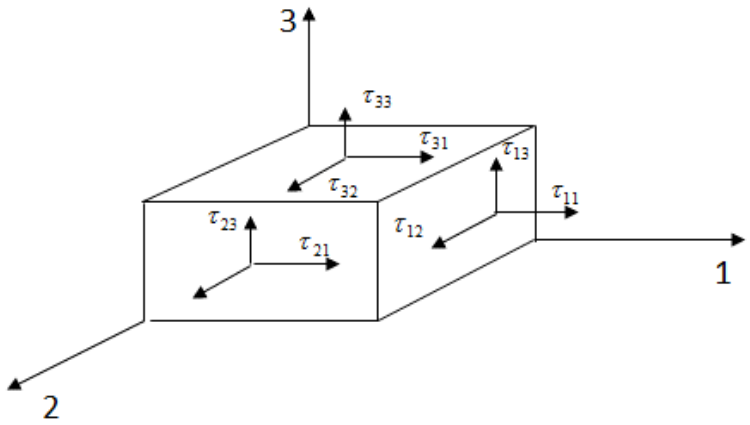

Figure 3-9 Stress tensor components on an element

Some material functions that could be measured via rotational rheometer under a steady shear (i.e. when $\dot{\zeta}(t) = constant = \dot{\gamma}_0$ and small amplitude oscillatory shear (SAOS) flow (i.e. when $\dot{\zeta}(t)$ is a sinusoidal function of time. Figure 3.10 summarizes these two types of tests, further information is also given in Table 3.1[68].

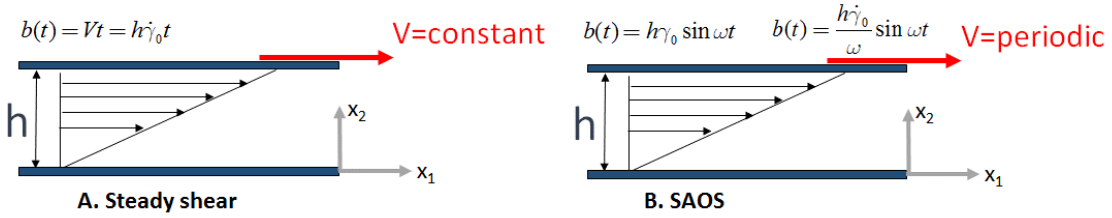

Figure 3-10 In steady shear flow (A) shear is produced by the constant rotation of the upper plate whereas in the SAOS (B), rotation is periodic. (b(t) is the time dependent displacement of the upper plate.)

Table 3-1 Flow kinematics and related material functions of rotation rheometer

Definition	Kinematics	Material Function
Steady Shear Viscosity, $\eta(\dot{\gamma})$	$\dot{\zeta}(t)=\dot{\gamma}_0=\text{constant}$	$\eta(\dot{\gamma})=\frac{\tau_{21}}{\dot{\gamma}_0}$
Storage Modulus, $G'(\omega)$	$\dot{\zeta}(t)=\dot{\gamma}_0\cos\omega t$ $\dot{\gamma}_0=\omega\gamma_0$	$G'(\omega)=\frac{\tau_0}{\gamma_0}\cos\delta$
Loss Modulus, $G''(\omega)$	$\dot{\zeta}(t)=\dot{\gamma}_0\cos\omega t$ $\dot{\gamma}_0=\omega\gamma_0$	$G''(\omega)=\frac{\tau_0}{\gamma_0}\sin\delta$

3.3 Isothermal titration Calorimetry

Examination of the dynamics and structure of the colloid-nanoparticle interactions via light scattering and rheology do not give much insight about the energetic forces that drive the resulting phase behavior, possible complex formation and stability of formed complexes[(69)]. In order to gain a compressive understanding of the interactions with an ultimate goal to fine tune them, thermodynamic signatures behind the interactions have to be explored.

Isothermal titration calorimetry is a powerful tool which directly measures the enthalpy change of interactions without the need of a predetermined model owing to its unique design, which is depicted in Figure 3.11.

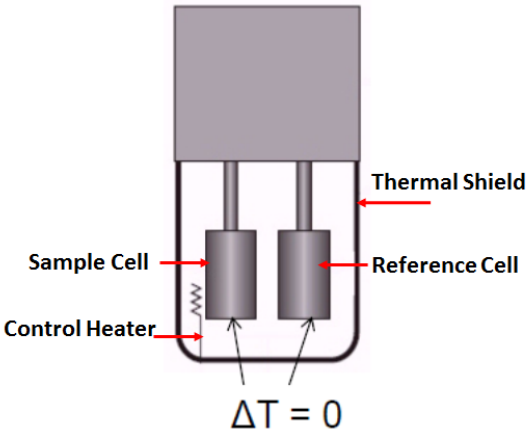

Figure 3-11. Schematic of a typical ITC unit. Source: TA Instruments

The sample cell and the reference cell are located in an adiabatic jacket in which the temperature is kept constant in a differential manner. As aliquots of guest solutions are injected through a syringe into the calorimeter sample cell that contains the host solution, the heat change in the sample cell is compensated by the applied power to maintain thermal equilibrium with the reference cell that contains the solvent of the solution. If heat is released, the sample cell would require less power input (negative signal), whereas absorption of heat would require more power input (positive signal). Each single injection will create a peak and as the reaction saturates, the magnitudes of the peaks will decrease gradually until a point that they don't change anymore. At this point the only heat associated with injection will result from the titration blanks such as heat of injection, heat of dilution and heat of mixing. Since this blank heats is not related to the host guest molecules interactions directly their subtraction is crucial.

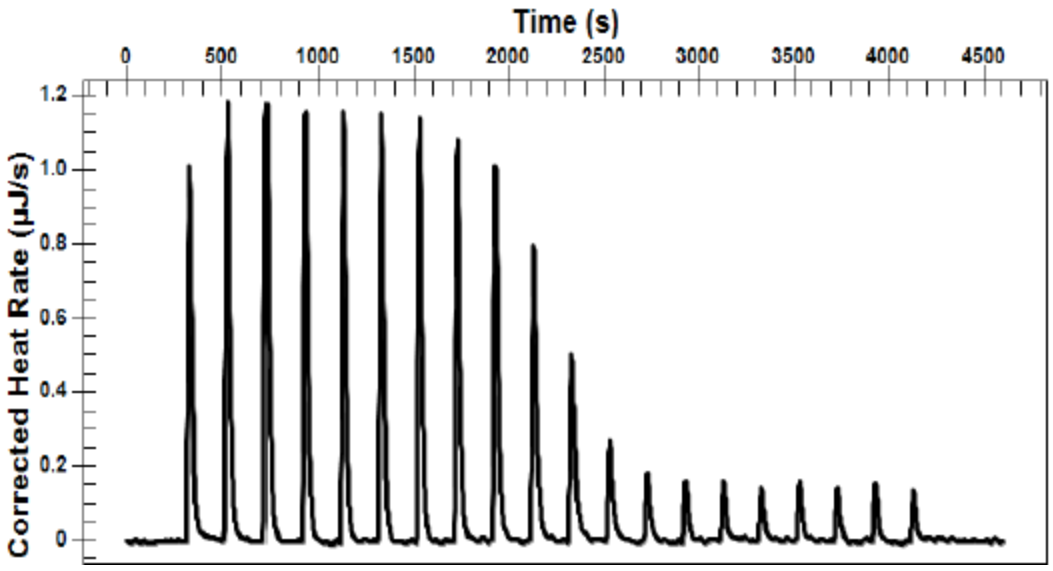

Figure 3-12 ITC raw data: power required to compensate the heat released or absorbed during the injections.Source TA Instruments

The raw data of a typical ITC experiment is the power (heat rate) versus time plot that is composed of the peaks of each injection (Figure 3.12). The raw data peaks has to be integrated with respect to time to determine the molar enthalpy of interaction (the measured quantity is power and has to be converted to heat and assuming constant volume and pressure, heat change is equal to the enthalpy change). Once the molar enthalpy of interaction is plotted against the mole ratio, thermodynamic parameters of interaction such as overall enthalpy, binding constant and stoichiometry is determined from the depth, slope and the inflection point of the curve, respectively (Figure 3.13).

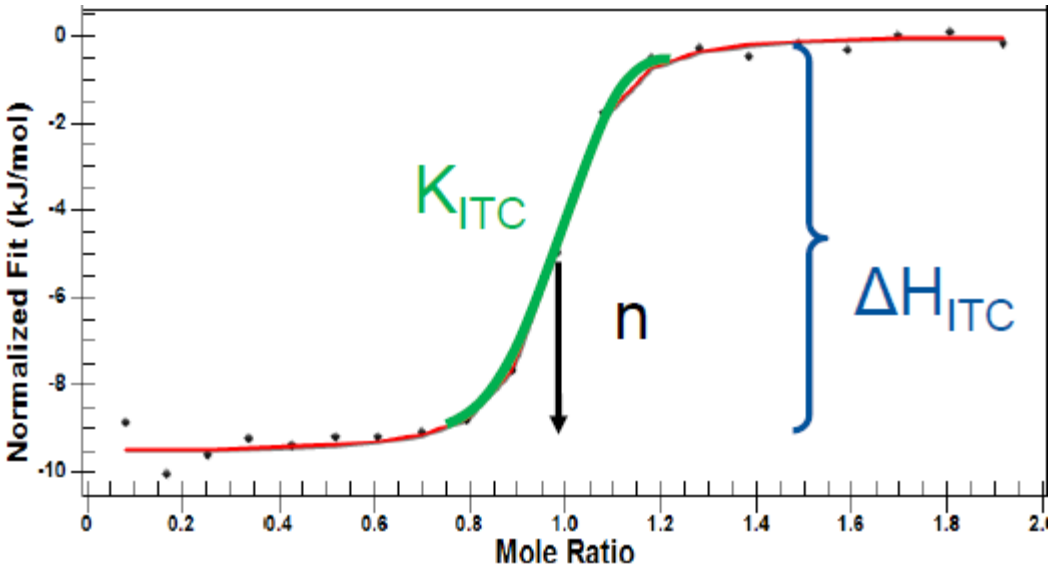

Figure 3-13 Heat Profile obtained from a typical ITC experiment. Source: TA Instruments

Obtaining the thermodynamic parameters form the heat profile requires the selection of a suitable binding model. All the possible reactions should be considered to be able to pick a theoretical framework for describing the binding phenomenon. The two simplest frameworks of binding analysis are depicted in Figures 3.14 and 3.15. Both of them allow closed-form expressions (equation 3.24 and equation 3.25) for Q (heat) as a function of total ligand concentration[(70)].

$$Q = V[M]\frac{n\Delta HK[L]}{1+K[L]} \tag{3.24}$$

$$Q = V[M]\left(\frac{n_1\Delta H_1K_1[L]}{1+K_1[L]} + \frac{n_2\Delta H_2K_2[L]}{1+K_2[L]}\right) \tag{3.25}$$

Where ΔH_i is the enthalpy of binding to binding sites of set i, L is the free ligand concentration, K_i is the binding constant, M is the total concentration of macromolecule available for binding, V is the volume.

Once the thermodynamic parameters are obtained by fitting, standard thermodynamic equations (equation 2.16: $RT\ln K = -\Delta G$ and 2.9: $\Delta G = \Delta H - T\Delta S$) can be used to calculate the free energy and discrimination of free energy into enthalpy and entropy contributions as further described in section 2.3.

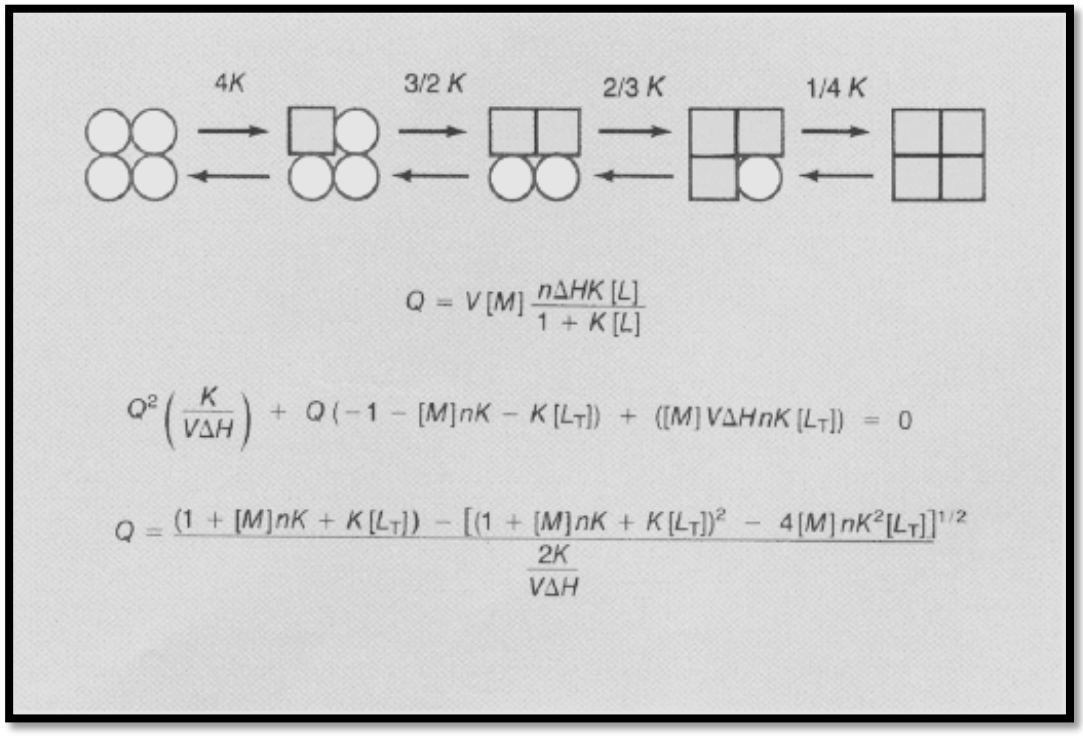

Figure 3-14 One set independent ligand-binding sites mode. Source: *Anal. Chem*, 1990, 62 (18), pp 950A-959A

It is important to note that the two equations given above apply for the systems depicted in Figures 3.14 and 3.15 and although literature often use these models they may not represent the true binding kinetics and they should be taken with caution.

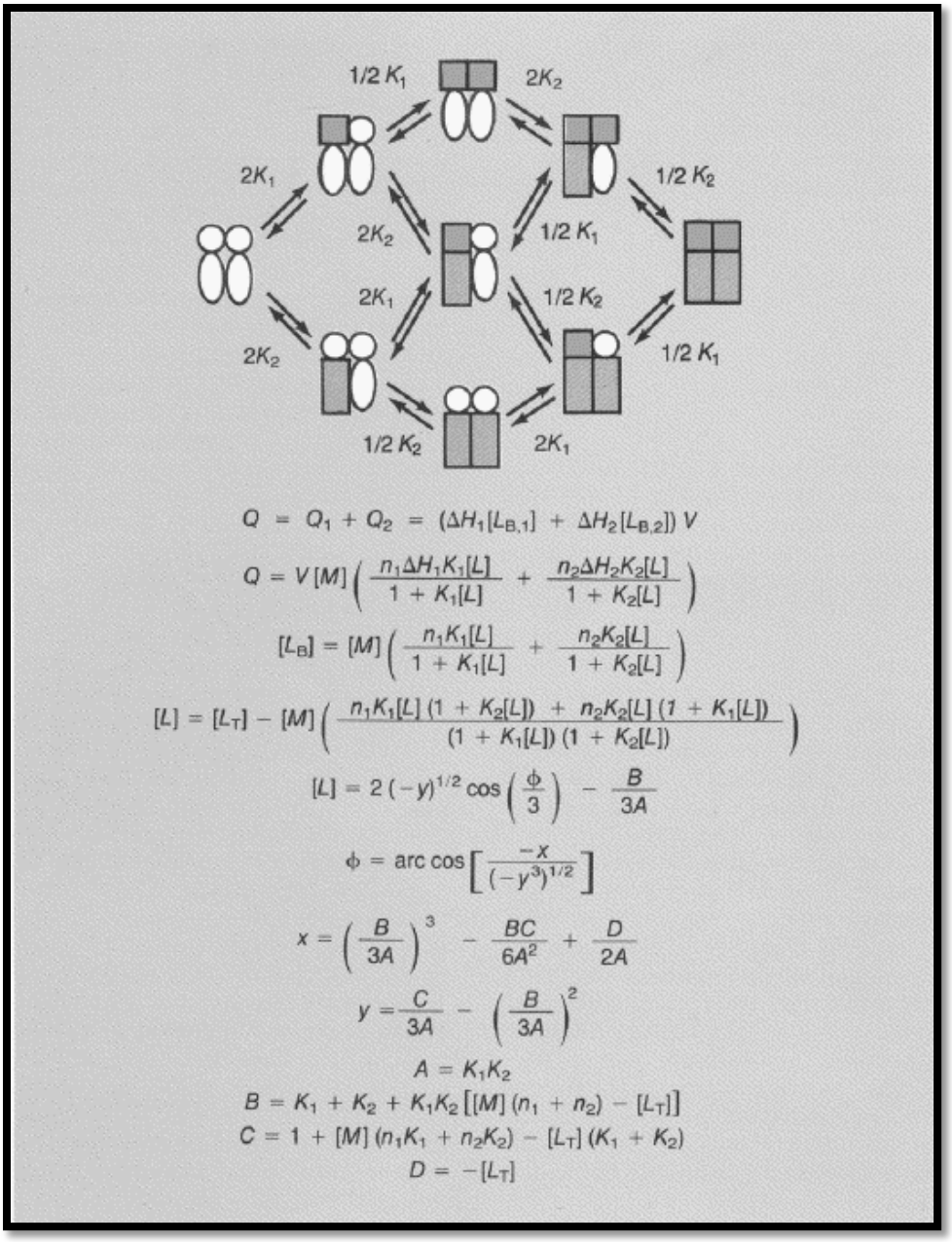

$$Q = Q_1 + Q_2 = (\Delta H_1[L_{B,1}] + \Delta H_2[L_{B,2}])\,V$$

$$Q = V[M]\left(\frac{n_1\Delta H_1K_1[L]}{1 + K_1[L]} + \frac{n_2\Delta H_2K_2[L]}{1 + K_2[L]}\right)$$

$$[L_B] = [M]\left(\frac{n_1K_1[L]}{1 + K_1[L]} + \frac{n_2K_2[L]}{1 + K_2[L]}\right)$$

$$[L] = [L_T] - [M]\left(\frac{n_1K_1[L]\,(1 + K_2[L]) + n_2K_2[L]\,(1 + K_1[L])}{(1 + K_1[L])\,(1 + K_2[L])}\right)$$

$$[L] = 2\,(-y)^{1/2}\cos\left(\frac{\phi}{3}\right) - \frac{B}{3A}$$

$$\phi = \arccos\left[\frac{-x}{(-y^3)^{1/2}}\right]$$

$$x = \left(\frac{B}{3A}\right)^3 - \frac{BC}{6A^2} + \frac{D}{2A}$$

$$y = \frac{C}{3A} - \left(\frac{B}{3A}\right)^2$$

$$A = K_1K_2$$

$$B = K_1 + K_2 + K_1K_2\left[[M]\,(n_1 + n_2) - [L_T]\right]$$

$$C = 1 + [M]\,(n_1K_1 + n_2K_2) - [L_T]\,(K_1 + K_2)$$

$$D = -[L_T]$$

Figure 3-15 Two sets of independent ligand-binding sites model. Source: *Anal. Chem*, 1990, 62 (18), pp 950A-959A

3.4 Physicochemical Properties of Colloidal Silica

3.4.1 Introduction to Colloidal Silica

Silica (SiO_2) is the major component of the crust of the earth. Quite proportional to its abundance, there are many forms of silica (crystalline, amorphous, soluble, chemically combined, etc...). Regardless the form, the building unit of silica is $[SiO_4]^{4-}$ is a tetrahedron (Figure 3.16.A). Various silica forms have different structural organization of $[SiO_4]^{4-}$units. For example amorphous form of silica is composed by a random packing of $[SiO_4]^{4-}$ whereas crystalline silica has a three dimensional framework structure (Figure 3.16.B,C). The density of amorphous silica is lower than crystalline ones due to the non-periodic structural organization[71].

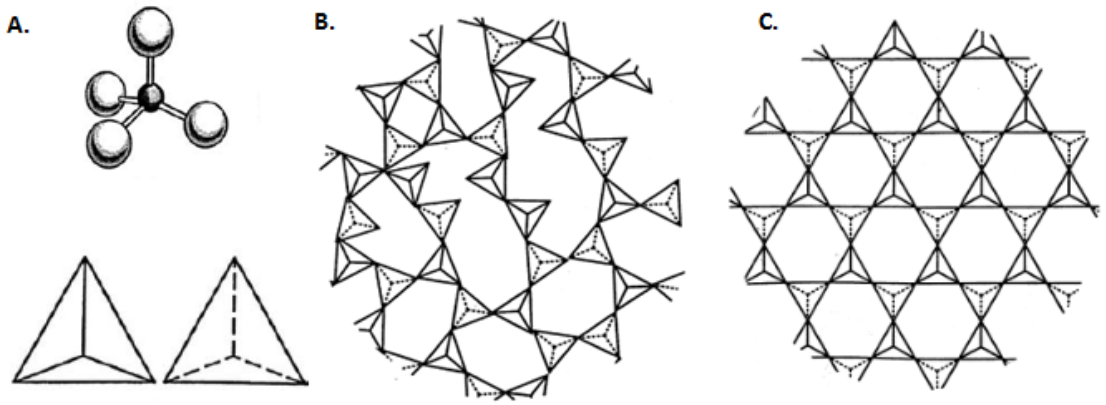

Figure 3-16 A. Tetrahedral coordination of oxygen ions with Silicon B. Random packing of $(Si\text{-}O_4)^4$ tetrahedra: Amorphous Silica C. Regular packing of $(Si\text{-}O_4)^{4-}$ tetrahedra: Crystalline Silica. Source[71]

Colloidal silica is a dispersion of synthetic amorphous silica. A stable dispersion of silica in a liquid is called a sol. Silica sols are stable in a sense that do not settle or agglomerate at a significant rate. Agglomeration is the cohesion of colloidal particles by any possible way such as gelation, coagulation, flocculation and coacervation. In gelation

(Figure 3.17.A) particles are linked together in a way that they span the all volume of the original sol, there is no local increase in the particle concentration in any macroscopic region of the total volume and the liquid phase is entrapped by the coherent network of the particles due to capillary action. In coagulation (Figure 3.17.B), particles come together as close packed clumps and there are macroscopic regions in which silica is more concentrated than in the original sol. In flocculation (Figure 3.17.C) particles are linked together by a sufficiently long flocculating agent and the resultant structure is open and voluminous compared to the coagulated ones. Sol to gel process is easier to capture and differentiate, however in a concentrated mixture it is difficult to differentiate between coagulate and flocculate. If a dilute sol is coagulated or flocculated a precipitate is formed and settles out quickly, whereas in concentrated sols the precipitate may be too voluminous to settle out and might stay as a thixotropic mass. In coacervation, the silica particles are linked together by relatively short adsorbate that makes the silica less hydrophilic but not form bridges between particles[(72)].

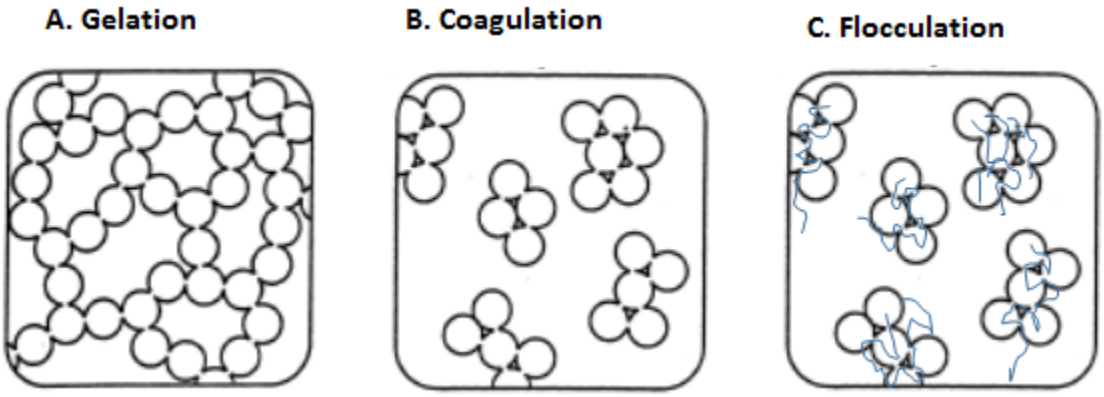

Figure 3-17 Agglomeration of Colloidal particles in different ways: A. Gelation B. Coagulation C. Flocculation. Source[(72)]

3.4.2 "Anomalous" Stability of Colloidal Silica

Aqueous silica sols are the only colloidal particles that do not follow the general patterns of the conventional DLVO theory. They are very stable around their isoelectric point and in high salt concentrations at near-neutral pH. Silica's unusual behavior is compared with the common behavior of colloidal particles in Figure 3.18

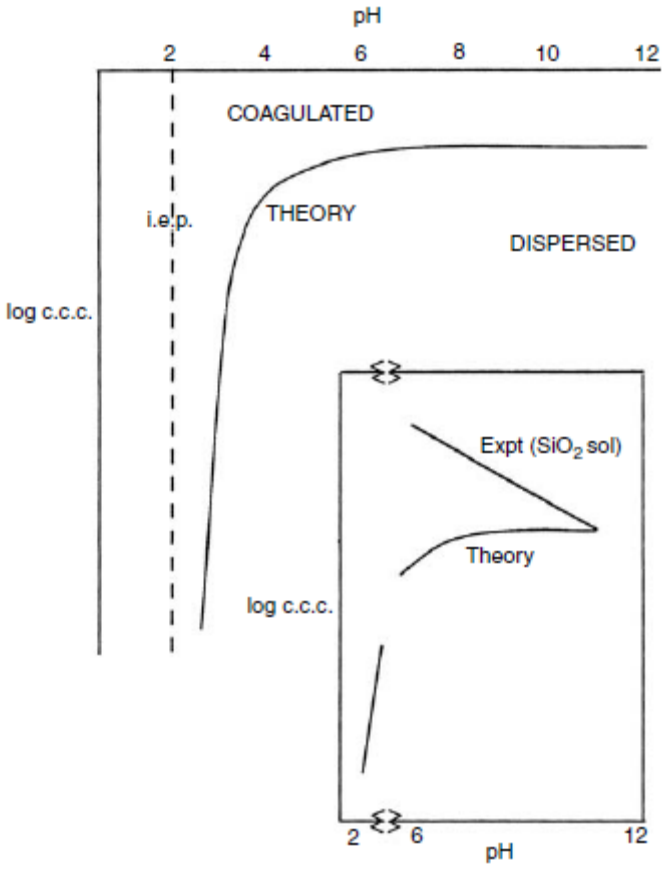

Figure 3-18. Figure shows the usual theoretical stability behavior of colloidal particles that has an isoelectric point (i.e.p) of 2. As the pH decreases their stability decreases. Inset Figure compares theoretical stability of a usual colloidal particle (theory) with silica's unusual behavior (expt) (ccc stands for the critical coagulation concentration. Silica is unusually stable around its isoelectric point)[71]

3.4.3 Surface Chemistry of Silica

Most of the practical applications where silica is used such as adsorption, adhesion, catalysis and many others are driven by the surface chemistry of silica. Surface area, surface ionization and interactions of surface groups play the most important role in the dynamic interplay between the silica surface and surrounding aqueous media.

Surface area of silica can be determined by using the Brunauer-Emmett-Teller (BET) isotherm that is based on adsorption of nitrogen on the silica surface. Geometrical surface area of non-porous silica is usually very close to the surface area determined by the BET isotherm, whereas porous silica shows a higher BET surface area compared to its geometrical surface area.

Silanol groups (≡Si–OH), siloxane bridges (≡Si–O–Si≡) and physically adsorbed water to the hydroxyl (OH) groups of silanols are responsible for the intricate interfacial characteristics of silica (Figure 3.18 A-C). Stability of silanol groups is usually achieved in alkaline media with ions such as Na^+, K^+ and $NH4^+$ by proton exchange.

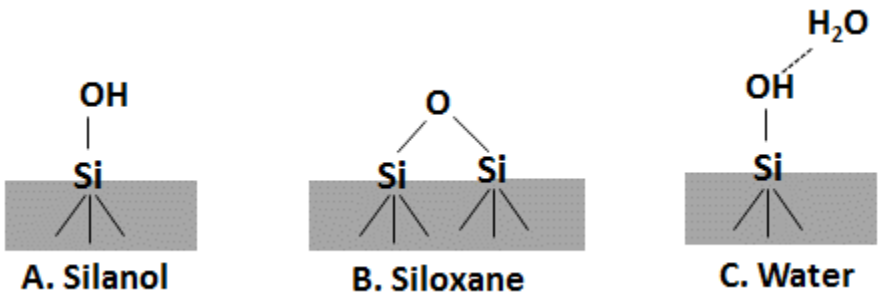

Figure 3-19 Surface Chemistry of Silica

The concentration of silanol groups is usually expressed in number of hydroxyl groups per square nanometers and called “silanol number”. Silanol number (α_{OH}) of

dehydrated but fully hydroxylated amorphous silica is widely accepted to be a constant physicochemical constant (α_{OH} =4.6) that is independent of the origin and structure of silica. The hydroxylated surface with predominance of silanols groups is hydrophilic whereas dehydroxylated surface with predominance of siloxane bridges is hydrophobic.

CHAPTER 4. CHANGES IN THE REOLOGY OF NANO-STRUCTURED SUSPENSIONS BY ADSORPTION OF THE PROTEIN ALPHA-LACTALBUMIN ON THE SURFACE OF SILICA PARTICLES

4.1 Abstract

A rheological phenomenon associated to the adsorption of a soluble protein in the surface of silica nanoparticles is reported along the mechanisms that could explain it. Rheological behavior and structural relaxation of hydrophilic fumed silica suspensions in the absence and presence of α-lactalbumin were studied at pH values 2, 4, and 6 using rheological tests and dynamic light scattering (DLS). The addition of α-lactalbumin caused an increase in viscosity and elasticity of the samples at pH 2 and pH 4, whereas an opposite effect was observed at pH 6. Structural relaxation of the nanoparticles forming the suspensions slowed down upon protein addition at pH's 2 and 4 but did not change significantly at pH 6. Changes in rheological properties and structural relaxation were attributed to electrostatic interactions induced by the changes in the silica surface charges at the different pH studied; also by perturbation of the short range interactions (pH 2), protein bridging (pH 4) and better-dispersion of particles (pH 6).

4.2 Introduction

The interaction of biopolymers such as proteins and nanoparticles has attracted considerable attention in recent years not only due to the increasing popularity of nanotechnology in areas such as pharmacy, medicine[(73)] and biotechnology [(74)] but also due to advantages provided by the large surface area of nanoparticles towards a better understanding of structure and function of immobilized proteins [(75)].

When a protein in a solution interacts with a solid surface, adsorption of the protein at the solid liquid interface usually occurs unless the surface is specifically designed to avoid it [(76)]. Protein adsorption might be promoted (or prevented) by (1) structural rearrangements in the protein molecule that may affect the adsorption on the surface, (2) protein-surface polarity, (3) redistribution of charged groups in the interfacial layer and (4) dehydration of the sorbent surface [(77)]. By considering these 4 main possible causes for protein adsorption on solid surfaces, kinetics and thermodynamics of adsorption as well as the structure and function of the adsorbed protein on flat surfaces and colloidal particles have been extensively studied and critical conclusions in regards to this phenomenon have been established [(78)]. However, protein adsorption on nanoparticles is less understood and has to be explored more [(79)] in order to develop various biocompatible nanomaterials ranging from nano-vaccines and nano-scale drugs [(80)] to biosensors [(81)]; also in order to address concerns regarding the transport of nanomaterials in living systems through membranes, organelles and biological fluids [(82)].

The interest in the current research stems from recent findings reported in the literature on nanoparticle-protein interactions focusing on the kinetics and thermodynamics of the system [83, 84], structure, stability and activity of the adsorbed protein [85, 86] as well as the resultant nano-composite microstructure [87, 88]. The current study is aimed to investigate the consequences of nanoparticle-protein interactions using a multi-perspective approach ranging from a meso and micro scale characterized by spectroscopic techniques such as DLS and UV absorption to a macroscale characterized by rheological measurements in order to build a bridge between the microstructure and macrostructure of systems that includes such composites.

This will contribute to a better understanding of how to control protein-nanoparticle interactions and the resultant complexes in order to modify the bulk properties (especially rheological) of the system. Once the mechanism is understood and controlled using a model system that is composed of low cost materials, it is envisaged that application of these principles to other fields such as 3-dimensional printing, wastewater purification, ceramic slurry processing and many others would be facilitated.

The composite system used in this study is formed with the protein α-lactalbumin and fumed silica. α-lactalbumin is a soft protein, with a molecular weight of approximately 14,000 Da that is prone to adsorb on surfaces even under high electrostatic repulsion barriers since it can go through structural arrangements due to its low structural stability. The fumed silica used in the study is built up of almost spherical primary particle, which are approximately 12 nm in size. Fumed silica does

not exist as single particles, instead they line up with each other to form fractal aggregates of 100-200 nm in size[89]. Although fumed silica has a complex structure compared to other types of silica such as Ludox or Stober, and α-lactalbumin exhibits some degree of polydispersity, the choice of fumed silica and this type of protein was made based on their abundance, los cost and commercial availability.

Since various types of silica and polymers such as proteins are commonly used as the nanoparticle source for investigation in the development and design of novel nano-composite materials [90] it is important to know how the silica nanoparticle interacts with a protein molecule either as a part of a composite system like the one used in this research or during its in vivo transportation. When silica interacts with a protein, changes in the phase behavior of silica due to silica protein interactions are expected with the resulting changes in the rheological behavior and structural relaxation of the composite system, all of which is investigated in the present study.

4.3 Materials and Methods

Hydrophilic fumed silica, SiO_2 (Aerosil200) used in the study was provided by the Evonik-Degussa Corporation (NJ, USA). α-lactalbumin was provided by Davisco Foods International Inc. (MN, USA) and used without further purification or modification. Silica suspensions with the desired concentrations were preparedfrom a stock solution of silica by adding the protein from a concentrated solution in the same buffer. Sodium acetate buffer (10 mM), used for preparation and dilution of all samples, were prepared at pH 2, 4, and 6 using sodium acetate and acetic acid from Sigma-Aldrich (MO,USA). 1M HCl solution (Sigma-Aldrich, MO, USA) was used to

finely adjust pH to the appropriate value. Sodium phosphate buffer (10mM) at pH 8 used to test the stability of silica by DLS was prepared by using disodium hydrogen phosphate and 0.1 M NaOH from Sigma-Aldrich (MO, USA) was used to adjust the pH.

Rheological properties of 5% (w/w) silica suspensions were determined by using a rotational AR-G2 Rheometer with Smart Swap™ geometry (TA Instruments, USA). Flow curves at 25oC were obtained using a 4-blade vane rotor (radius= 14mm, height=42 mm) to minimize slip and shear banding. Apparent viscosity was measured as a function of decreasing shear rate in a range 300 s-1 - 0.05 s-1 after a steady pre-shear step of 100 s-1 and 60 sec followed by a resting step of 30 sec was applied to the samples.

A cone and plate geometry with a 40 mm diameter and 2° cone angle was used to determine the viscoelastic properties of the samples at a constant temperature of 25 °C. Strain sweep tests were performed at 1Hz/6.283 rad.s^{-1} in order to determine the linear viscoelastic region of the silica suspensions which was determined to be around 1% strain (data not shown). Viscoelastic properties were determined in the linear viscoelastic region (1% strain) over an angular frequency range of 0.05-60 rad/s^{-1}. In order to remove any shear history created by the loading of the samples on the rheometer, a steady pre-shear step at a shear rate of 100 s^{-1} for 120 sec was applied to each sample before rheological testing.

The measuring gaps were 3000 microns for the vane rotor and cone and plate, respectively. The biggest aggregate in the system measured by DLS and estimated to

be 2.6 microns by the cumulant method was considered to be small compared to both measuring gaps (Table 1).

Silica suspensions of 2 % (w/w) with or without 0.2% (w/w) α-lactalbumin were similarly prepared with an additional homogenization of the samples for 1 minute in an ultra-Turrax type homogenizer (Polytron PT 10/35, Brinkmann Instruments, NY, USA) in order to break large aggregates prior to DLS measurements. Suspensions were diluted to a final concentration of 0.2% (w/w) silica and 0.02% (w/w) protein using 10 mM sodium acetate buffer at the desired pH value for measurement of UV absorbance and zeta-potential.

Dynamic Light Scattering on a light scattering goniometer (ALV/CGS-3 Compact Goniometer, ALV, Langen, Germany) were measured using 10 mm diameter glass tubes and illuminated with a HeNe laser (wavelength is 632.8 nm, output power is 22 mW). Scattered light was detected with dual ALV-High QE APD (avalanche photo diode) photon detectors in Pseudo-Cross-Correlation Mode at an angle of 90° for 120 seconds. Cross- Correlation technique is one of the main modifications to a classical DLS experiment to overcome multiple scattering effects due to relatively high concentrations of the sample. The coherence factor (intercept of the correlation function) was larger than 0.8 in all measurements conducted in the current study, which is the minimum value to neglect multiple scattering contributions according to ISO 13321 (ISO13321, 1996).

The objective of DLS measurements was to detect gelation/ aggregation and to relate structural relaxation of the system to its rheological properties at a higher concentration rather than obtaining particle size distributions. Information on the

structural relaxation of the silica suspensions was determined directly from plots of the correlation function.

To study protein adsorption, diluted suspensions were transferred into centrifuge tubes. Centrifuge tubes were rotated end over end in a hybridization oven (Big Shot, Boekel Scientific, PA, USA) at 25C° to ensure steady state adsorption, centrifuged at 20,000 rpm for 40 min at 25 C° (Avanti J-25I, Beckman Instruments, CA, USA) following the procedure described by Larsericsdotter et al [(91)]. Absorbance of supernatants was measured at 280 nm, in 1 cm path length quartz cells (Perkin Elmer, MA, and USA) with a UV-Visible Spectrometer (Lambda25, Perkin Elmer, MA, USA) against the corresponding buffer blank at 25 C°.

Electrophoretic mobility at 25 C° was determined in disposable folded capillary cells (DTS1070, Malvern, Worcestershire, UK) with a zeta-sizer that combines laser Doppler velocimetry and phase analysis light scattering (Zeta-sizer Nano ZS, Malvern, Worcestershire, UK). Electrophoretic mobility (U_E) was converted to zeta potential (z) using Henry Equation, ($U_E = 2\varepsilon z f(ka)/3\mu$)) along the Smoluchowski approximation ($f(ka) = 1.5,$), where ε and μ are the dielectric constant and the viscosity of the continuous phase was assumed to be 78.6 and 0.89cp, respectively (a is the particle radius and κ^{-1} is the thickness of electrical double layer) The scattering angle was 173° and refractive index of silica and protein was assumed as 1.33 and 1.45, respectively[(92)]. The protein's refractive index was used for silica-protein mixtures. To achieve a good phase signal, samples were sonicated in a sonication bath prior to reading to break aggregates that might affect the reproducibility of results in the dilute suspension. The capillary cells were rinsed first

with isopropanol then with deionized water and dried with nitrogen gas between samples.

Concentrations were chosen to meet recommendable upper and lower concentration limits of all the instruments used in the study to be able to get reliable and reproducible data. However, a silica protein ratio of 10:1 was kept constant for all studied samples. Rheological changes observed at higher concentration (5 %) were related to the interactions and adsorption phenomena which can only be examined at lower concentrations (2% or 0.2%).

All experiments were performed in triplicate and mean values were plotted with the standard error of the mean unless otherwise stated.

4.4 Results

4.4.1 Zeta Potential and Protein Adsorption

The experimental isoelectric point (IEP) of silica typically falls within a range of pH values between 2.0 and 3.0, which depends on the material geometry and the type of the measurement technique [(93)]. Protonation ($\equiv Si–OH_2^+$) or deprotonation ($\equiv Si–O^-$) of silanol ($\equiv Si–OH$) groups provides the surface charge below and above the IEP, respectively (pK_a of SiOH2 < -2.5)[(94, 95)]. As shown in Figure 4.1, at pH 2 silica particles possessed an almost neutral net charge (0.59 ±0.16 mV). As pH increases beyond the isoelectric point, particles become negatively charged and the magnitude of the zeta-potential increases significantly to -3.9±0.1 mV at pH 4 and -21.0±0.4 mV at pH 6. As illustrated in Figure 4.1, zeta potential decreased with continued increases in pH.

The isoelectric point of α-lactalbumin was determined to be around 4.8 which is in good agreement with reported values that have ranged from 4.8-3.5, depending on the salt concentration present in the solvent [96]. Thus, as illustrated in Figure 4.2 there are three distinct zones to study the protein nano-silica interactions. At pH 2, silica is neutral/ slightly positive and protein is positively charged, at pH 4, silica is negatively charged and protein is positively charged and at pH 6 both silica and protein are both negatively charged.

In order to have another insight on the nature of interactions between α-lactalbumin and silica in these distinct pH zones, protein adsorption on the nano-silica surface was investigated by removing silica particles with the protein that has been attached by centrifugation and measuring the visible light absorption of the supernatant as an indicator of the presence of unattached protein [91]. Significant decrease in the absorbance of protein samples after mixing with silica and centrifugation provides clear evidence of protein adsorption on the silica surface. As shown in Figure 4.3, silica suspensions had hardly any absorbance due to the separation of silica particles upon centrifugation regardless of the pH. In contrast, α-lactalbumin keeps suspended in the solution after centrifugation at all pH values. So, the hypothesis is that if α-lactalbumin is not strongly adsorbed on the silica surface it should stay in the solution and have a similar absorbance than pure α-lactalbumin solution with the same concentration (Figure 4.3). There was not a significant decrease in the absorbance of protein at pH's 2 and 6 after centrifugation in the presence of silica. However, a large decrease in the measured protein absorbance was observed at pH 4 after centrifugation. This is a clear indication of a strong protein

adsorption on the nano-silica surface at this pH because the protein will be kept attached to the silica particles and separated with them upon centrifugation. The strong adsorption of the α-lactalbumin protein on the silica surface is due to strong electrostatic interactions at pH 4 induced by particles strongly charged with charges of opposite signs (Figure 4.2).

4.4.2 Viscosity, Viscoelasticity and Structural Relaxation of Nano-Structured Silica

Effects of colloidal interactions, arising from differences in the zeta potential of silica, on rheological properties of the concentrated suspensions were determined under steady and small strain oscillatory dynamic shear tests. Steady shear flow curves of concentrated silica suspensions were obtained at the three different studied pH's. As shown in 4.4a, viscosity of silica suspensions increased slightly with increased pH, which was attributed to the increase in negative charge of the silica. For sols of equal silica concentration, viscosities of highly charged particles (in this case pH=6) has already been reported higher compared to the viscosity of suspensions of slightly charged particles (in this study pH=2)[97]. This rheological behavior observed in suspensions has been attributed to electro viscous effects [98] generated by an immobilized water layer[99, 100] on particles, a concept that was later extended to an immobilized gel layer on the silica particle surface[101]. In both cases these layers were considered responsible for short-range interactions that affect the rheology of the suspensions [97, 102, 103].

Mewis and Wagner (2012) discuss measurement concerns during testing colloidal suspensions which have been associated to violations of the assumed

theoretical shear viscometric flows used to estimate the sample viscosity. These concerns include wall slip, shear banding and secondary flows. Given the moderate shear rates used and the relatively high viscosities of the suspensions, the presence of secondary flows can be ruled out from the measurements. The presence of wall slip tends to reduce the truly applied shear rate from the calculated value and thus the calculated apparent viscosity is lower than the real viscosity of the sample. The geometric constraints created by the cone and plate and the parallel plates geometries induce layers of different particle concentration from the vicinity of the geometry wall to the suspension bulk resulting in slip zones with sizes on the order of the particle size. The formation of fluid layers with different particle concentration and viscosities is a phenomenon known as shear banding that often occurs when testing complex fluids such as suspensions. Both slip and shear banding become evident by the presence of an apparent stress plateau, where the shear stress becomes nearly independent of shear rate or possibly even decreases with increasing shear rate [(104)].That pattern was observed in this work during steady shear measurements using smooth and rough cone and plate and parallel plates geometries which indicated these geometries induced either slip or shear banding or both effects. The use of rotating vane geometries for the measurement of flow properties of structured liquids and suspensions has been suggested as an alternative to alleviate these unavoidable artifacts when testing suspensions [(105)] and was used in this work.

Shear banding has been reported to occur during steady shear tests at moderate shear rates but not when the suspensions are measured under small strain oscillatory rheological tests[(106)]. Thus, a cone and plate geometry was used to

characterize the viscoelasticproperties of the samples under small strain oscillation tests. In addition, the use of small strain oscillatory rheology provides a more direct indication of the microstructure of concentrated silica sols than steady shear rheology because under the small strain applied during the test there is no disruption of the sample structure [(107)]. As shown in Figure 4.5. a, storage modulus of silica suspensions increased with increasing pH, which indicated an increased in structure as the charge of the silica increases. Moreover, it is worth to note that the angular frequency dependence of the storage modulus decreased with increases in pH, which is attributed to the development of a more elastic structure in these samples. The larger values of the storage modulus compared to the loss modulus indicate that all samples show an elastic gel-like characteristic (4.5b-d).

Differences in the rheological properties of silica suspensions were attributed to interparticle interactions among silica particles and aggregates, which can be investigated via DLS, in an indirect manner, i.e. by examining the structural relaxation of particles. The faster decay of the correlation function at pH 6 in comparison with pH's 2 and 4, illustrated in Figure 4.6, indicates that the structure formed at this higher pH values relaxes more quickly within the suspension. Conversely, the correlation functions of silica particles in buffers at pH 2 and 4 decay more slowly, which clearly indicated that structural relaxation of silica particles was slowed down by lowering the pH of the suspension and thus reducing the charge of the silica particles. Silica's stability at higher pH's had been well established [(108)] and faster decay of correlation function at pH 8 (Figure 4.6) was a clear support of slower dynamics that were observed at lower pH's.

4.4.3 Rheological and Physico-chemical Changes due to interactions between α-Lactalbumin and Silica Particles

At pH 2, incorporation of α-lactalbumin into silica suspensions caused a significant increase in the viscosity of the mixture (Figure 4.4b), and the storage and loss moduli (Figure 4.7). The higher values of storage modulus compared to the loss modulus are indicating the presence of a more structured and gel-like network. This is supported with the slower dynamics (delayed structural relaxation) of the protein-silica mixtures compared to pure silica suspensions at the same pH (Figure 4.8). The observed structured network was attributed to the formation of silica clusters that are able to entrap water and form a gel-like structure. At this pH, α-lactalbumin is positively charged and silica is neutral/slightly positively charged. Theoretically electrostatic interactions between silica and protein are mainly repulsive or weak. Experimentally, adsorption of protein on silica was not confirmed. Since an associative electrostatic interaction would not be expected under these conditions, clusters of nanoparticles are thought to be formed due to perturbation of short range repulsions upon protein addition. The interaction of α-lactalbumin molecules with silica particles might lead to a decrease in the thickness of water or gel layer thought to be responsible for short range repulsion which is mentioned above [(109)].

At pH 4 α-lactalbumin and silica particles are oppositely charged and electrostatic interactions induce the adsorption of protein on the silica surface. The silica α-lactalbumin mixture shows significantly higher values of viscosity (Figure 4.4c), and storage and loss moduli (Figure 4.9), indicating the formation of a gel-like structure upon protein adsorption. This gel-like structure is generated mainly due to

bridging aggregation induced by the protein in between silica particles. Similar results have been reported on the adsorption of lysozyme onto silica surfaces at a range of pH between the isoelectric points of silica and lysozyme, which promoted bridging aggregation of the silica particles [(87)]. The dramatic shift of structural relaxation to longer lag times is considered as strong evidence that further supports bridging aggregation (Figure 4.10). The shift of structural relaxation to longer times has been explained by Kroon et al to describe sol-gel transition of amorphous systems [(110)] or when the colloidal systems governed by slower dynamics [(111)].

At pH 6, both silica and α-lactalbumin were above its isoelectric points and are negatively charged so there is a barrier against adsorption due to electrostatic repulsion with the negatively charged silica (Figure 4.2). As shown in Figure 4.11, there was no significant change in the correlation function determined from the DLS experiments upon addition of the negatively charged α-lactalbumin, although the viscosity (Figure 4.4.d) and the storage and loss moduli decreased (Figure 4.12). At pH 6 silica particles are quite stable due to strong negative charges on their surface and incorporation of a negatively charged protein is not expected to disturb the electrostatic double layer on the silica surface. However a better dispersion of the particles in the suspension created by the strong repulsive forces might be the reason behind the observed change in rheology, since a significant change in structural relaxation is not observed in the DLS profiles.

4.5 Discussion

The objective of the current study is to relate the rheological changes to the structural relaxation and interactions of particles in order to build a microscopic insight that affect the macroscopic rheological properties of the system. However, rheological attributes are determined at significant higher concentrations (5%, w/w) when compared to the concentrations used to assess the dynamics of the system by DLS, which was 2% (w/w). So, even though while interpreting the rheology data at relatively high concentrations, interparticle forces among aggregates, effects of particle crowding and short range interactions have to be accounted for, and those attributes appear to be affected for the pH studied and rheological changes can be still considered a consequence of interactions [(29)].

Moreover, as opposed to a general misunderstanding, aggregation is not necessarily a preliminary step inducing gelation, so might not lead an increase in the structured network of the system as shown in the pure silica system (Figure 4.4a). Even though silica is much more stable than other materials at the vicinity of its IEP, it is clear from the DLS data that silica is aggregating as the pH is decreased. Slight decrease in viscosity with decreased pH indicates that aggregates were not able to create a gel like network. If aggregates are able to entrap water during the formation of a structured network the resulting phase behavior will be similar to gelation rather than phase separation (Figure 4.4b and 4.4c) [(43)].

The mixing of α-lactalbumin with fumed silica sols changes the structural relaxation and rheology of the system through interactions and structural arrangements. After addition of protein into the nanoparticle suspension, depending

on pH, the adsorption of protein at the solid liquid interface is one of the expected phenomena. The driving force for adsorption might be the preferential interaction of the protein with the nanoparticle or an unfavorable interaction between protein and the solvent [(45)]. At pH 4 electrostatic interactions between protein and silica are strong due to their oppositely charged surfaces; in addition water is not a very good solvent for α-lactalbumin at the vicinity of its isoelectric point (IEP 4.8). These conditions create suitable thermodynamic conditions for protein adsorption. At pH 6 neither UV-Vis nor DLS results indicate adsorption of protein on the silica surface. The decrease in viscosity and the storage and loss moduli of the suspension might be attributed to re-dispersion of silica aggregates in the strong repulsive environment at those conditions [(87)] or to changes on the water/gel layer thickness without disturbing the electrostatic double layer . At pH 2 silica does not have a considerable amount of charge to counteract the protein binding and high absorbance after centrifugation indicates the absence of adsorption. Then the increase in viscosity at pH 2 might be attributed to formed silica clusters that are able to entrap water due to perturbation of short range repulsions upon protein addition.

4.6 Conclusion

Protein interaction with fumed silica under different electrostatic environments was studied via rheological, electrophoretic mobility, DLS, and UV-VIS characterization. Protein adsorption on silica can be clearly identified at pH 4 and bridging aggregation was considered to be the reason that can explain the increase in viscosity/ viscoelasticity and retardation in structural relaxation of the suspensions at

pH 4. At pH 2, rheological and physic-chemical changes were attributed to the perturbation of short range interactions. At pH 6 the rheological changes are thought be the result from re-dispersion of the structured silica aggregates. To sum up, it has been observed that by changing the charge of the silica and protein the structural relaxation of the system can be tuned according to their electrostatic interactions and significantly affect its microstructure and macrostructural rheological properties. The focus of this work was based on fumed silica which is inexpensive and abundant as well as the protein used. A quantitative analysis of the adsorption of a polymer (protein) on silica nanoparticles is being studied using a model system includes silica particles of uniform size and less molecularly dispersed protein.

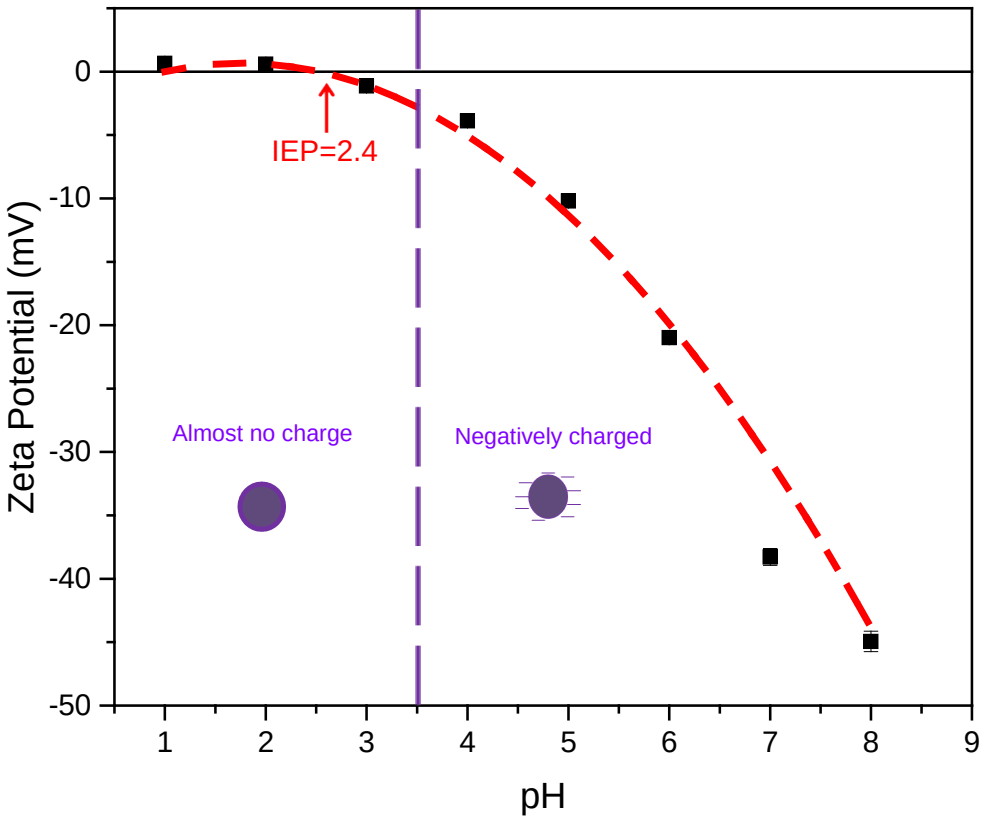

Figure 4-1 Zeta Potential curve of silica suspensions (0.2% w/w) as a function of pH

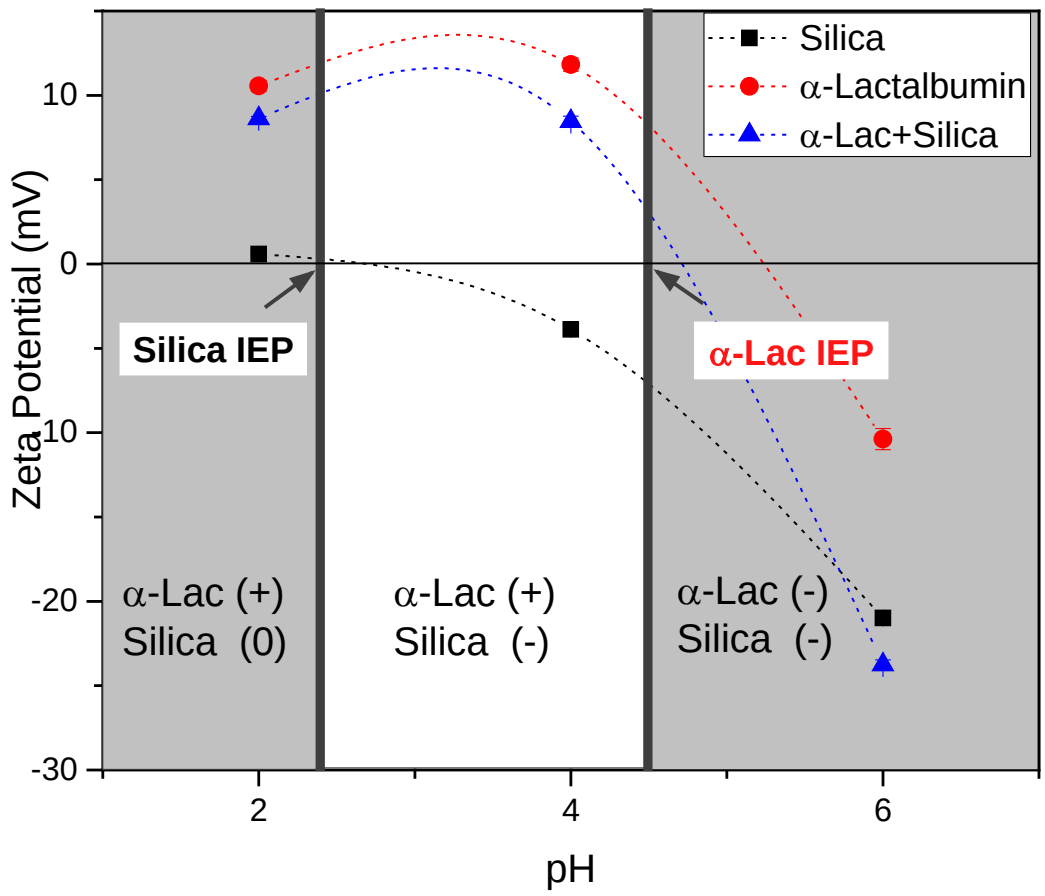

Figure 4-2 Zeta Potential of silica suspensions (0.2% w/w) and silica+ α-lactalbumin (0.2% and 0.02% w/w, respectively) in 10 mM sodium acetate buffer.

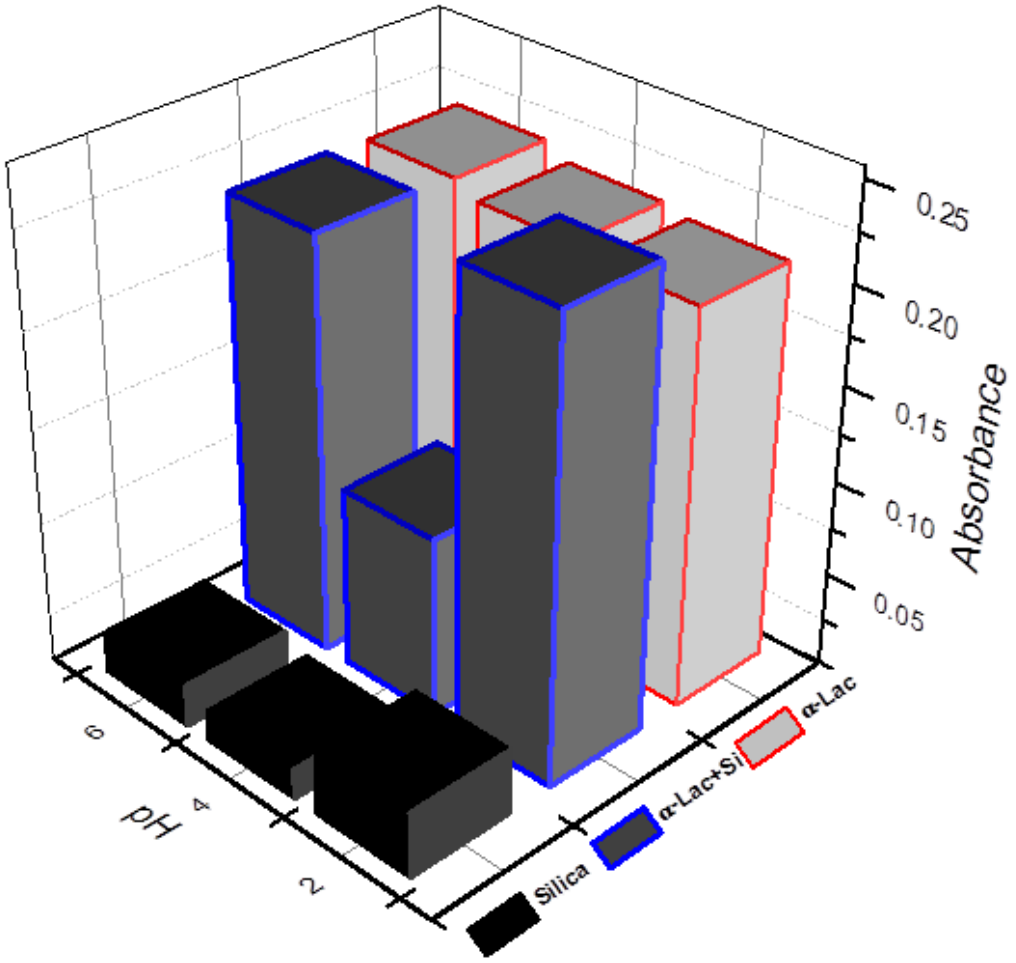

Figure 4-3 Absorbance of silica, silica + α-lactalbumin and α-lactalbumin measured at 280 nm after centrifugation

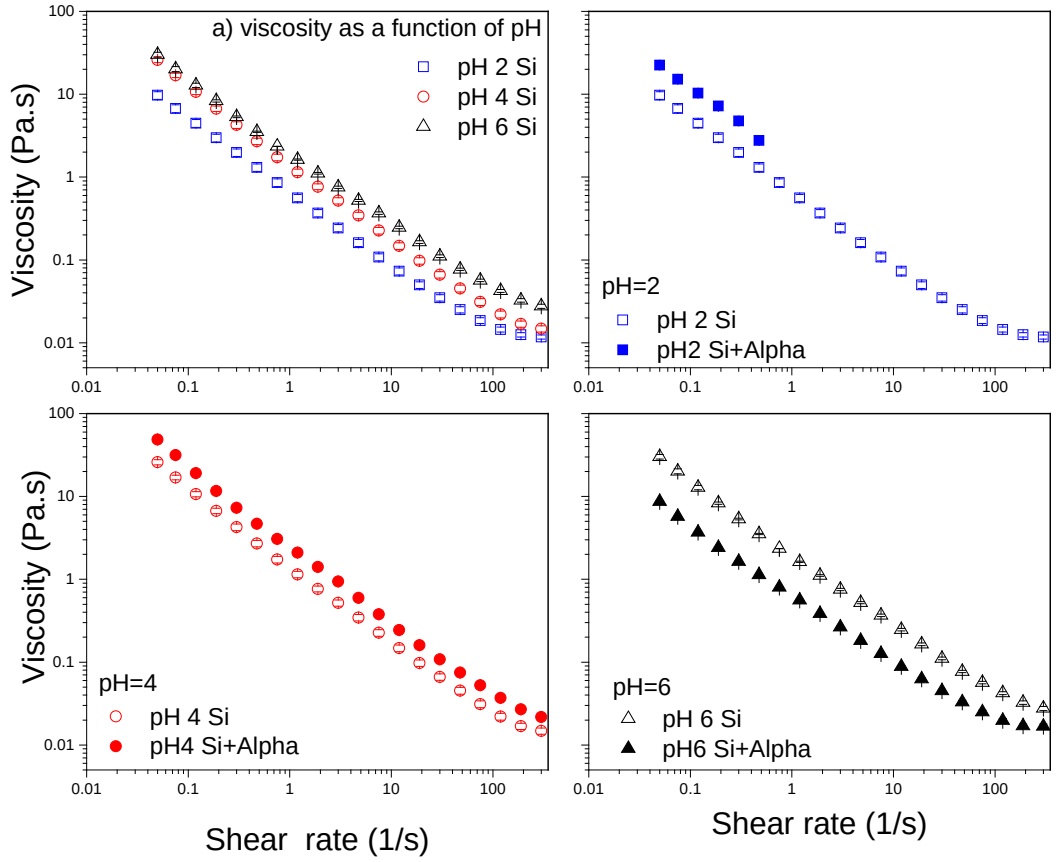

Figure 4-4 Steady shear viscosity of silica suspensions (5% w/w) and silica + α-lactalbumin(5% and 0.5% w/w, respectively) in 10 mM sodium acetate buffer. : (a) Viscosity at different pH's b)pH=2, c) pH=4 d) pH=6,

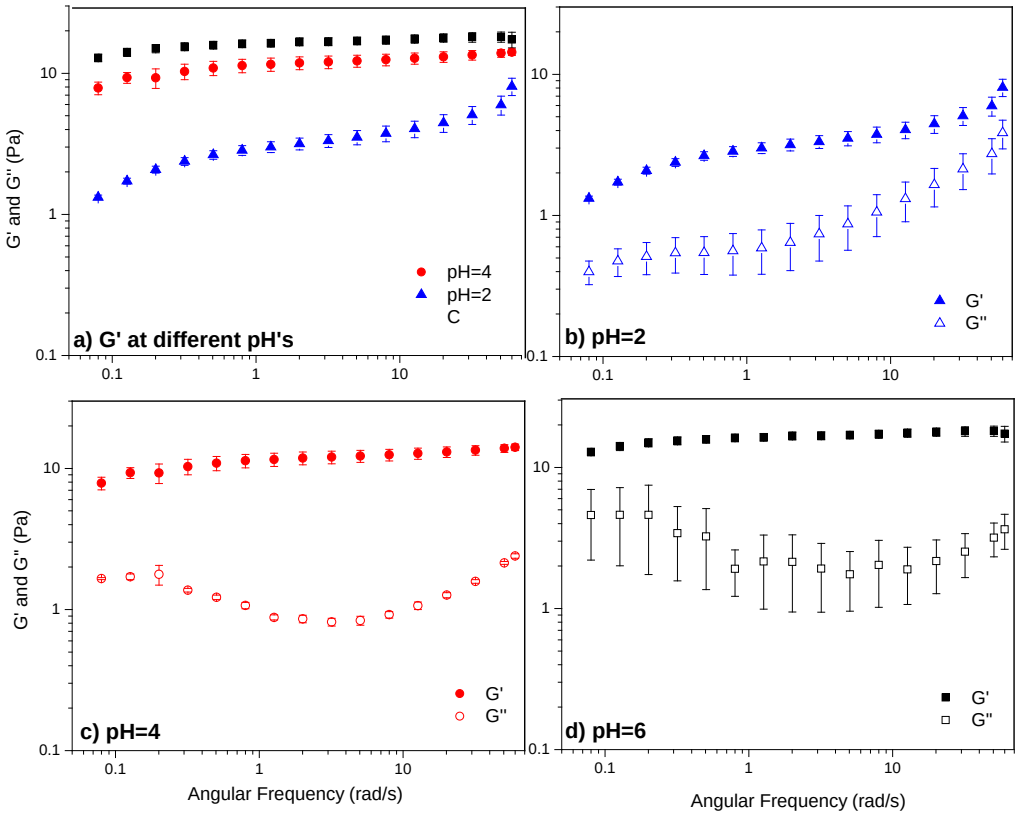

Figure 4-5 Viscoelastic properties of silica suspensions (5% w/w) in 10 mM sodium acetate buffer: (a) Storage modulus at different pH's b)pH=2, c) pH=4 d) pH=6,

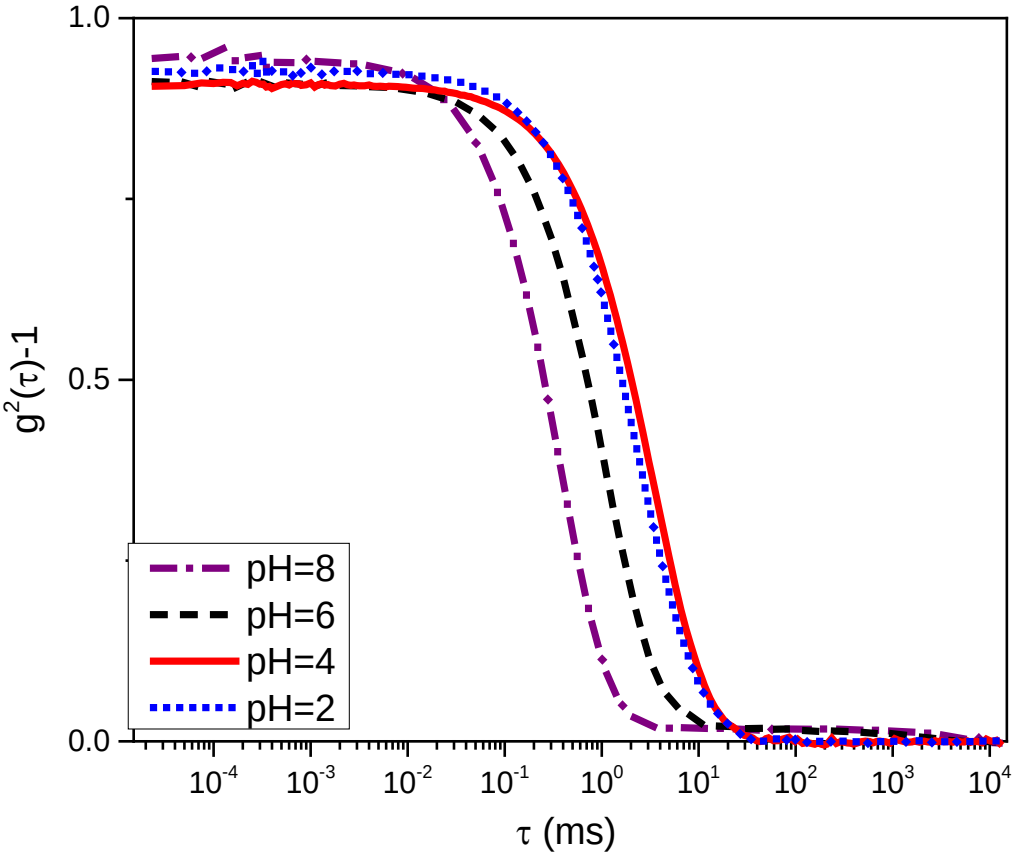

Figure 4-6 Correlogram of Silica Suspensions (2%) in 10 mM sodium acetate and sodium phosphate buffers. The ordinate is $g^2(t)-1$, where $g^2(t)$ denotes the second order intensity autocorrelation function and t is the lag time.Variability was less than 1% so error bars were not inluded in the plot in order to avoid effecting the clarity of the curves.

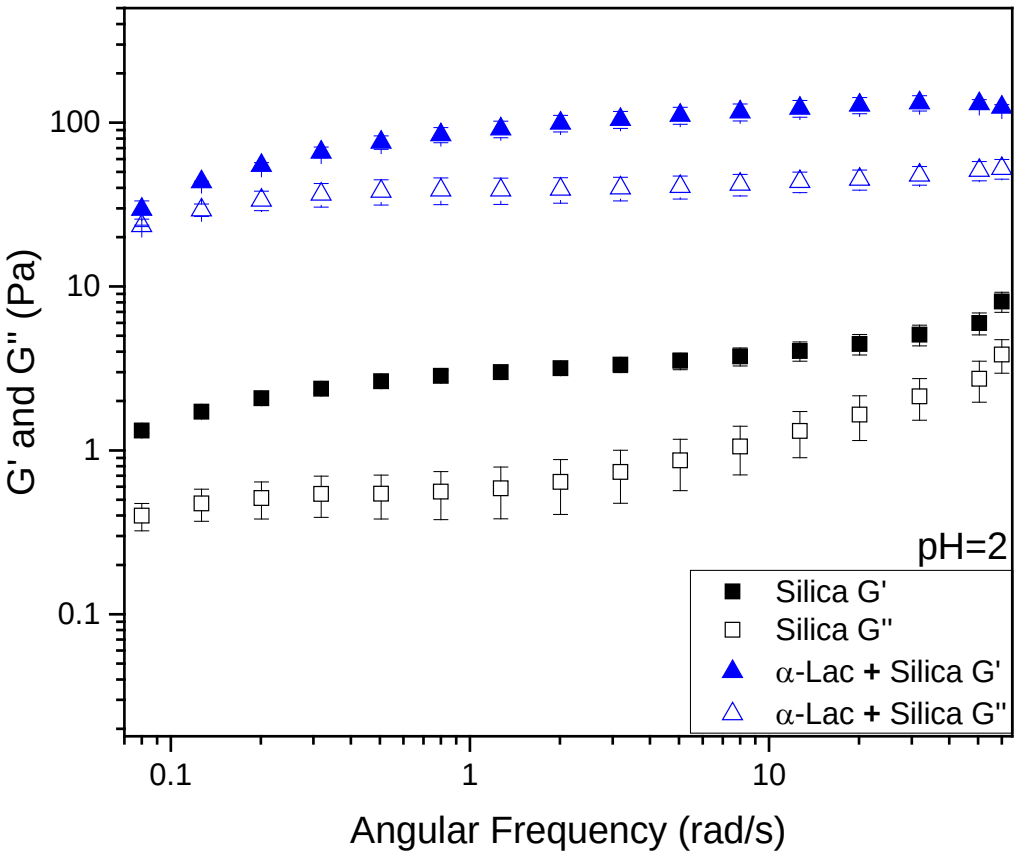

Figure 4-7 Viscoelasticity of Silica (5%) and Silica + a-Lactalbumin(5:0.5%) in 10 mM sodium acetate buffer at pH=2

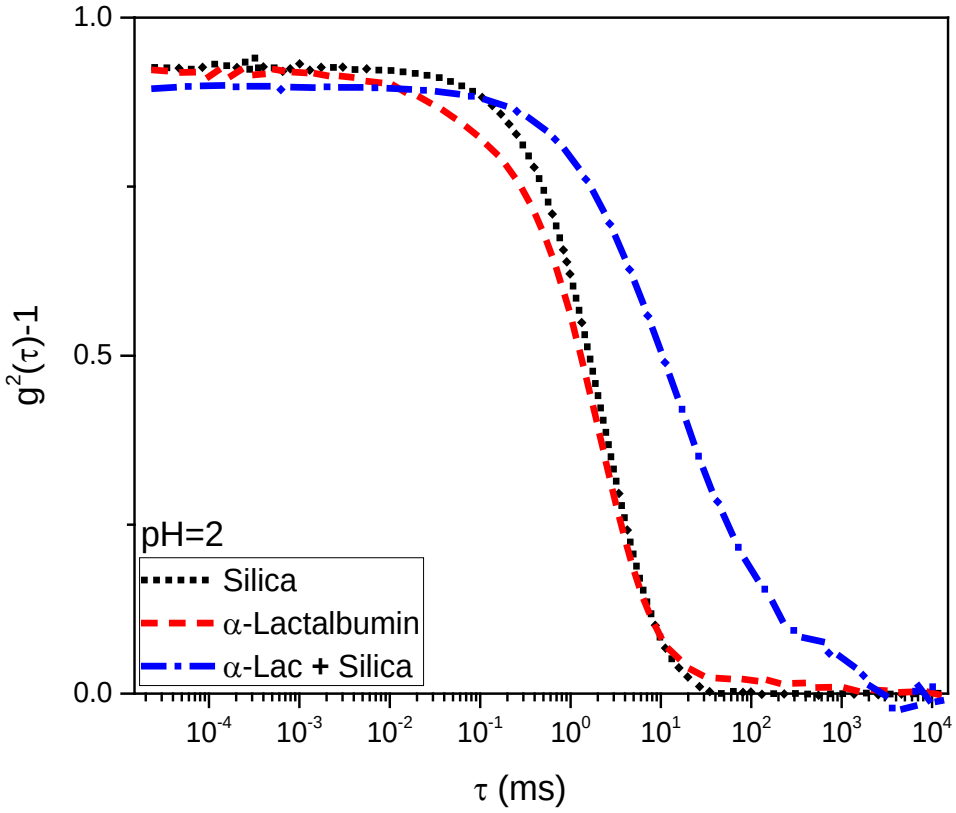

Figure 4-8 Correlogram of Silica (0.2%), a-Lactalbumin(0.02%) and Silica + a-Lactalbumin (0.2:0.02%) in 10 mM sodium acetate buffer at pH=2. . The ordinate is $g^2(t)-1$, where $g^2(t)$ denotes the second order intensity autocorrelation function and t is the lag time.Variability was less than 1% so error bars were not inluded in the plot in order to avoid effecting the clarity of the curves.

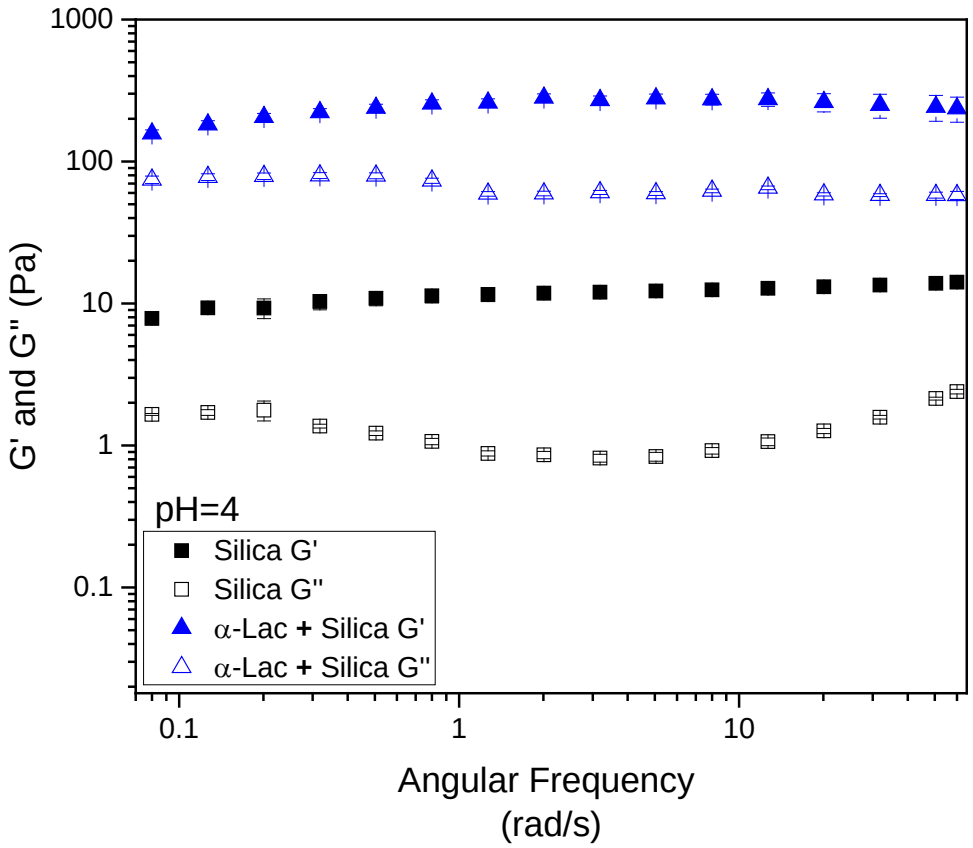

Figure 4-9 Viscoelasticity and viscosity of Silica (5%) and Silica + a-Lactalbumin(5:0.5%) in 10 mM sodium acetate buffer at pH=4

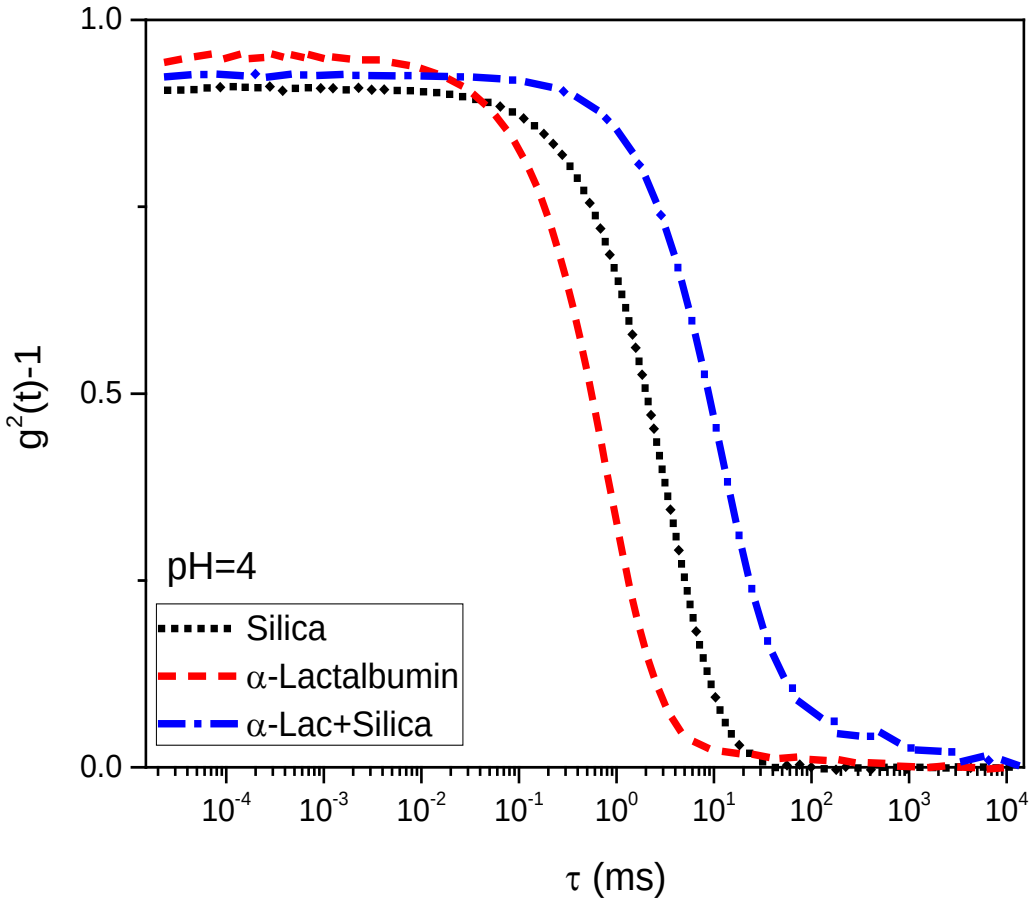

Figure 4-10 Correlogram of Silica (0.2%) and Silica + a-Lactalbumin(0.2:0.02%) in 10 mM sodium acetate buffer at pH=4. The ordinate is $g^2(t)-1$, where $g^2(t)$ denotes the second order intensity autocorrelation function and t is the lag time.Variability was less than 1% so error bars were not inluded in the plot in order to avoid effecting the clarity of the curves.

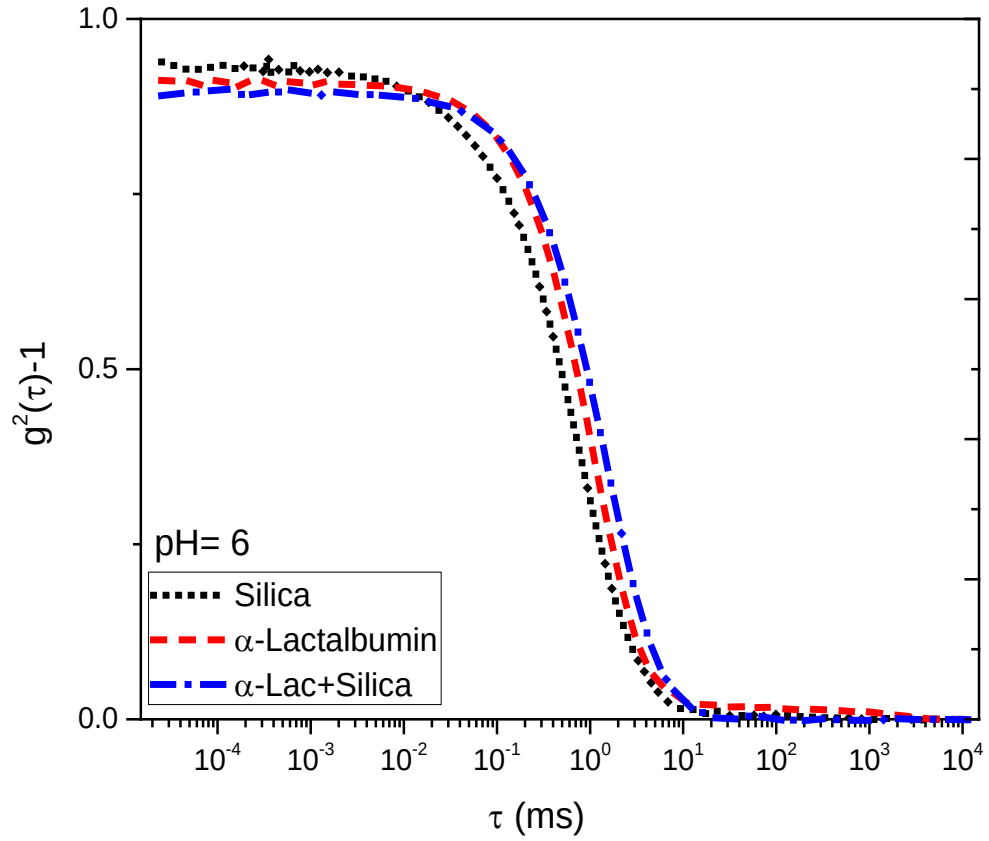

Figure 4-11 Correlogram of Silica (0.2%) and Silica + a-Lactalbumin(0.2:0.02%) in 10 mM sodium acetate buffer at pH=6. The ordinate is $g^2(t)-1$, where $g^2(t)$ denotes the second order intensity autocorrelation function and t is the lag time.Variability was less than 1% so error bars were not inluded in the plot in order to avoid effecting the clarity of the curves.

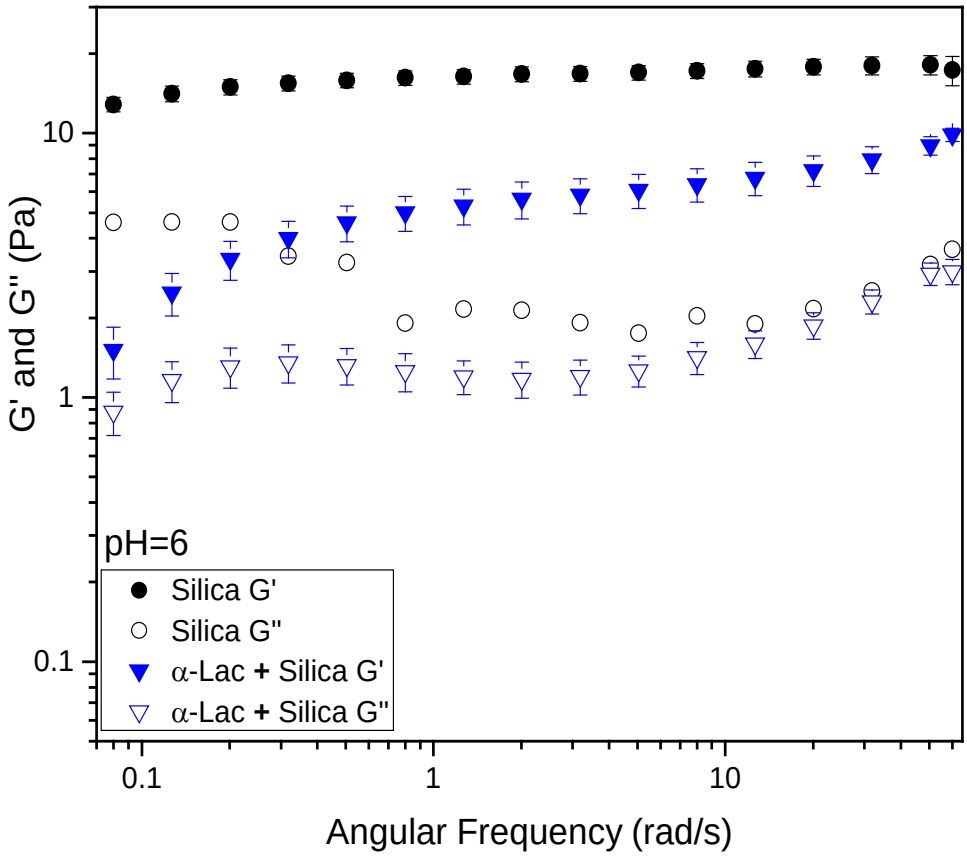

Figure 4-12 Viscoelasticity and viscosity of Silica (5%) and Silica+ a-Lactalbumin(5:0.5%) in 10 mM sodium acetate buffer at pH=6

Table 4-1Information on hydodynamic radius of the different systems studied.

	Γ (1/ms)	D ($\mu m^2/s$)	Polydispersity Parameter	Rh (Hydrodynamic Radius,nm)	Linear Regression Coefficient
pH 2 Silica	0.400^{a}	0.789^{a}	0.2326^{ab}	310.1685^{a}	0.9991
pH 2 Silica+ α-Lac	0.047^{b}	0.093^{b}	0.4627^{a}	2631.429^{b}	0.9731
pH 4 Silica	0.310^{c}	0.612^{c}	0.168^{ab}	399.874^{c}	0.999
pH 4 Silica+ α-Lac	0.074^{b}	0.146^{b}	0.2609^{ab}	1676.184^{b}	0.9993
pH 6 Silica	1.349^{d}	2.662^{d}	0.0907^{b}	91.93197^{d}	0.993
pH 6 Silica+ α-Lac	0.637^{e}	1.257^{e}	0.4085^{ab}	194.6881^{e}	0.9994

Means with the same letter are not significantly different (Tukey's Studentized Test (HSD), $P>0.05$)

CHAPTER 5. LYSOZYME ADSOPTION INDUCED BRIDGING FLOCCULATION: THE DOMINANT ENTROPIC PATHWAY OF NANO-BIO COMPLEXATION

5.1 Abstract

Lysozyme-silica interactions and complexation were investigated via adsorption isotherms, isothermal titration calorimetry (ITC), dynamic and electrophoretic light scattering and circular di-chroism (CD). Comparison of Langmuir and Hill adsorption models highlighted the significance of protein-protein interactions during the adsorption and multiple site binding model was adapted to describe the overall complexation events including protein-nanoparticle and protein-protein interactions. The complexation mechanism accounted for both enthalpic and entropic contributions and was supported by a number of experimental techniques performed using the same model system and under the same conditions (e.g. temperature, ionic strength, the concentration ratios, mixing time, equilibration time) for each technique. Even though each experimental method has its own limitations and modeling the binding is only feasible after a few assumptions, thermal footprints of lysozyme-silica complexation indicated two types of interactions. The first type of interaction has higher binding affinity, lower equilibrium stoichiometry and is driven by a higher entropic contribution compared to the second type. The bound protein undergoes a structural reorganization on the surface that further contributes to a favorable entropy gain. Zeta potential of silica- protein complex aggregates reaches

equilibrium at the concentration ratio that refers to the equilibrium of second type of interaction which is in agreement with the growth of flocs according to the measured hydrodynamic radius. Based on all these findings, it is proposed that lysozyme adsorption on nano-silica is a result of protein-nanoparticle and protein-protein interactions that further leads spontaneous, non-directional and random complexation of silica through bridging flocculation.

5.2 Introduction

Nanoparticle-protein interactions are at the heart of today's nanotechnology research [1-5, 7, 112]. Not only do they determine the biological response to nano-medical tools [6, 8, 113], but they also determine the functionality of all the non-medical nano-practices that interface nanoparticles with proteins[13]. Immobilization of enzymes, design of biosensors and nano-bio hybrid materials are examples of nano-practices that are not directly related to medicine[10, 11]. Among those, nano-bio hybridization with proteins can be defined as a spontaneous complexation process in which specific and weak interactions between proteins and nanoparticles triggers the bottom up self-assembly of organic and inorganic components into two-dimensional networks and three dimensional structures ([12, 14, 15]). Functional properties of the those networks and structures depend on at least the surface characteristics [114], size[88] and shape[115] of the nanoparticles, supra-chemical reactivity [116, 117] and internal structure rigidity [118]of biopolymers, the physicochemical characteristics of the surrounding solvent [119, 120] and the nanoparticles/biopolymer concentration ratio[88, 114, 116-118, 120]. Despite the fact that the wide range window of the parameters

offers increased functional diversity, this makes complexation mechanism too sophisticated that we are still far away to offer design strategies to produce nano-bio complexes with targeted functional properties[3]. This gap most probably stems from the lack of understanding of universal principles that are involved in the nano-bio complexation “chaos”.

The current study was stimulated to initiate a central curiosity about the thermodynamic details of a “spontaneous” complexation process. In order to be able to focus more on the mechanism of the complexation, rather than system component characterization, complexation of lysozyme with hydrophilic silica was chosen as a model system.

The rationale behind the model system selection can be summarized as follow: 1) structure, size, shape and surface characteristics of each component is well-documented [71, 121, 122] 2) interactions of lysozyme with silica was already extensively studied with different approaches which is expected to complement the thermodynamic approach[123-127] utilized in this work 3) both component are abundant, inexpensive and preparation of samples for experiments does not require specific expertise and longtime purification procedures.

The model system interactions were investigated via adsorption isotherms, isothermal titration calorimetry (ITC), dynamic and electrophoretic light scattering and circular di-chroism (CD). Langmuir and Hill models were compared to quantitatively assess the adsorption of the protein on the nano-particles and a complexation mechanism that accounts for both enthalpic and entropic contributions was adapted to model overall all heat of binding which is measured directly with ITC.

The model system was verified to be a good selection to show the case of the well-known complexity of interactions governing nanoparticle-protein complexation. Even though we are still far away from drawing a general mechanism for bio-nano complexation, it is shown that the thermodynamic nature of interactions deserves further attention. As more studies conducted with different model systems, under different conditions with a similar approach; mechanism of interactions at the nano-bio interface will be understood better. Finally a better fundamental understanding will lead more specific applications that use or include proteins and nanoparticles either as disordered fractal like microstructures[(128)]or highly ordered crystals[(15)]. .

5.3 Experimental

Silica nanoparticles (Ludox-TM50) used in the study were kindly donated by Grace& Co.-Conn (MD, USA). Chicken egg white lysozyme (L6876) is purchased from Sigma-Aldrich (MO, USA). Both protein and silica solutions/suspensions were prepared in sodium phosphate buffer (pH=7.4) at various concentrations to obtain Lysozyme/Silica molar ratios ranging from 5 to 200. All the experiments were conducted in a similar manner and mimic the ITC method; complexation was assumed to reach equilibrium in 5 minutes after each injection corresponding to the particular molar ratio. All the experiments were conducted at room temperature and in triplicate.

To obtain the adsorption isotherms: Norde's depletion method[(129)] was followed with slight modifications: 1) Unbound protein concentration was determined with the BCA assay according to the manufacturer's protocol (Thermo Scientific,

IL,USA). 2) Silica suspensions with the same concentration were titrated with protein solutions in a similar manner than the ITC technique.

Dynamic Light Scattering on a light scattering goniometer (ALV/CGS-3 Compact Goniometer, ALV, Langen, Germany) was measured using 10 mm diameter glass tubes and illuminated with a HeNe laser (wavelength is 632.8 nm, output power is 22 mW). Scattered light was detected with dual ALV-High QE APD (avalanche photo diode) photon detectors in Pseudo-Cross-Correlation Mode at an angle of 90° for 120 seconds. The cumulant method was used to determine the mean hydrodynamic radius (Rh) of the lysozyme-silica complexes[(49)].

Electrophoretic mobility at 25 °C was determined in disposable folded capillary cells (DTS1070, Malvern, Worcestershire, UK) with a zeta-sizer that combines laser Doppler velocimetry and phase analysis light scattering (Zeta-sizer Nano ZS, Malvern, Worcestershire, UK). Electrophoretic mobility (U_E) was converted to zeta potential (z) using Henry Equation, ($U_E = 2\varepsilon z f(ka)/3\mu$)) along the Smoluchowski approximation ($f(ka) = 1.5$), where ε and μ are the dielectric constant and the viscosity of the continuous phase and were assumed to be 78.and 0.89 cP, respectively. The scattering angle was 173° and refractive index of silica and protein was assumed as 1.33 and 1.45, respectively[(92)]. The protein's refractive index was used for silica-protein mixtures.

CD spectrum was collected between 260-185 nm with a Jasco J-1500 CD spectrometer equipped with a temperature controller. The bandwidth was 1nm and scanning speed was 50 nm/min. Collected spectra in mdeg was converted to mean

residual ellipticity[130] and deconvolution was performed with DichroWeb online server using CDSSTR algorithm and the reference data set 3[131, 132].

Isothermal titration calorimetry was carried out with a Nano ITC calorimeter (TA Instruments, DE, USA). The reference cell was filled with water, whereas reaction cell filled with silica suspensions. Protein solution in syringe was injected to the reactions cell with an interval of 300 sec at a stirring speed of 350 rpm until saturation (if necessary, a second syringe was injected after the first load). All the blank experiments (heat of dilution, heat of injection, heat of mixing) were conducted under the same conditions[133]. Heat profile was fitted with multiple site model to obtain the thermodynamic parameters.

5.4 Results

5.4.1 Protein Adsorption

Different types of adsorption isotherms were constructed by plotting the surface coverage (Γ) versus equilibrium protein concentration (Ceq), the adsorbed protein mass versus Ceq, the surface coverage fraction (Γ/Γ_{max}) versus mole ratio (lysozyme/silica) and Ceq vs mole ratio (Figure 5.1 A-D). Figure 1A is the most traditional way to depict the characteristics of polymer adsorption on solid surfaces, and under specific assumptions (summarized below in the discussion section) the thermodynamic equilibrium constant of the protein surface interactions could be calculated by using the Langmuir model given below:

$$\Gamma = \frac{\Gamma_{\max} C_{eq}}{K_{app} + C_{eq}} \tag{5.1}$$

Where Γ is the surface coverage (mg/m^2), Γ_{max} is the maximum surface coverage (mg/m^2), C_{eq} is the equilibrium protein concentration (mg/mL) and K_{app} is the apparent dissociation constant (mg/mL).

By fitting the experimental data with the Langmuir model the maximum surface coverage Γ_{max} is calculated as 1.54 mg/m^2. It could be noted that even without using any assumption or fitting model the experimental data shows that the adsorption isotherm reaches a plateau around 1.3 mg/m^2 (Figure 5.1 A). This is in agreement with previously reported maximum surface coverage of lysozyme on hydrophilic silica at neutral pH and low ionic strength and this well-defined plateau corresponds to full coverage of the surface [(129)]. Also the initial steep of the isotherm reflects the high binding affinity of lysozyme on oppositely charged hydrophilic silica which is quite reasonable for a globular, structurally stable protein[(77)].

Also it is important to mention that the current procedure used for the batch depletion method is slightly different than Norde's method[(129)] because it was designed with the purpose of mimicking the adsorption process that occurs during an isothermal titration calorimetry (ITC) experiment. Usually, in the batch depletion method, a constant adsorbent surface is exposed to protein solutions of varying concentrations to provide a spectrum of surface coverages as a function of free protein concentration in the mixtures (Ceq). Also to ensure the equilibrium/ steady state adsorption the adsorbent and adsorbate are incubated under mild rotation for usually 16 hours. Conversely in the ITC test a concentrated protein solution is titrated into the silica suspension as small aliquots of volume and equilibrium time between injections and total experiment time are shorter compared to batch depletion method.

In order to test any potential discrepancy that could result from the difference in equilibrium time between traditional depletion method and ITC, the depletion method was conducted in both ways; first using the timeframe of ITC and second extending the equilibrium time to 16 hours. The “ITC mimic” depletion method and traditional depletion method did not show any significant differences and were quite in line with Norde’s isotherm results. So the two conclusions from this particular experiment were: (1) Using constant volumes of protein solutions with varying concentrations or adding more volume of protein solution with the same concentration does not affect the isotherm plateau as long as the mass balance is conducted in a careful manner and (2) lysozyme adsorption on hydrophilic silica reaches to an equilibrium within the timeframe of the experiments that are conducted in ITC.

5.4.2 Protein Adsorption Induced Silica Flocculation

The zeta potential (ζ) and hydrodynamic radius [(87)] of lysozyme-silica complexes were determined for various molar ratios to track the electrostatic interactions driving the complex formation and to roughly quantify the size of formed complexes, respectively (Figure 5.2 A and Figure 5.2 B).

Protein adsorption modifies the silica surface charge dramatically even at low protein loadings, followed by the charge neutralization (at a molar ratio between 18.8 and 23.5) and charge is reversed until the charge of complex is equal to that of native free lysozyme (10mV). Charge neutralization and reversal is a quite expected outcome of the electrostatic interactions between oppositely charged surfaces [(134)].

The other consequence of lysozyme adsorption on hydrophilic silica is bridging flocculation [87, 88, 120]. Even at the very low protein loading (molar ratio=4.7, ζ=-33.2), hydrodynamic radius of lysozyme-silica complex (469 nm) is much larger than that of silica (20 nm) and lysozyme (2 nm) indicating the formation of a silica aggregate linked via adsorbed lysozyme (Figure 5.2 B). At higher protein loadings aggregate size exceeds 2 μm which is similar to the aggregate size of silica/lysozyme flocculate that is determined by the sedimentation velocity technique[87].

5.4.3 Protein Denaturation upon Adsorption

CD spectra of native lysozyme and silica-lysozyme mixtures at 2 different molar ratios (lysozyme/silica=47.2 and lysozyme/silica=94.3) were collected. Control refers to the native protein in buffer without any silica (Figure 5.3 A). It is important to note that while converting the CD raw signal (millidegrees) to mean residual ellipticity (MRE), initial protein concentration (bound plus free) of silica-lysozyme mixtures was used in order to obtain the total conformational change in the whole system that is composed of bound and free protein. The focus was not to isolate the CD signal of the adsorbed state or determine the surface coverage dependent structural changes since those aspects have been already reported in great detail[135].

According to BCA assay, at a MR =47.2, almost 90% of the total protein in the system is bound to silica nanoparticles. At this molar concentration CD signal is mostly coming from the bound protein since free protein concentration (Ceq=0.05) is very low for the provided relatively small path length (0.01 cm). On the other hand, at

MR=100, bound protein accounts for the 50% of the total protein in the system which refers to the equilibrium stoichiometry.

Perturbation of the secondary structure upon binding is clear from the changes in the CD spectra even without further de-convolution. If not, CD spectra should have overlapped once plotted in MRE unit. Upon adsorption, magnitudes of the negative peaks at 222 nm and 208 nm as well as the magnitude of the positive peak at 193nm decreased. Also, negative peak shifted towards to 218 nm and positive peak shifts towards to 195 nm. This clearly indicates a decrease in the alpha-helix conformation and an increase in beta-sheet and random coil conformation, which is in agreement with earlier reports examining lysozyme structural changes upon adsorption on solid surfaces [83, 86, 129, 135-137].

To further understand the changes in the protein CD spectra upon adsorption on the silica surface, fractions of secondary structure components were calculated by deconvolution of the CD spectra. According to the deconvolution of CD spectra, native lysozyme has a conformation composing 33.7 % helix, 18.7 % sheet, 22.5% turn and 25.7% unordered structures which is generally in a general agreement with the secondary structure fractions of lysozyme reported from X-Ray data [138] (helix:0.39, sheet:0.11, turn:0.34 and unordered:0.16), ATR/FTIR[137] (helix:0.40, sheet:0.07, turn:0.4 and unordered: 0.13) and CD in phosphate buffer[130] (helix:0.34 sheet:0.17 turn:0.23 unordered:0.26). To compare the secondary structure components of native protein and bound protein at different molar ratios, the three situations described above are plotted together (Figure 5.3 B).

According to the deconvolution results, the structure of lysozyme is perturbed significantly upon adsorption (18% loss in the helical structure, 14 % gain in the sheets and 4% gain in the random coil). The extent of the conformational changes is quite comparable with earlier reports that investigated the perturbation of lysozyme on similar hydrophilic silica particles at neutral pH (20-32 % loss in the helical structure [83, 135], 14% gain in the sheets and 6% gain in the random coil [135])

5.4.4 Thermal Footprints of Adsorption Induced Flocculation

The thermodynamic nature of the interactions between lysozyme and silica were further investigated using isothermal titration calorimetry (ITC) in order to resolve the contributions of the driving forces that possibly dominate the complex formation. As lysozyme is titrated into the calorimeter sample cell that contains silica, the heat change in the sample cell is compensated by the applied power to maintain the thermal equilibrium with the reference cell. If the heat is released, the sample cell would require less power input (negative signal), whereas absorption of heat would require more power input (positive signal). Observed negative signal through the entire range of titration reflects the overall exothermic nature of the all interactions among the system components: protein, nanoparticle and solvent (Figure 5.4 A). Raw data peaks were (1) integrated with respect to time, (2) corrected for the heat of dilution, heat of injection and heat of mixing, (3) normalized with respect to molarity of titrant to obtain the molar enthalpy of the interactions (Figure 5.4 B). To further quantify the association constant (K_a), enthalpy change (ΔH) and stoichiometry (n)

from the heat profile, curve-fitting analysis was performed. Gibbs free energy change (ΔG) and entropy change (ΔS) were calculated via:

$$\Delta G = -RT \ln K_a \tag{5.2}$$

$$\Delta G = \Delta H - T\Delta S \tag{5.3}$$

Thermodynamic parameters of nanoparticle-protein interactions (K_a, n, ΔH, ΔG, ΔS) obtained from the experimental data are summarized in Table 1.

According to curve fitting analysis the nanoparticle-protein complexation features two distinct binding processes with significantly different affinities, stoichiometry's and enthalpies. The first site binds with larger affinity and enthalpy whereas the second site binds with weaker affinity and larger stoichiometry/population of sites that results in a weaker enthalpy per molecule. Even though both binding modes feature favorable enthalpic changes (ΔH<0), and entropic changes (ΔS>0), favorable entropic contribution is less pronounced in the second binding mode.

Observation of two discrete binding events is quite rare among titration calorimetry studies. Nevertheless, there are a few influential works that successfully resolved the binding curve for two binding modes [(139-141)]. Also in one of those studies, a detailed protein-nanoparticle complexation mechanism that accounts for both non-covalent complex formation and solvent reorganization was proposed[(140)]. De's mechanism is adapted to the current contribution in order to draw the whole thermodynamic picture behind the lysozyme interactions with hydrophilic silica.

According to De's mechanism, the complexation of nanoparticles with proteins could be exothermic or endothermic depending the nature of interactions

driving the complex formation. As long as favorable enthalpy contribution ($\Delta H<0$, exothermic) is not offset by the unfavorable entropy loss ($\Delta S<0$) or unfavorable enthalpy contribution ($\Delta H>0$, endothermic) is compensated by the favorable entropy gain ($\Delta S>0$), free energy of the process (ΔG) will be negative. Negative free energy change is the thermodynamic requirement for a process to occur spontaneously.

Based on this, the overall lysozyme-silica complexation process (reaction 3) could be described as a combination of non-covalent complex formation (reaction 1) and solvent reorganization (reaction 2).

Lysozyme + Silica ⇋ Lysozyme-Silica $\Delta H<0$ and $\Delta S<0$ (1)

xH_2O**lys** + yH_2O**si** ⇋ $(x+y-z)H_2O$**lys-si** + zH_2O $\Delta H>0$ and $\Delta S>0$ (2)

Lyzozyme·xH_2O**lys** + Silica· yH_2O**si** ⇋ Lysozyme-Silica·(x+y-z) H2Olys-**si** + zH_2O (3)

Whereas H_2O**lys**, H_2O**si**, H_2O**lys-si** are water molecules bound to lysozyme, silica and lysozyme-silica complexes, respectively.

In Process 1, formation of non-covalent bonds are favorable and could compensate the loss of conformational entropy due to complex formation[(139)]. In Process 2 energy is required for disruption of the bound water at the nanoparticle-protein interface ($\Delta H>0$), but the increasing conformational entropy of water ($\Delta S>0$) due to the release of highly ordered solvent from interface to bulk could compensate the unfavorable enthalpy contribution. So the enthalpy and entropy in process 3 would be a sum of those contributions.

So it is clear that in each binding mode the contribution of those processes weight differently. For the first binding mode increase in entropy is the dominating

driving force for the complexation and for the second mode complexation is driven by a moderate favorable enthalpy and a moderate favorable entropy contribution (Figure 5.5).

5.5 Discussion

5.5.1 Non-Direct Methods to evaluate Mechanism of Protein Adsorption

When a small gas molecule approaches to a solid interface, only two things might happen: adsorption on or desorption from the surface. On the other hand, when a protein molecule approaches to a solid surface, protein might undergo structural arrangements, interact with each other, change the surface affinity depending the surface coverage, form multiple layers all of which complicates the adsorption and desorption process. In this respect, groups that have and currently study protein adsorption on surfaces widely accept the Langmuir model and hypotheses that allow the development of this model. The Langmuir adsorption theory and model has been developed for gases and could serve only as a starting point to model the complicated protein adsorption behavior [76, 77, 142, 143] . Thus, in order to characterize the mechanistic details of the protein adsorption process, high resolution real time kinetic experimental data should be described with advance mathematical models that account for all the violations to the hypotheses used to develop the Langmuir theory[143]. Alternatively, thermodynamic models can reveal the energetic aspects of the adsorption process and can be applied by using final equilibrium state concentrations and surface coverages to calculate equilibrium constants and the associated thermodynamic properties, notably the Gibbs Free Energy.

In the current contribution, Langmuir model was used as a starting point to set the stage for the forthcoming discussion on the thermodynamic model that is obtained from ITC data analysis. Results showed that it is important to lower expectations from the Langmuir model by considering the fact that lysozyme changes its native conformation upon adsorption on the silica surface (Figure 5.3). In addition unfolded protein might favor lateral interactions[(135)] and protein bridging (silica-lysozyme-silica) might occur through a single lysozyme molecule, also multiple lysozyme bridges (silica-(lysozyme)$_n$-silica).

The Langmuir model predicted a maximum surface coverage of 1.5 mg/m^2 and an equilibrium dissociation constant of 0.038 mg/mL. Predicted maximum surface coverage is between the experimental saturation (1.3 mg/m^2) and calculated theoretical value based on monolayer coverage (1.7 mg/m^2). In addition to Langmuir, the same adsorption data was successfully modeled with the Hill equation ($\Gamma = \frac{\Gamma_{\max} C_{eq}^n}{K_d + C_{eq}^n}$) as well. Hill equation predicted the cooperativity term (n) as 2.1, which was assumed to be 1 in Langmuir (Langmuir is a special case of Hill model, and assumes no-cooperativity). Incorporating the cooperativity term improves the fitting of the data, which is further supporting the non-Langmuir like behavior of the adsorption isotherm of lysozyme on silica. Shift in the binding site properties with surface cioverage implies lateral protein-protein interactions Predicted surface coverage was more accurate (1.3 mg/m^2) and equilibrium dissociation constant (K_{app}=0.00045 mg/mL) was significantly different than that obtained from the Langmuir model.

Based on the experimental surface coverage and contradicting equilibrium constants, it could be assumed that the adsorption of lysozyme on silica could be explained by at least three “possible” scenarios: 1) Projected cross sectional area of an unfolded protein might be slightly larger than that of the folded native one. If this were the case, the silica surface would be covered with less protein. That would support the slight discrepancy between the predictions and the observations. 2) At least two silica particles are bridged by the same single protein through two binding sites. If this were the case, available surface for adsorption would be dynamically decreasing and the saturation would occur at a lower protein loading than predicted. 3) Centrifugal forces applied to separate the free protein during the non-direct adsorption technique, detach some of the bound protein on the silica as well. If this were the case, detached proteins would be assumed to be weakly bound compared to the ones resisting centrifugal forces.

Equilibrium constants that are predicted via Langmuir or Hill models were further compared with the ones that are obtained from ITC in the following section.

5.5.2 ITC directly provides More Details on the Mechanism of Protein Adsorption and Resulting Bridging Flocculation

The most important objective of the current contribution was to investigate the thermodynamic nature of the complex formation between silica and protein (lysozyme) in which protein adsorption plays a key role by inducing bridging flocculation. In this context, the thermodynamic nature of the complex formation was

further investigated by directly measuring the heat of interactions with isothermal titration calorimetry (ITC).

The most impressive outcome of the ITC results was the consistent (see the ITC master curve in Graphical Abstract) bimodal characteristic of the heat profile (Figure 5.4 B) that cannot be simply attributed to only one type of lysozyme-silica interaction. Considering the fact lysozyme-silica complexation would occur through two sub-processes, results show that it is possible to conclude that each sub-process weighted differently in each interaction mode and thus there were two distinct heats (or enthalpies in this case due to constant pressure and volume) associated with interactions leading to complexation.

Further analysis of the thermodynamic signature associated to the complexation process requires to assume a binding model for complexation and obtain the equilibrium constant from the known total concentrations of lysozyme and silica since the heat associated to binding is proportional to the change in the concentration of the bound lysozyme through each injection. By using two sets of independent binding sites model, it was possible to discriminate the free energy of the interactions into its enthalpy and entropy components by using the apparent association/dissociation constants. Even though the measured heat is the cumulative heat of all simultaneous binding interactions including the silica flocculation, since as demonstrated this is promoted by lysozyme bridging, it would not be unreasonable to propose that lysozyme binds to silica at least by two distinct modes.

The higher affinity binding mode seems to be resulting from the direct interactions of lysozyme with silica at low surface coverage’s that leads the most

important portion of silica flocculation (see the initial jump in figure 5.2 B). Higher calculated positive entropy changes supports the assumption of significant disruption of the structurally organized water at the silica surface. Release of the bound water to the bulk or reorganization to a more disordered state at the silica-lysozyme interface is the most possible explanation behind the favorable entropic contribution that compensates unfavorable entropic contribution due to the restriction of the protein in between the silica particles. It is also important to remember that the partial transition in the secondary structure of protein from helical to sheets and random coil (Figure 3 B) might be also contributing to the favorable entropy.

The lower affinity binding mode observed at higher surface coverages seems to be resulting from an additional protein-protein interaction to the already existing protein-silica interactions. Lower positive entropy supports the less pronounced effect of the water reorganization on the silica surface or at the binding interface. It is not very clear whether the pure protein-protein interactions on the silica surface are favorable or not due to complexity brought by the conformational change, but incorporation of protein-protein interactions significantly decreases the affinity of binding.

It is already mentioned that, since complexation includes both protein adsorption and silica flocculation simultaneously, the equilibrium constants and the free energy and entropy obtained from these values are apparent parameters and absolute numbers should be evaluated carefully. However it is quite interesting to observe that the high affinity binding dissociation constant has the same order of magnitude as the one obtained from Hill equation ($3.15x10^{-8}$) and the low affinity

binding dissociation constant has the same order of magnitude as the one obtained from the Langmuir model ($2.65x10^{-6}$). This gives us enough confidence to assume a binding mechanism (multiple binding site model) and resolve the affinity of the lysozyme binding on hydrophilic nano-silica.

Definitely, stoichiometry constants (*n*) that are obtained via multiple binding site model would have been more meaningful without the messed up molarity of silica due to random flocculation. However, with the numbers in hand, it seems like the high affinity binding mode is saturated with less protein compared to the low affinity binding mode.

5.6 Conclusion

Thermodynamic details of protein-nanoparticle interactions and complexation were studied with a well-defined model system (lysozyme-silica). Interactions governing protein nanoparticle complexation is concluded to be complex yet resolvable with a multi-experimental approach. Electrostatically initiated protein adsorption plays the key-role in complexation by inducing the bridging flocculation. According to ITC data analysis complexation shows a bimodal character due to two distinct binding modes. Higher affinity binding mode that is driven by a larger entropic contribution is followed by the low affinity binding mode that is a consequence of moderate enthalpy and entopic contributions. Higher affinity mode requires less protein to reach equilibrium and is seen at lower surface coverages. Solvent re-organization plays the most important role in the complexation process by contributing the favorable entropy gain. In addition to solvent reorganization, changes in the secondary structure of lysozyme upon adsorption might be contributing to the

favorable entropy gain. The dominant entropic pathway of complexation, showed the case that the assembly of the supra colloidal micro-structures by using nanoparticles and biopolymers as building blocks might not be limited by unfavorable enthalpic restrictions.

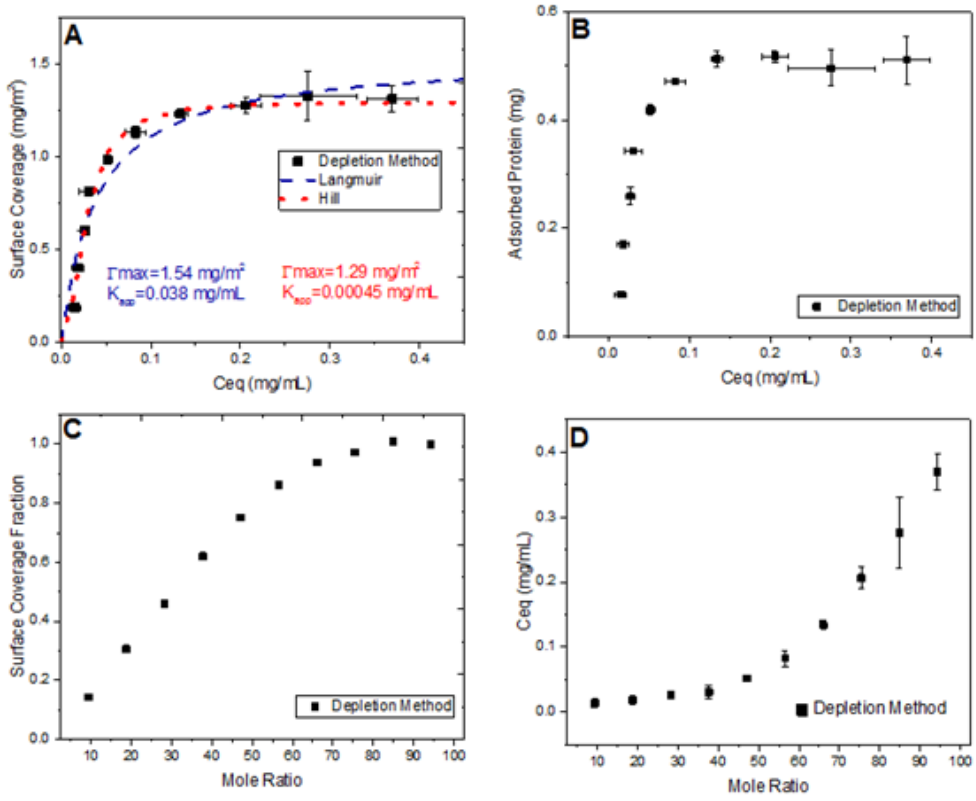

Figure 5-1 Adsorption isotherms: Squares and brackets represent mean and standard error of the mean (n=6, triplicate short equilibrium times, triplicate 16 hours equilibrium), respectively. Blue and red lines in A represents the predicted adsorption isotherms via Langmuir and Hill models, respectively. B represent the raw adoption data before normalizing the adsorbed amount with respect to surface area. Surface coverage fraction in C was calculated by normalizing the surface coverage with respect to the maximum experimental surface coverage. Molar ratio in D is the ratio of the total protein molarity to the theoretical total molarity of silica.

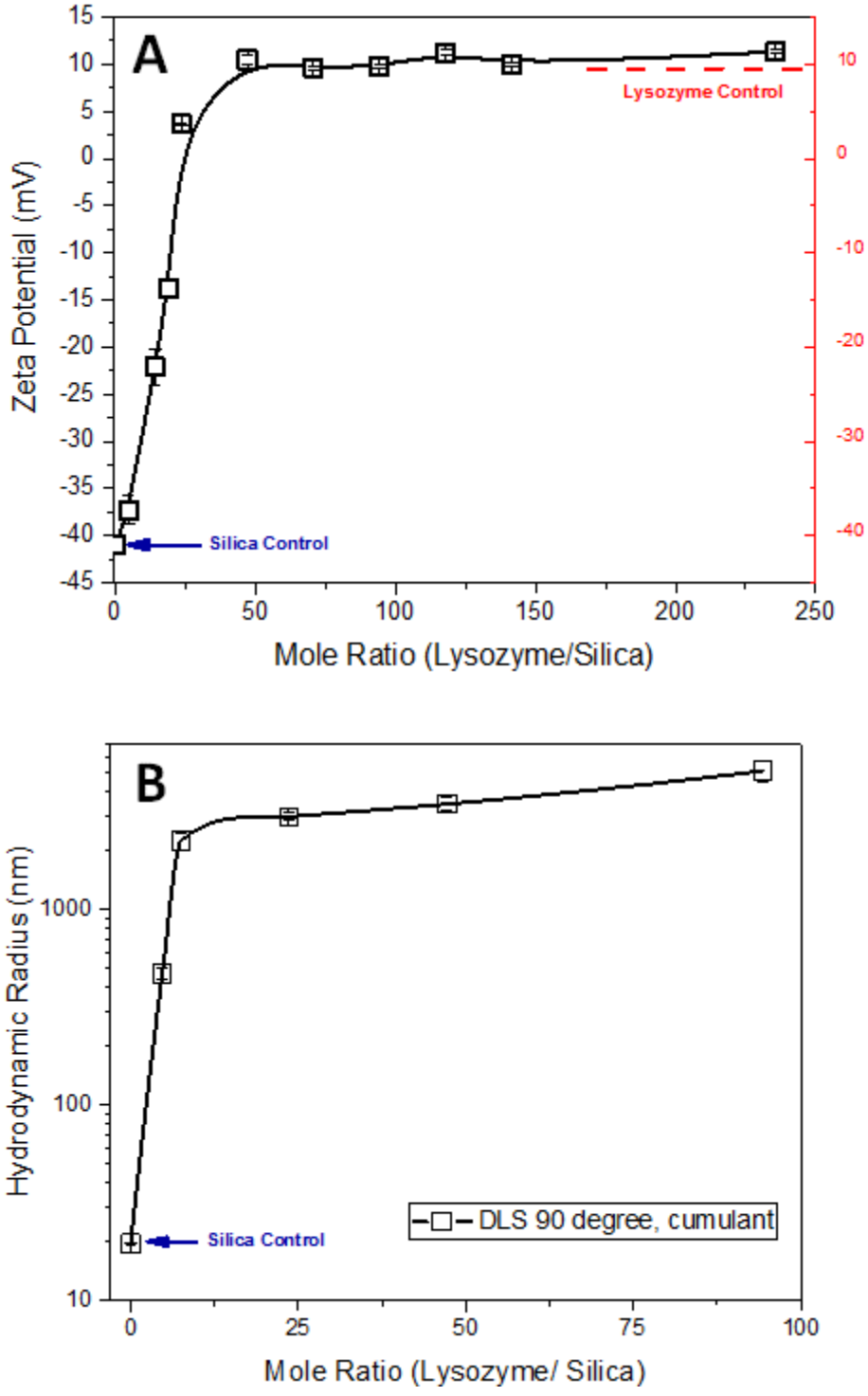

Figure 5-2 Light Scattering results. 2A. Zeta Potential of lysozyme-silica complexes. Charge of silica particles before any protein incorporation (Mole Ratio=0) is marked with a blue arrow. Second y-axis (red) represents the charge scale for lysozyme. 2B. Hydrodynamic radius of lysozyme-silica complex. Radius of silica particles before any protein incorporation (Mole Ratio=0) is marked with a blue arrow.

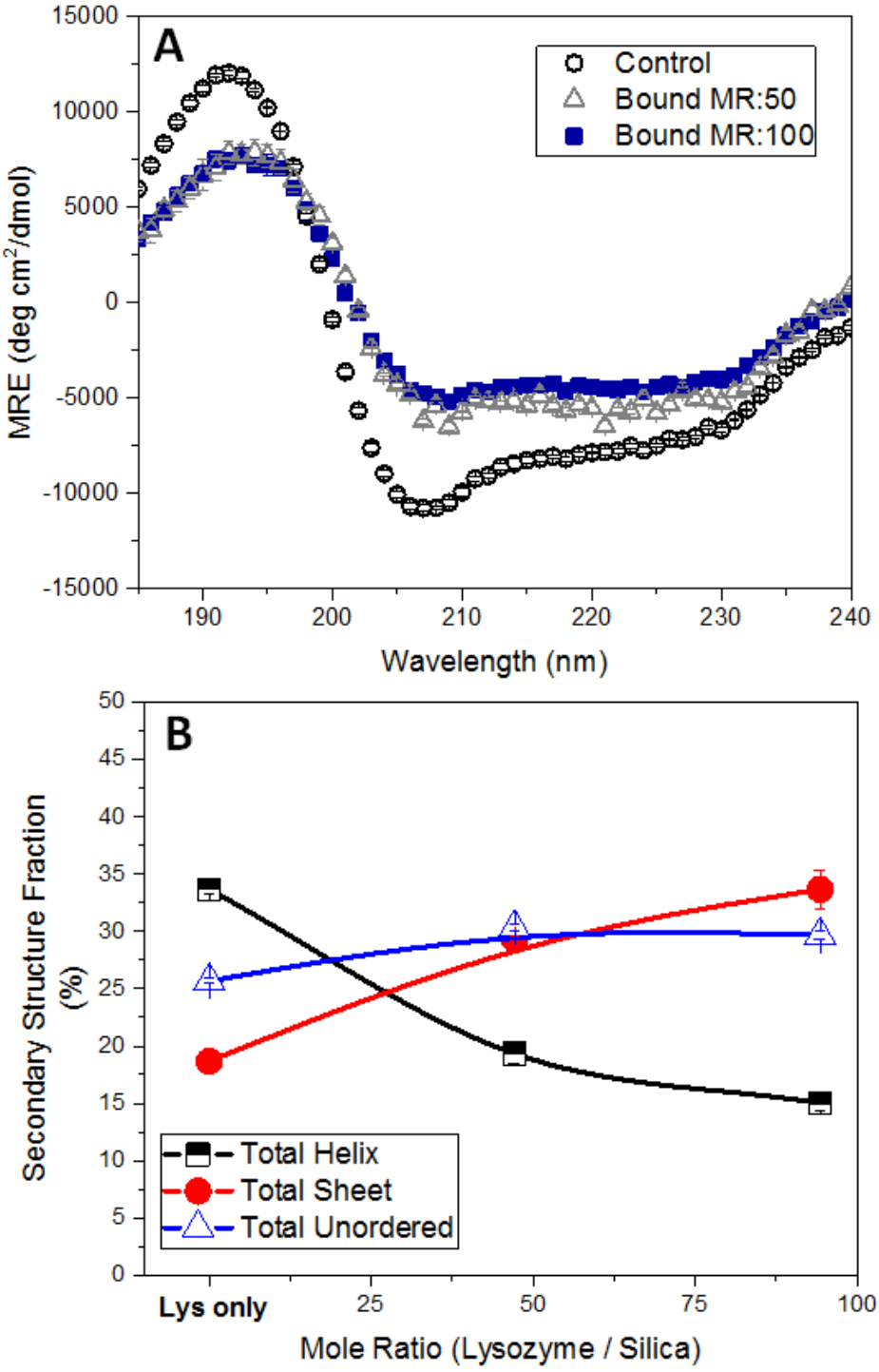

Figure 5-3 Circular Dichroism. 3A. CD spectra of control and bound proteins. MRE stands for mean residue ellipticity. 3B. Deconvolution of CD spectra enable to determine the fractions of secondary structure as helix, sheet and turn.

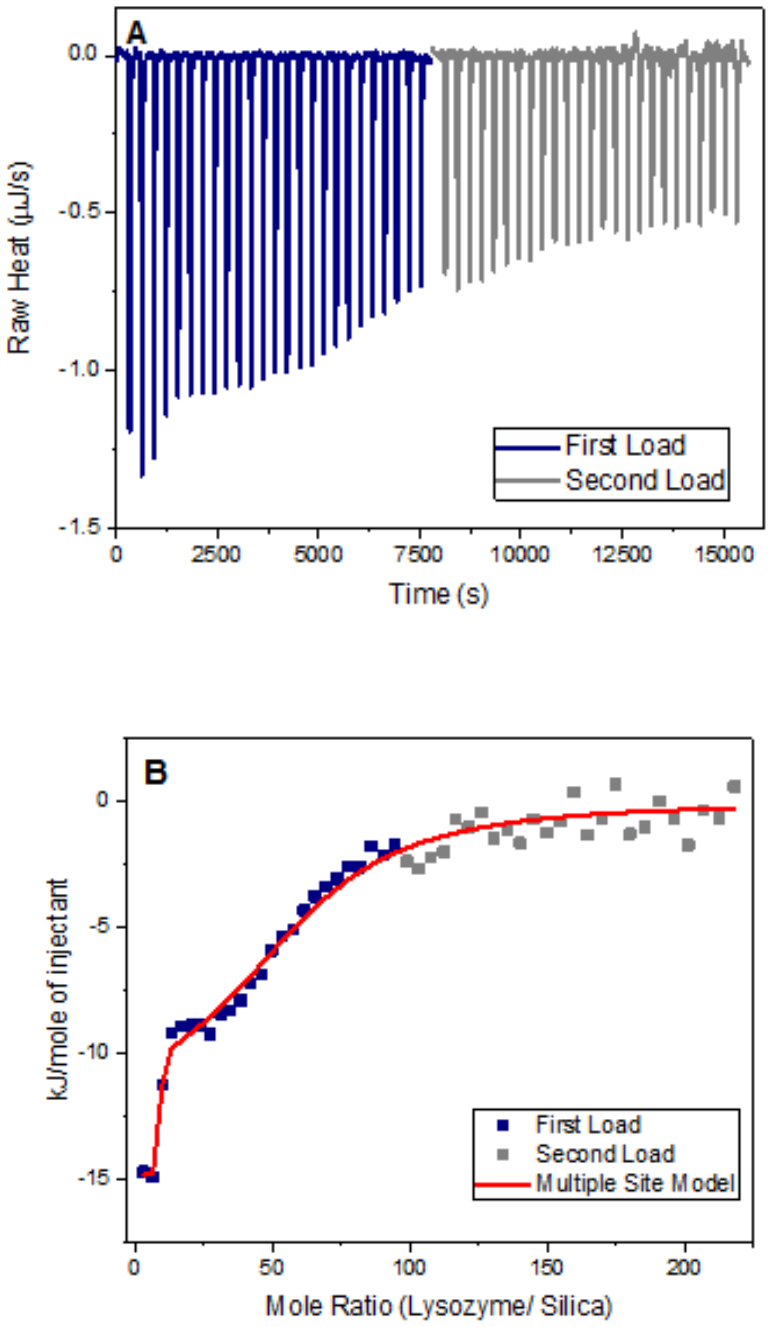

Figure 5-4 ITC 4A. ITC raw data before integration: After the "first load", syringe re-filled with the same protein solution and injected to the cell that includes the silica and lysozyme to collect the "second load" heats. 4B. Integrated peaks after normalization with respect to mole of injectant: After integrating the peaks of raw data with respect to time, obtained heats were normalized with respect to initial protein molarity. Red line represents the heat profile predicted with the multiple site model.

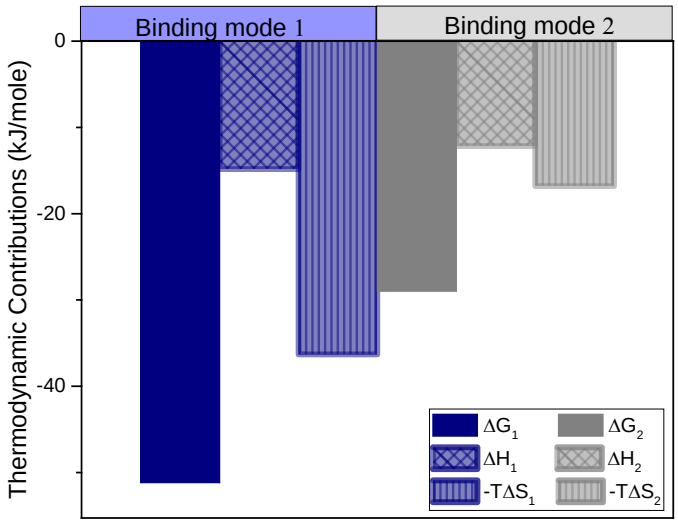

Figure 5-5ITC thermodynamic signature. ΔH is measured directly with ITC, ΔG and ΔS were calculated based on the equilibrium constant as explained in the text. T is the test temperature, which is 298.15K in this case

Table 5-1ITC Apparent binding parameters

ITC Parameter	Site 1	Site 2
K_a (M^{-1})	4.65E+08	3.2E+05
K_d (M)	2.15E-09	8.40E-06
n	7.549	54.72
ΔH (kJ/mol)	-14.84	-12.16
ΔS (J/mol.K)	122	56.4
ΔG (kJ/mol)	-51.15	-28.96

CHAPTER 6. SUMMARY AND OUTLOOK

The main objective of the current PhD research was to develop a design paradigm to engage nano-bio hybridization/complexation into the macro-structure/rheology manipulation with the aim of developing new and functional biomaterials. Specifically, supra-colloidal assembly of disordered fractal microstructures was studied with two complementary approaches.

First, rheological attributes of bio-polymer nanoparticle interactions were investigated with dynamic light scattering and rheology. Concentrated nano-structured suspensions of silica and α-lactalbumin were formed under different electrostatic conditions by changing the suspension pH. Electrostatic interactions were shown to significantly affect the rheological characteristics of the suspensions. Changes in the rheological behavior was indirectly attributed to attraction and repulsion between the inorganic (silica) and organic component (protein, α-lactalbumin) of the suspension. Possibility of tuning the rheological characteristic of nano-structured suspension was directly attributed to the formation of disordered fractal microstructures under the influence of electrostatic interactions.

Second, the thermodynamic nature of complexation at the silica nanoparticles with lysozyme was investigated using isothermal titration calorimetry and circular dichroism. A new model was developed to quantitatively asses the complexation that is promoted by the protein adsorption. Formation of disordered fractal aggregates

shows a bimodal character due to two distinct binding modes. A higher affinity binding mode that is driven by a larger entropic contribution is followed by a low affinity binding mode that is a consequence of moderate enthalpy and entopic contributions. Dominant entropic pathway of interactions offered an alternative self-assembly route to the enthalpically restricted complexation.

6.1 Spin Off Of the Current Contribution: Short Term Outcomes

As already mentioned, tunable rheology and entropic pathway of complexation is expected to open up the floor for application of these principles in 3-dimensional printing, wastewater purification, ceramic slurry processing, fuel design with increased safety, personal care products with desired rheology and function, artistic paints with fine-tuned consistency among others.

The first step logical continuation of this study could be defining the specific rheological needs of industry and applying a similar physicochemical-thermodynamic approach to address their needs by fine tuning the rheological behavior of end products.

6.2 Fundamental Gaps: Medium Term Outcomes

Even though this study proposed a bi-modal binding mode for the thermodynamic nature of interactions, it left open questions that merit attention. Answering those questions is expected to fill some of the fundamental gaps associated with supra-colloidal assembly.

What is the real stoichmetry of binding? Could an advanced binding model be developed that accounts for a stoichiometry distribution for the random complexation?

Is the protein-denatured protein interactions favorable? Are these interactions bridging the nanoparticles, or is one single protein molecule bridging at least two silica nanoparticles via two binding site?

6.3 Future Direction: Long Term Outcomes

As already mentioned, this study demonstrated the fact that interactions of disordered fractal aggregates changes the rheological behavior of nano-structured suspensions. Given the influential studies on the microstructure of disordered aggregates, this rheological approach could be combined with those studies. Studies on microstructure should be expanded to investigate the fractal structure with other techniques such as small angle neutron scattering to draw a relationship between fractal aggregate structure, rheology and thermodynamics. This multi-disciplinary approach could lead fruitful interdisciplinary research projects.

LIST OF REFERENCES

LIST OF REFERENCES

1. Nel, A. E., Mädler, L., Velegol, D., Xia, T., Hoek, E. M. V., Somasundaran, P., Klaessig, F., Castranova, V., and Thompson, M. (2009) Understanding biophysicochemical interactions at the nano–bio interface, *8*.

2. Niemeyer, C. M. (2001) Nanoparticles, Proteins, and Nucleic Acids: Biotechnology Meets Materials Science, *Angewandte Chemie International Edition 40*, 4128-4158.

3. You, C.-C., Verma, A., and Rotello, V. M. (2006) Engineering the nanoparticle-biomacromolecule interface, *Soft Matter 2*, 190-204.

4. Leszczynski, J. (2010) Bionanoscience: Nano meets bio at the interface, *Nat Nano 5*, 633-634.

5. Moyano, D. F., and Rotello, V. M. (2011) Nano Meets Biology: Structure and Function at the Nanoparticle Interface, *Langmuir 27*, 10376-10385.

6. Lynch, I., Cedervall, T., Lundqvist, M., Cabaleiro-Lago, C., Linse, S., and Dawson, K. A. (2007) The nanoparticle-protein complex as a biological entity; a complex fluids and surface science challenge for the 21st century, *Advances in Colloid and Interface Science 134-135*, 167-174.

7. Lynch, I., and Dawson, K. A. (2008) Protein-nanoparticle interactions, *Nano Today 3*, 40-47.

8. Lynch, I., Salvati, A., and Dawson, K. A. (2009) Protein-nanoparticle interactions: What does the cell see?, *Nat Nano 4*, 546-547.

9. Ungyu Paik, J. Y. K., Vincent A. Hackley. (2005) Rheological and electrokinetic behavior associated with concentrated nanosize silica hydrosols, *Materials Chemistry and Physics*, 205-211.

10. Asuri, P., Bale, S. S., Karajanagi, S. S., and Kane, R. S. (2006) The protein–nanomaterial interface, *Current Opinion in Biotechnology 17*, 562-568.

11. Kane, R. S., and Stroock, A. D. (2007) Nanobiotechnology: Protein-Nanomaterial Interactions, *Biotechnology Progress 23*, 316-319.

12. Grzelczak, M., Vermant, J., Furst, E. M., and Liz-Marzán, L. M. (2010) Directed Self-Assembly of Nanoparticles, *ACS Nano 4*, 3591-3605.

13. Katz, E., and Willner, I. (2004) Integrated Nanoparticle–Biomolecule Hybrid Systems: Synthesis, Properties, and Applications, *Angewandte Chemie International Edition 43*, 6042-6108.

14. Li, F., Josephson, D. P., and Stein, A. (2011) Colloidal Assembly: The Road from Particles to Colloidal Molecules and Crystals, *Angewandte Chemie International Edition 50*, 360-388.

15. Velev, O. D., and Gupta, S. (2009) Materials Fabricated by Micro- and Nanoparticle Assembly – The Challenging Path from Science to Engineering, *Advanced Materials 21*, 1897-1905.

16. Hiemenz, P. C., and Rajagopalan, R. (1997) *Principles of Colloid and Surface Chemistry, Third Edition, Revised and Expanded*, Taylor & Francis.

17. Hunter, R. J. (2001) *Foundations of Colloid Science*, Oxford University Press.

18. Larson, R. G. (1999) *The Structure and Rheology of Complex Fluids*, OUP USA.

19. Morrison, I. D., and Ross, S. (2002) *Colloidal Dispersions: Suspensions, Emulsions, and Foams*, Wiley.

20. Vold, R. D., and Vold, M. J. (1983) *Colloid and Interface Chemistry*, Addison-Wesley.

21. Dzina, K., Remco, T., and Peter, R. L. (2008) Direct measurements of polymer-induced forces, *Journal of Physics: Condensed Matter 20*, 073101.

22. Netz, R. R., and Andelman, D. (2003) Neutral and charged polymers at interfaces, *Physics Reports 380*, 1-95.

23. Asakura, S., and Oosawa, F. (1954) On interaction between two bodies immersed in a solution of macromolecules, *Chemical Physics*, 1255-1256.

24. Asakura, S., and Oosawa, F. (1958) Interaction between particles suspended in solutions of macromolecules, *Journal of polymer science 33*, 183-192.

25. Sieglaff, C. L. (1959) Phase separation in mixed polymer solutions, *Journal of Polymer Science 41*, 319-326.

26. Feigin, R. I., and Napper, D. H. (1980) Depletion stabilization and depletion flocculation, *Journal of Colloid and Interface Science 75*, 525-541.

27. Heath, D., and Tadros, T. F. (1983) Rheological investigations of the effect of addition of free polymer to concentrated sterically stabilised polystyrene latex dispersions, *Faraday Discussions of the Chemical Society 76*, 203-218.

28. Patel, P. D., and Russel, W. B. (1988) A mean field theory for the rheology of phase separated or flocculated dispersions, *Colloids and Surfaces 31*, 355-383.

29. Tadros, T. F. (1996) Correlation of viscoelastic properties of stable and flocculated suspensions with their interparticle interactions, *Advances in Colloid and Interface Science 68*, 97-200.

30. Shah, S., Chen, Y.-L., Schweizer, K., and Zukoski, C. (2003) Viscoelasticity and rheology of depletion flocculated gels and fluids, *The Journal of chemical physics 119*, 8747-8760.

31. Lu, P. J., Zaccarelli, E., Ciulla, F., Schofield, A. B., Sciortino, F., and Weitz, D. A. (2008) Gelation of particles with short-range attraction, *Nature 453*, 499-503.

32. Napper, D. H. (1977) Steric stabilization, *Journal of Colloid and Interface Science 58*, 390-407.

33. Heller, W., and Pugh, T. L. (1954) ``Steric Protection"of Hydrophobic Colloidal Particles by Adsorption of Flexible Macromolecules, *The Journal of Chemical Physics 22*, 1778-1778.

34. Papir, Y. S., and Krieger, I. M. (1970) Rheological studies on dispersions of uniform colloidal spheres: II. Dispersions in nonaqueous media, *Journal of Colloid and Interface Science 34*, 126-130.

35. Woods, M. E., and Krieger, I. M. (1970) Rheological studies on dispersions of uniform colloidal spheres I. Aqueous dispersions in steady shear flow, *Journal of Colloid and Interface Science 34*, 91-99.

36. Willey, S. J., and Macosko, C. (1978) Steady shear rheological behavior of PVC plastisols, *Journal of Rheology (1978-present) 22*, 525-545.

37. Liang, W., Tadros, T. F., and Luckham, P. F. (1992) Rheological studies on concentrated polystyrene latex sterically stabilized by poly(ethylene oxide) chains, *Journal of Colloid and Interface Science 153*, 131-139.

38. Prestidge, C., and Tadros, T. F. (1988) Viscoelastic properties of aqueous concentrated polystyrene latex dispersions containing grafted poly(ethylene oxide) chains, *Journal of Colloid and Interface Science 124*, 660-665.

39. de L. Costello, B. A., Luckham, P. F., and Tadros, T. F. (1992) Investigations of the properties of aqueous sterically stabilized dispersions, *Journal of Colloid and Interface Science 152*, 237-246.

40. Luckham, P. F., Ansarifar, M. A., de L. Costello, B. A., and Tadros, T. F. (1991) The relationship between interparticle forces and the bulk rheology of suspensions, *Powder Technology 65*, 371-379.

41. Liang, W., Tadros, T. F., and Luckham, P. F. (1993) Influence of addition of electrolyte and/or increase of temperature on the viscoelastic properties of concentrated sterically stabilized polystyrene latex dispersions, *Langmuir 9*, 2077-2083.

42. van de Ven, T. G. M., and Hunter, R. J. (1979) Viscoelastic properties of coagulated sols, *Journal of Colloid and Interface Science 68*, 135-143.

43. Quemada, D., and Berli, C. (2002) Energy of interaction in colloids and its implications in rheological modeling, *Advances in Colloid and Interface Science 98*, 51-85.

44. Çengel, Y. A., and Boles, M. A. (2002) *Thermodynamics: An Engineering Approach*, McGraw-Hill.

45. Norde, W. (2003) *Colloids and Interfaces in Life Sciences*, Taylor & Francis.

46. Tinoco, I., Sauer, K., and Wang, J. C. (1995) *Physical Chemistry: Principles and Applications in Biological Sciences*, Prentice Hall.

47. Norde, W. (2011) *Colloids and interfaces in life sciences and bionanotechnology*, CRC Press.

48. Berne, B. J., and Pecora, R. (2000) *Dynamic Light Scattering: With Applications to Chemistry, Biology, and Physics*, Dover Publications.

49. Koppel, D. E. (1972) Analysis of Macromolecular Polydispersity in Intensity Correlation Spectroscopy: The Method of Cumulants, *The Journal of Chemical Physics 57*, 4814-4820.

50. Ostrowsky, N., Sornette, D., Parker, P., and Pike, E. R. (1981) Exponential Sampling Method for Light Scattering Polydispersity Analysis, *Optica Acta: International Journal of Optics 28*, 1059-1070.

51. Provencher, S. W. (1982) CONTIN: A general purpose constrained regularization program for inverting noisy linear algebraic and integral equations, *Computer Physics Communications 27*, 229-242.

52. Frisken, B. J. (2001) Revisiting the method of cumulants for the analysis of dynamic light-scattering data, *Appl Optics 40*, 4087-4091.

53. Bargeron, C. B. (1974) Analysis of intensity correlation spectra of mixtures of polystyrene latex spheres: A comparison of direct least squares fitting with the method of cumulants, *The Journal of Chemical Physics 60*, 2516-2519.

54. Lee, S. P., and Chu, B. (1974) Application of least-squares (difference-integration) method to cumulants analysis in intensity fluctuation spectroscopy, *Applied Physics Letters 24*, 575-576.

55. Roig, A. R., and Alessandrini, J. L. (2006) Particle Size Distributions from Static Light Scattering with Regularized Non-Negative Least Squares Constraints, *Particle & Particle Systems Characterization 23*, 431-437.

56. Berberan-Santos, M. N. (2008) A luminescence decay function encompassing the stretched exponential and the compressed hyperbola, *Chem Phys Lett 460*, 146-150.

57. Berberan-Santos, M. N., Bodunov, E. N., and Valeur, B. (2005) Mathematical functions for the analysis of luminescence decays with underlying distributions 1. Kohlrausch decay function (stretched exponential), *Chemical Physics 315*, 171-182.

58. Berberan-Santos, M. N., and Valeur, B. (2007) Luminescence decays with underlying distributions: General properties and analysis with mathematical functions, *Journal of Luminescence 126*, 263-272.

59. Zhu, X. J., Shen, J., Liu, W., Sun, X. M., and Wang, Y. J. (2010) Nonnegative least-squares truncated singular value decomposition to particle size distribution inversion from dynamic light scattering data, *Appl Optics 49*, 6591-6596.

60. Kim, J., Ahn, S., Lee, H., and Lee, M. (2013) Estimation of particle size distribution using photon autocorrelation function from dynamic light scattering considering unknown baseline, *Opt Lett 38*, 1757-1759.

61. Pusey, P. N., and van Megen, W. (1984) Detection of small polydispersities by photon correlation spectroscopy, *The Journal of Chemical Physics 80*, 3513-3520.

62. Morrison, I. D., Grabowski, E. F., and Herb, C. A. (1985) Improved techniques for particle size determination by quasi-elastic light scattering, *Langmuir 1*, 496-501.

63. Bryant, G., Abeynayake, C., and Thomas, J. C. (1996) Improved particle size distribution measurements using multiangle dynamic light scattering .2. Refinements and applications, *Langmuir 12*, 6224-6228.

64. Bryant, G., and Thomas, J. C. (1995) Improved Particle-Size Distribution Measurements Using Multiangle Dynamic Light-Scattering, *Langmuir 11*, 2480-2485.

65. Briggs, J., and Nicoli, D. F. (1980) Photon-Correlation Spectroscopy of Polydisperse Systems, *J Chem Phys 72*, 6024-6030.

66. Podzimek, S. (2011) Light Scattering, In *Light Scattering, Size Exclusion Chromatography and Asymmetric Flow Field Flow Fractionation*, pp 37-98, John Wiley & Sons, Inc.

67. Hunter, R. J., Ottewill, R. H., and Rowell, R. L. (2013) *Zeta Potential in Colloid Science: Principles and Applications*, Elsevier Science.

68. Morrison, F. A. (2001) *Understanding Rheology*, Oxford University Press.

69. Ladbury, J. E., and Doyle, M. L. (2005) *Biocalorimetry 2: Applications of Calorimetry in the Biological Sciences*, Wiley.

70. Freire, E., Mayorga, O. L., and Straume, M. (1990) Isothermal titration calorimetry, *Analytical Chemistry 62*, 950A-959A.

71. Bergna, H. E., and Roberts, W. O. (2005) *Colloidal Silica: Fundamentals and Applications*, CRC Press.

72. Dobias, B., and Stechemesser, H. (2005) *Coagulation and Flocculation, Second Edition*, CRC Press.

73. Saptarshi, S. R., Duschl, A., and Lopata, A. L. (2013) Interaction of nanoparticles with proteins: relation to bio-reactivity of the nanoparticle, *J Nanobiotechnol 11*.

74. Ge, J., Lu, D. N., Liu, Z. X., and Liu, Z. (2009) Recent advances in nanostructured biocatalysts, *Biochem Eng J 44*, 53-59.

75. Devineau, S., Zanotti, J. M., Loupiac, C., Zargarian, L., Neiers, F., Pin, S., and Renault, J. P. (2013) Myoglobin on Silica: A Case Study of the Impact of Adsorption on Protein Structure and Dynamics, *Langmuir 29*, 13465-13472.

76. Nakanishi, K., Sakiyama, T., and Imamura, K. (2001) On the adsorption of proteins on solid surfaces, a common but very complicated phenomenon, *Journal of Bioscience and Bioengineering 91*, 233-244.

77. Haynes, C. A., and Norde, W. (1994) Globular proteins at solid/liquid interfaces, *Colloids and Surfaces B: Biointerfaces 2*, 517-566.

78. Norde, W. (2003) *Adsorption of Bio(Polymers), with Special Emphasis on Globular Proteins*, Marcel Dekker, INC, New York.

79. Lynch, I., and Dawson, K. A. (2008) Protein-nanoparticle interactions, *Nano Today 3*, 40-47.

80. Nel, A. E., Madler, L., Velegol, D., Xia, T., Hoek, E. M. V., Somasundaran, P., Klaessig, F., Castranova, V., and Thompson, M. (2009) Understanding biophysicochemical interactions at the nano-bio interface, *Nat Mater 8*, 543-557.

81. Kondo, A., Murakami, F., and Higashitani, K. (1992) Circular dichroism studies on conformational changes in protein molecules upon adsorption on ultrafine polystyrene particles, *Biotechnol Bioeng 40*, 889-894.

82. Cedervall, T., Lynch, I., Lindman, S., Berggard, T., Thulin, E., Nilsson, H., Dawson, K. A., and Linse, S. (2007) Understanding the nanoparticle-protein corona using methods to quantify exchange rates and affinities of proteins for nanoparticles, *P Natl Acad Sci USA 104*, 2050-2055.

83. Vertegel, A. A., Siegel, R. W., and Dordick, J. S. (2004) Silica Nanoparticle Size Influences the Structure and Enzymatic Activity of Adsorbed Lysozyme, *Langmuir 20*, 6800-6807.

84. Henzler, K., Haupt, B., Lauterbach, K., Wittemann, A., Borisov, O., and Ballauff, M. (2010) Adsorption of β-Lactoglobulin on Spherical Polyelectrolyte Brushes: Direct Proof of Counterion Release by Isothermal Titration Calorimetry, *Journal of the American Chemical Society 132*, 3159-3163.

85. Shang, W., Nuffer, J. H., Muñiz-Papandrea, V. A., Colón, W., Siegel, R. W., and Dordick, J. S. (2009) Cytochrome c on Silica Nanoparticles: Influence of Nanoparticle Size on Protein Structure, Stability, and Activity, *Small 5*, 470-476.

86. Wu, X., and Narsimhan, G. (2008) Effect of surface concentration on secondary and tertiary conformational changes of lysozyme adsorbed on silica nanoparticles, *Biochimica et Biophysica Acta (BBA) - Proteins and Proteomics 1784*, 1694-1701.

87. Bharti, B., Meissner, J., and Findenegg, G. H. (2011) Aggregation of Silica Nanoparticles Directed by Adsorption of Lysozyme, *Langmuir 27*, 9823-9833.

88. Kumar, S., Aswal, V. K., and Kohlbrecher, J. (2011) SANS and UV–vis Spectroscopy Studies of Resultant Structure from Lysozyme Adsorption on Silica Nanoparticles, *Langmuir 27*, 10167-10173.

89. Technical Bulletin 11, C. p. (1967) Basic Characteristics of Aerosil Fumed Silica.

90. Barik, T. K., Sahu, B., and Swain, V. (2008) Nanosilica - from medicine to pest control, *Parasitol Res 103*, 253-258.

91. Larsericsdotter, H., Oscarsson, S., and Buijs, J. (2001) Thermodynamic Analysis of Proteins Adsorbed on Silica Particles: Electrostatic Effects, *Journal of Colloid and Interface Science 237*, 98-103.

92. Reference Manual, M. I. (2007) Sample Dispersion and Refractive Index Guide.

93. Herman, D., and Walz, J. Y. (2013) Stabilization of Weakly Charged Microparticles Using Highly Charged Nanoparticles, *Langmuir 29*, 5982-5994.

94. Brown, M. A., Huthwelker, T., Redondo, A. B., Janousch, M., Faubel, M., Arrell, C. A., Scarongella, M., Chergui, M., and van Bokhoven, J. A. (2012) Changes in the Silanol Protonation State Measured In Situ at the Silica-Aqueous Interface, *J Phys Chem Lett 3*, 231-235.

95. Liu, X., Cheng, J., Lu, X., and Wang, R. (2014) Surface acidity of quartz: understanding the crystallographic control, *Physical Chemistry Chemical Physics 16*, 26909-26916.

96. Zittle, C. A. (1956) Solubility Transformation of Alpha-Lactalbumin, *Arch Biochem Biophys 64*, 144-151.

97. Paik, U., Kim, J. Y., and Hackley, V. A. (2005) Rheological and electrokinetic behavior associated with concentrated nanosize silica hydrosols, *Materials Chemistry and Physics 91*, 205-211.

98. Krieger, I. M., and Eguiluz, M. (1976) The Second Electroviscous Effect in Polymer Latices, *Transactions of The Society of Rheology (1957-1977) 20*, 29-45.

99. Israelachvili, J. N., and Adams, G. E. (1978) Measurement of forces between two mica surfaces in aqueous electrolyte solutions in the range 0-100 nm, *Journal of the Chemical Society, Faraday Transactions 1: Physical Chemistry in Condensed Phases 74*, 975-1001.

100. Peschel, G., Belouschek, P., Müller, M. M., Müller, M. R., and König, R. (1982) The interaction of solid surfaces in aqueous systems, *Colloid & Polymer Sci 260*, 444-451.

101. Vigil, G., Xu, Z., Steinberg, S., and Israelachvili, J. (1994) Interactions of Silica Surfaces, *Journal of Colloid and Interface Science 165*, 367-385.

102. Rubio-Hernández, F. J., Ayúcar-Rubio, M. F., Velázquez-Navarro, J. F., and Galindo-Rosales, F. J. (2006) Intrinsic viscosity of SiO2, Al2O3 and TiO2 aqueous suspensions, *Journal of Colloid and Interface Science 298*, 967-972.

103. Iler, R. K. (1979) *The Chemistry of Silica: Solubility, Polymerization, Colloid and Surface Properties and Biochemistry of Silica*, Wiley.

104. Mewis, J., and Wagner, N. J. (2011) *Colloidal Suspension Rheology*, Cambridge University Press.

105. Barnes, H. A., and Nguyen, Q. D. (2001) Rotating vane rheometry - a review, *J Non-Newton Fluid 98*, 1-14.

106. Cohen, I., Davidovitch, B., Schofield, A. B., Brenner, M. P., and Weitz, D. A. (2006) Slip, yield, and bands in colloidal crystals under oscillatory shear, *Phys Rev Lett 97*, 215502.

107. Raghavan, S. R., Walls, H. J., and Khan, S. A. (2000) Rheology of silica dispersions in organic liquids: New evidence for solvation forces dictated by hydrogen bonding, *Langmuir 16*, 7920-7930.

108. Brinker, C. J., and Scherer, G. W. (1990) *Sol-gel Science: The Physics and Chemistry of Sol-gel Processing*, Academic Press.

109. Gunko, V. M., Turov, V. V., Zarko, V. I., Dudnik, V. V., Tischenko, V. A., Kazakova, O. A., Voronin, E. F., Siltchenko, S. S., Barvinchenko, V. N., and Chuiko, A. A. (1997) Aqueous suspensions of fumed silica and adsorption of proteins, *Journal of Colloid and Interface Science 192*, 166-178.

110. Kroon, M., Wegdam, G. H., and Sprik, R. (1996) Dynamic light scattering studies on the sol-gel transition of a suspension of anisotropic colloidal particles, *Phys Rev E 54*, 6541-6550.

111. Ruzicka, B., Zulian, L., and Ruocco, G. (2004) Routes to gelation in a clay suspension, *Phys Rev Lett 93*.

112. Nel, A. E., Madler, L., Velegol, D., Xia, T., Hoek, E. M. V., Somasundaran, P., Klaessig, F., Castranova, V., and Thompson, M. (2009) Understanding biophysicochemical interactions at the nano-bio interface, *Nat Mater 8*, 543-557.

113. Cedervall, T., Lynch, I., Lindman, S., Berggård, T., Thulin, E., Nilsson, H., Dawson, K. A., and Linse, S. (2007) Understanding the nanoparticle–protein corona using methods to quantify exchange rates and affinities of proteins for nanoparticles, *Proceedings of the National Academy of Sciences 104*, 2050-2055.

114. Costanzo, P. J., Patten, T. E., and Seery, T. A. P. (2004) Protein−Ligand Mediated Aggregation of Nanoparticles: A Study of Synthesis and Assembly Mechanism, *Chemistry of Materials 16*, 1775-1785.

115. Salem, A. K., Chen, M., Hayden, J., Leong, K. W., and Searson, P. C. (2004) Directed Assembly of Multisegment Au/Pt/Au Nanowires, *Nano Letters 4*, 1163-1165.

116. Bayraktar, H., Srivastava, S., You, C.-C., Rotello, V. M., and Knapp, M. J. (2008) Controlled nanoparticle assembly through protein conformational changes, *Soft Matter 4*, 751-756.

117. Yadav, I., Kumar, S., Aswal, V. K., and Kohlbrecher, J. (2014) Small-angle neutron scattering study of differences in phase behavior of silica nanoparticles in the presence of lysozyme and bovine serum albumin proteins, *Physical Review E 89*, 032304.

118. Shi, L., Carn, F., Boue, F., Mosser, G., and Buhler, E. (2013) Control over the electrostatic self-assembly of nanoparticle semiflexible biopolyelectrolyte complexes, *Soft Matter 9*, 5004-5015.

119. Bharti, B., Meissner, J., and Findenegg, G. H. (2011) Aggregation of Silica Nanoparticles Directed by Adsorption of Lysozyme, *Langmuir, 2011, 27 (16), pp 9823–9833 27*, 9832-9833.

120. Kumar, S., Aswal, V. K., and Callow, P. (2014) pH-Dependent Interaction and Resultant Structures of Silica Nanoparticles and Lysozyme Protein, *Langmuir 30*, 1588-1598.

121. Blake, C. C., Koenig, D. F., Mair, G. A., North, A. C., Phillips, D. C., and Sarma, V. R. (1965) Structure of hen egg-white lysozyme. A three-dimensional Fourier synthesis at 2 Angstrom resolution, *Nature 206*, 757-761.

122. Deželić, G., and Kratohvil, J. P. (1960) Determination of size of small particles by light scattering. experiments on ludox colloidal silica, *Kolloid-Zeitschrift 173*, 38-48.

123. Ball, V., and Ramsden, J. J. (1997) Absence of Surface Exclusion in the First Stage of Lysozyme Adsorption Is Driven through Electrostatic Self-Assembly, *The Journal of Physical Chemistry B 101*, 5465-5469.

124. Daly, S. M., Przybycien, T. M., and Tilton, R. D. (2003) Coverage-Dependent Orientation of Lysozyme Adsorbed on Silica, *Langmuir 19*, 3848-3857.

125. Hildebrand, N., Köppen, S., Derr, L., Li, K., Koleini, M., Rezwan, K., and Colombi Ciacchi, L. (2015) Adsorption Orientation and Binding Motifs of Lysozyme and Chymotrypsin on Amorphous Silica, *The Journal of Physical Chemistry C 119*, 7295-7307.

126. Rezwan, K., Meier, L. P., and Gauckler, L. J. (2005) Lysozyme and bovine serum albumin adsorption on uncoated silica and AlOOH-coated silica particles: the influence of positively and negatively charged oxide surface coatings, *Biomaterials 26*, 4351-4357.

127. Xu, K., Ouberai, M. M., and Welland, M. E. (2013) A comprehensive study of lysozyme adsorption using dual polarization interferometry and quartz crystal microbalance with dissipation, *Biomaterials 34*, 1461-1470.

128. Eren, N., Jones, O., and Campanella, O. (2015) Changes in the rheology of nano-structured suspensions by adsorption of the protein α-lactalbumin on the surface of silica particles, *Rheol Acta*, 1-10.

129. Norde, W., and Favier, J. P. (1992) Structure of adsorbed and desorbed proteins, *Colloids and Surfaces 64*, 87-93.

130. Greenfield, N. J. (2006) Using circular dichroism spectra to estimate protein secondary structure, *Nature protocols 1*, 2876-2890.

131. Sreerama, N., and Woody, R. W. (2000) Estimation of protein secondary structure from circular dichroism spectra: Comparison of CONTIN, SELCON, and CDSSTR methods with an expanded reference set, *Analytical Biochemistry 287*, 252-260.

132. Whitmore, L., and Wallace, B. A. (2008) Protein secondary structure analyses from circular dichroism spectroscopy: Methods and reference databases, *Biopolymers 89*, 392-400.

133. Velazquez-Campoy, A., and Freire, E. (2006) Isothermal titration calorimetry to determine association constants for high-affinity ligands, *Nat. Protocols 1*, 186-191.

134. Turci, F., Ghibaudi, E., Colonna, M., Boscolo, B., Fenoglio, I., and Fubini, B. (2010) An Integrated Approach to the Study of the Interaction between Proteins and Nanoparticles, *Langmuir 26*, 8336-8346.

135. Felsovalyi, F., Mangiagalli, P., Bureau, C., Kumar, S. K., and Banta, S. (2011) Reversibility of the Adsorption of Lysozyme on Silica, *Langmuir 27*, 11873-11882.

136. Czeslik, C., and Winter, R. (2001) Effect of temperature on the conformation of lysozyme adsorbed to silica particles, *Physical Chemistry Chemical Physics 3*, 235-239.

137. Sethuraman, A., Vedantham, G., Imoto, T., Przybycien, T., and Belfort, G. (2004) Protein unfolding at interfaces: Slow dynamics of α-helix to β-sheet transition, *Proteins: Structure, Function, and Bioinformatics 56*, 669-678.

138. Kabsch, W., and Sander, C. (1983) Dictionary of Protein Secondary Structure - Pattern-Recognition of Hydrogen-Bonded and Geometrical Features, *Biopolymers 22*, 2577-2637.

139. Boczkowska, M., Rebowski, G., Kast, D. J., and Dominguez, R. (2014) Structural analysis of the transitional state of Arp2/3 complex activation by two actin-bound WCAs, *Nat Commun 5*.

140. De, M., Miranda, O. R., Rana, S., and Rotello, V. M. (2009) Size and geometry dependent protein-nanoparticle self-assembly, *Chemical Communications*, 2157-2159.

141. De, M., You, C.-C., Srivastava, S., and Rotello, V. M. (2007) Biomimetic Interactions of Proteins with Functionalized Nanoparticles: A Thermodynamic Study, *Journal of the American Chemical Society 129*, 10747-10753.

142. McGuire, J. (2014) Building a working understanding of protein adsorption with model systems and serendipity, *Colloids and Surfaces B: Biointerfaces 124*, 38-48.

143. Rabe, M., Verdes, D., and Seeger, S. (2011) Understanding protein adsorption phenomena at solid surfaces, *Advances in Colloid and Interface Science 162*, 87-106.

APPENDIX

APPENDIX

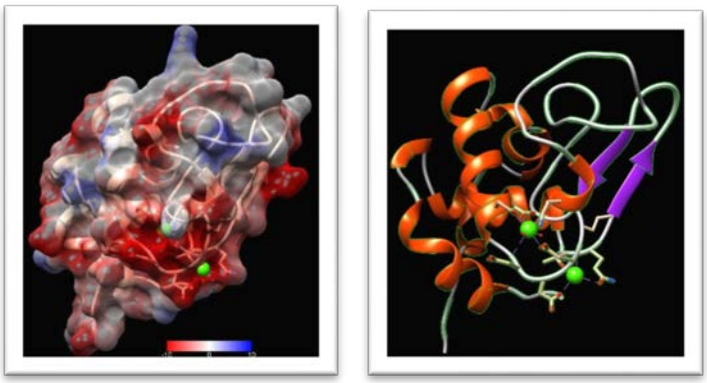

Figure A-1α-lactalbumin structure, PDB:1a4v is visualized with Chimera

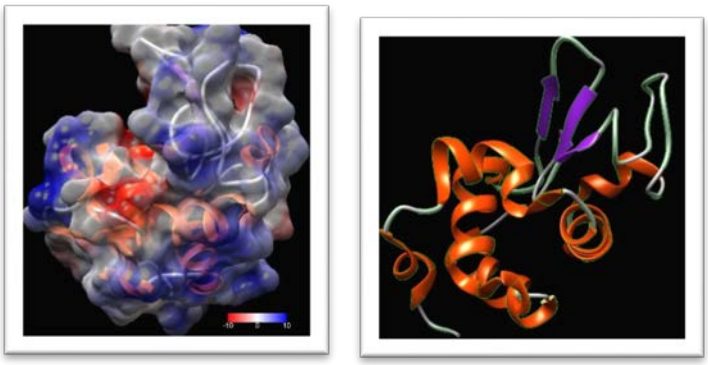

Figure A-2Lysozyme structure, PDB: 4RLM was visualized with Chimera

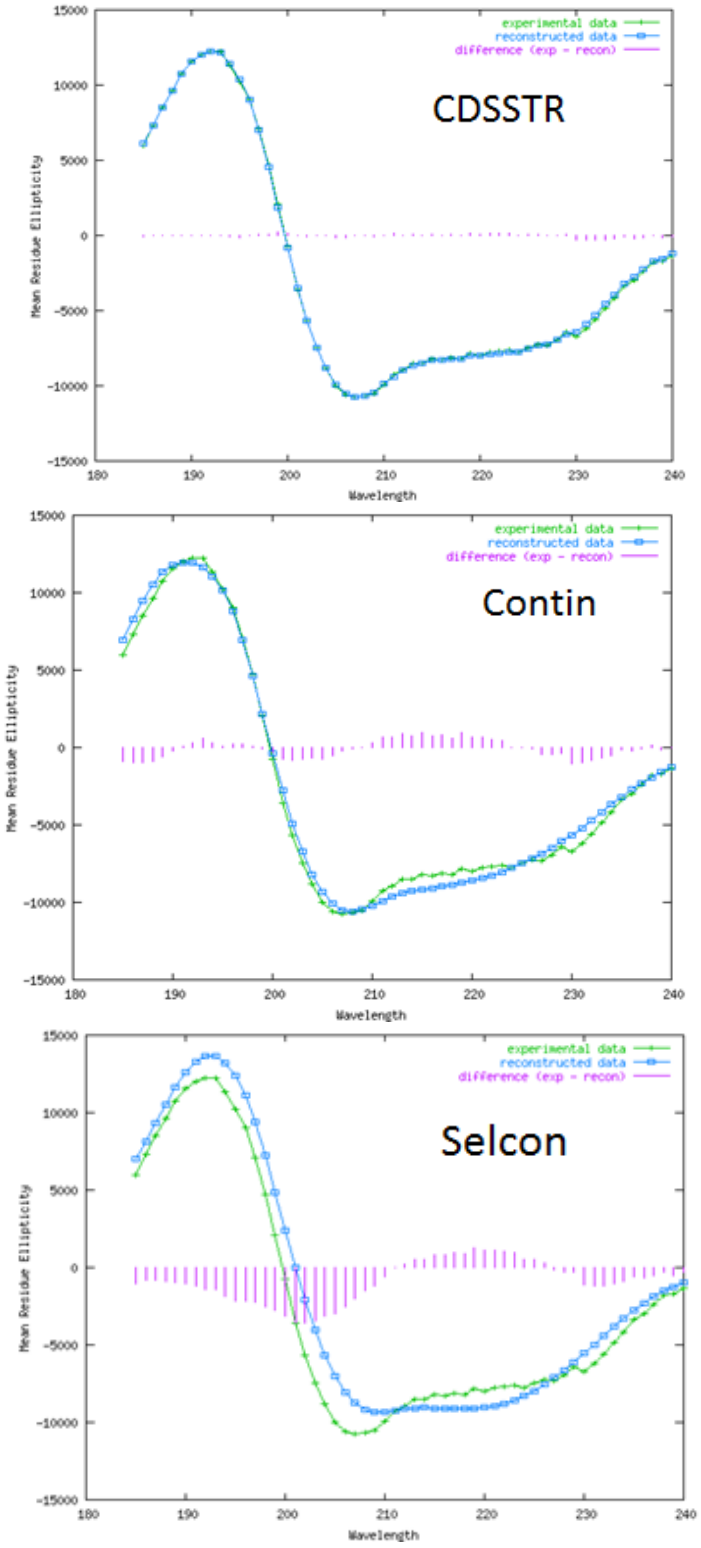

Figure A-3Different CD Deconvolution Algorithms

Surface Coverage Calculations for Protein Adsorption

$RSi := 11$ nm $\quad \rho si := 2.2$ g/cm^3

$Nav := 6.022 \cdot 10^{23}$ $\quad MwLys := 14307$ g/mol

$SASi := 4\pi \cdot (RSi)^2 = 1.521 \times 10^3$ nm^2 surface area of one silica

$VSi := \pi \cdot \frac{4}{3} \cdot RSi^3 = 5.575 \times 10^3$ nm^3 volume of one silica

$mSi := VSi \cdot 2.2 \cdot 10^{-21} = 0$ g mass of one silica

$SApermass := \frac{SASi}{mSi} \cdot 10^{-18} = 123.967$ m^2/g

BET Surface area is 110-150 m^2/g since my silica is non-porous geometric surface area matches with BET quite well

$RLyslong := 2.25$ nm

$RLysshort := 1.5$ nm

Lysozyme is an ellipsoid with dimensions 4.5x3x3 nm

$CALyslong := \pi \cdot RLyslong^2 = 15.904$ nm^2 Long Cross Sectional area

$CALysshort := \pi \cdot RLysshort^2 = 7.069$ nm^2 Short Cross Sectional area

Assuming the Lysozyme does not change the conformation, Surface Area of Silica at a distance of protein radius is:

$SAforLysshort := 4 \cdot \pi \cdot (RSi + RLyslong)^2 = 2.206 \times 10^3$ nm^2

$SAforLyslong := 4 \cdot \pi \cdot (RSi + RLysshort)^2 = 1.963 \times 10^3$ nm^2

hexagonel close packing of sphres on a flat surface would yield a 0.9069 density

$HCPlong := \frac{SAforLyslong \cdot 0.9069}{CALyslong} = 111.963$ number of protein bindindg side on (long diameter)

$HCPshort := \frac{SAforLysshort \cdot 0.9069}{CALysshort} = 283.054$ number of protein bindindg side on (short diameter)

$$\text{Longmass} := \text{HCPlong} \cdot \frac{\text{MwLys}}{\text{Nav}} \cdot 1000 = 2.66 \times 10^{-15} \quad \text{mg per Silica}$$

$$\text{Longcoverage} := \frac{\text{Longmass}}{\text{SASi}} \cdot 10^{18} = 1.749 \quad \text{mg/m^2}$$

$$\text{Shortmass} := \text{HCPshort} \cdot \frac{\text{MwLys}}{\text{Nav}} \cdot 1000 = 6.725 \times 10^{-15} \quad \text{mg per Silica}$$

$$\text{Shortcoverage} := \frac{\text{Shortmass}}{\text{SASi}} \cdot 10^{18} = 4.423 \quad \text{mg/m^2}$$

Table A-1Experimental design for ITC mimic adsorption test

	Reference Injection									
	n1	n2	n3	n4	n5	n6	n7	n8	n9	n10
	Inoculation Time									
Tube	0	5	10	15	20	25	30	35	40	45
1	S1									
2		S2								
3			S3							
4				S4						
5					S5					
6						S6				
7							S7			
8								S8		
9									S9	
10										S10

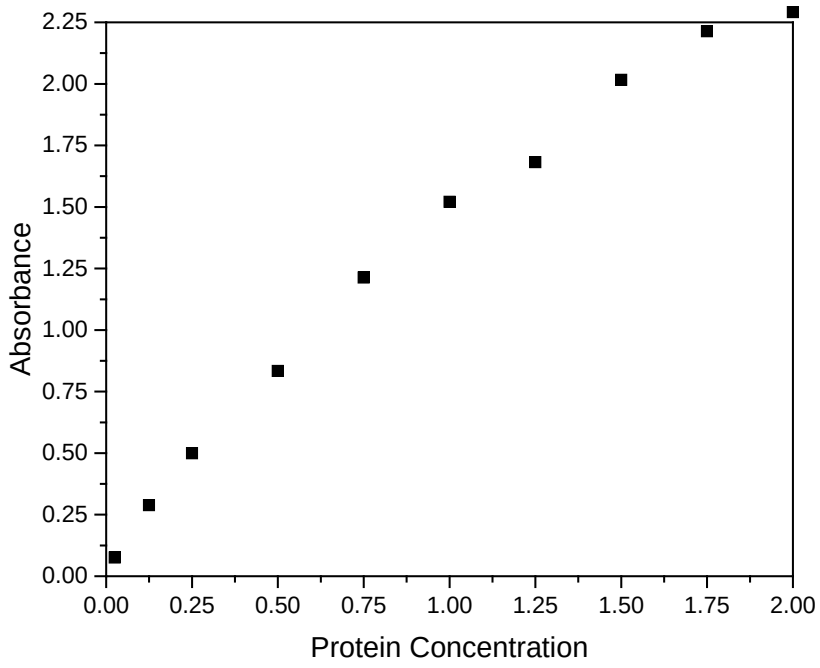

Figure A-4 Example of BCA assay internal standard curve for Lysozyme

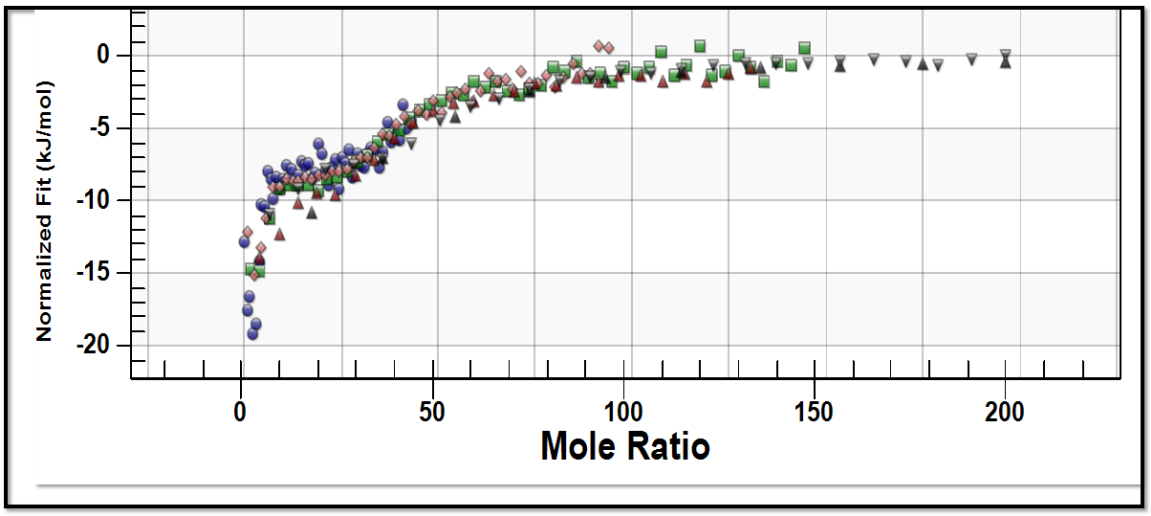

Figure A-5ITC data master curve. Each color represents a different initial mole ratio of Lysozyme and Silica.

VITA

VITA

Necla Mine Eren earned her BS degree from Ankara University in Food Engineering in 2009 and MSc degree from Purdue University in Biological Engineering in May 2012 and directly continued her PhD within the same research group which is supervised by Dr. Osvaldo Campanella Throughout her graduate studies, she has worked on collaborative projects with mechanical, aerospace and biomedical engineering and completed a 6 months internship in Industrial and Physical Pharmacy Department. Besides her research efforts, she mentored undergraduate students by serving as a teaching assistant in Thermodynamics, Physical Chemistry and Heat and Mass Transfer Courses and graduate students by leading the ABE Graduate Student Association as 2013-2014 President.